VISCOELASTIC FE MODELING OF ASPHALT PAVEMENTS AND ITS APPLICATION TO U.S. 30 PERPETUAL PAVEMENT

A dissertation presented to

the faculty of

the Russ College of Engineering and Technology of Ohio University

In partial fulfillment

of the requirements for the degree

Doctor of Philosophy

Yun Liao

November 2007

This dissertation titled

VISCOELASTIC FE MODELING OF ASPHALT PAVEMENTS

AND ITS APPLICATION TO U.S. 30 PERPETUAL PAVEMENT

by

YUN LIAO

has been approved for

the Department of Civil Engineering

and the Russ College of Engineering and Technology by

_____

Shad M. Sargand

Russ Professor of Civil Engineering

_____

Dennis Irwin

Dean, Russ College of Engineering and Technology

ABSTRACT

LIAO, YUN, Ph.D., November 2007. Integrated Engineering

VISCOELASTIC FE MODELING OF ASPHALT PAVEMENTS AND ITS APPLICATION TO U.S. 30 PERPETUAL PAVEMENT (146 pp.)

Director of Dissertation: Shad M. Sargand

The primary objective of this research consisted of incorporating laboratory-determined viscoelastic material properties into a three-dimensional finite element model to accurately simulate the behavior of a perpetual pavement structure subjected to vehicular loading at different pavement temperatures and vehicular speeds. With this finite element model, statistical models that were based on Falling Weight Deflectometer testing were developed to predict the structural response of a perpetual pavement.

In this research, the dynamic modulus test was chosen to determine viscoelastic properties of hot-mix-asphalt materials in the laboratory. A 5-term Prony series was used to describe the viscoelastic behavior of hot-mix-asphalt materials. Resilient modulus tests were performed to measure resilient moduli of hot-mix-asphalt mixtures and subgrade soils. All these laboratory-determined material properties were inputted into the developed viscoelastic finite element model to predict pavement response.

The developed viscoelastic finite element model was validated by and calibrated to field-measured pavement responses collected at the U.S. 30 perpetual pavement constructed in Wayne County, Ohio. The results demonstrated that the developed viscoelastic finite element model can predict pavement responses accurately.

Parametric studies revealed that the developed viscoelastic finite element model performed better in pavement thickness design compared with perpetual-pavement-

design-oriented software PerRoad which underestimated pavement responses. Layer modulus variation did not affect pavement response significantly. The ratio maximum-tensile-strain/load was independent of the axle load. The ratio maximum-tensile-strain/speed increased with decreasing in vehicular speeds. A nomograph was developed to correlate the maximum tensile strain to the pavement temperature depending on the thickness of the ODOT302 layer and the aggregate base.

Finally, the developed finite element model was tailored to work for Falling Weight Deflectometer tests. Statistical models were developed to estimate pavement response using the Falling Weight Deflectometer upon the completion of a perpetual pavement. These models are important in practice to assess pavement quality using the Falling Weight Deflectometer.

Outcomes of this research are significantly important to improve the accuracy of current design and analysis methods which are widely used in predicting pavement responses and to provide practical guidelines for perpetual pavement design and analysis.

Approved: _____

Shad M. Sargand

Russ Professor of Civil Engineering

DEDICATION

To my wife, Sherrie Y. Yang, and my Parents

ACKNOWLEDGEMENTS

Immeasurable debts are owed to many individuals who greatly assisted completion of this dissertation.

The research presented in this dissertation was completed at the Department of Civil Engineering of Ohio University.

First and foremost, my sincere gratitude goes to Dr. Shad Sargand for all his encouragement, guidance, and help. This dissertation would not have been possible without Dr. Sargand, who accepted me as a doctoral student and offered me financial support throughout my three-years of study at Ohio University.

I would like to give my sincere appreciation to Dr. Sang-Soo Kim who has always been extremely generous with his knowledge, ideas, and time.

I would also like to sincerely appreciate Dr. Ludwig Figueroa for his important advice and assistance and his great patience.

My thanks must go to my committee members: Dr. Hajrudin Pasic, Dr. Gregory Springer, and Dr. Martin Mohlenkamp for their help and the time they spent in serving on my committee.

My thanks also must go to Dr. Teruhisa Masada for his help on soil testing and Mr. Issam Khoury for his support.

Finally, I want to thank my wife, Sherrie Y. Yang, and my parents for their persistent support and love in pursuing my educational goals.

TABLE OF CONTENTS

ABSTRACT 3

DEDICATION 5

ACKNOWLEDGEMENTS 6

LIST OF TABLES 10

LIST OF FIGURES 12

1 INTRODUCTION 15

1.1 Research Objectives and Approach 15

1.2 Outline of the Research Presented 18

2 LITERATURE REVIEW 20

2.1 Elastic M-E Design 22

2.2 Viscoelastic M-E Design 24

3 VISCOELASTIC MODELING OF HMA MATERIALS 28

3.1 Theory of Linear Viscoelasticity 28

3.2 Mechanical Model Representing Linear Viscoelastic Behavior 32

3.3 Summary 35

4 MATERIAL CHARACTERIZATION 37

4.1 Dynamic Modulus Testing and Results 38

4.1.1 Complex Modulus, Dynamic Modulus, and Phase Angle 38

4.1.2 Experiments and Results 41

4.1.3 Conversion between Dynamic Modulus and Relaxation Modulus 47

4.1.4 Master Curve of Relaxation Modulus 50
4.1.5 Time Dependency and Prony Series 53
4.1.6 Temperature Dependency and WLF Equation 58
4.2 Resilient Modulus Testing and Results 63
4.2.1 HMA mixtures 63
4.2.2 Subgrade Soils 67
4.2.3 Aggregates 73
4.3 Summary 74
5 FE MODELING OF U.S. 30 PERPETUAL PAVEMENT 75
5.1 U.S. 30 Perpetual Pavement Project 75
5.1.1 Project Overview 75
5.1.2 Brief Introduction to Perpetual Pavement 77
5.1.3 Instrumentation Plan 78
5.1.4 Moisture Content 81
5.1.5 Temperature 83
5.1.6 Controlled Load Vehicle Testing 83
5.2 Viscoelastic FE Model Formulation 86
5.2.1 Model Idealization 86
5.2.2 Traffic Loading Simulation 90
5.3 Calibration of Viscoelastic FE Model 92
5.4 Predictability of Calibrated Viscoelastic FE Model 101
5.5 Comparative Study between Linear Elastic FE and Viscoelastic FE Models 104

6 PARAMETRIC STUDY OF VISCOELASTIC FE MODEL 110
6.1 The Effect of Layer Thickness 110
6.2 The Effect of Layer Modulus 117
6.3 The Effect of Pavement Temperature 119
6.4 The Effect of Load Level 123
6.5 The Effect of Traffic Speed 124
6.6 Summary 126
7 USING FWD TESTS TO PREDICT PAVEMENT RESPONSE 128
7.1 Overview 128
7.2 FWD FE Model 129
7.3 Factors Considered 130
7.4 Results 132
7.5 Summary 136
8 CONCLUSIONS AND RECOMMENDATIONS 137
9 LIST OF REFERENCES 141

LIST OF TABLES

Table 4.1 Dynamic Moduli and Phase Angles for SMA Mix 46

Table 4.2 Dynamic Moduli and Phase Angles for ODOT442 Mix 46

Table 4.3 Dynamic Moduli and Phase Angles for ODOT302 Mix 46

Table 4.4 Dynamic Moduli and Phase Angles for FRL Mix 47

Table 4.5 Relaxation Moduli of SMA Mix 49

Table 4.6 Relaxation Moduli of ODOT442 Mix 49

Table 4.7 Relaxation Moduli of ODOT302 Mix 49

Table 4.8 Relaxation Moduli of FRL Mix 50

Table 4.9 Constants of Prony Series 55

Table 4.10 WLF Equation Constants 61

Table 4.11 Measured and Calculated Shift Factors 61

Table 4.12 Atterberg Limits and Soil Classification 69

Table 4.13 Load Sequences Applied during Resilient Modulus Tests 70

Table 5.1 Perpetual Pavement Build-Up 77

Table 5.2 Load Response and Seasonal Instrumentation Details 81

Table 5.3 Results of Sensitive Analysis to Mesh Size 89

Table 5.4 Comparison of Loading Cases 1 and 2 90

Table 5.5 Effect of Non-linearity of Subgrade soils 100

Table 5.6 Comparison of the Calibrated and Measured Moduli 100

Table 6.1 Analysis Cases Used in Thickness Study 111

Table 6.2 Comparison of Thickness Design 116

Table 6.3 Variations of Layer Modulus 118

Table 6.4 Effect of Layer Modulus on Maximum Tensile Strain 118

Table 6.5 Selected Pavement Temperature Profiles 120

Table 7.1 ANOVA Results 133

Table 7.2 Average AC Temperature vs. Air Temperature Coefficients (after Figueroa) 135

LIST OF FIGURES

Figure 2.1 Critical analysis locations in a pavement structure 21

Figure 2.2 Elastic layered theory and its inputs 23

Figure 3.1 Stress-strain behavior between elastic (left) and viscoelastic materials (right) 29

Figure 3.2 Stress-strain behavior under linear viscoelastic cyclic loading against strain (left) and pseudo strain (right) (after Daniel, 2001) 31

Figure 3.3 The Maxwell model (left) and the Kelvin model (right) 33

Figure 3.4 The Generalized Maxwell model 34

Figure 4.1 Typical dynamic modulus test curves (no tension force applied) 39

Figure 4.2 Complex representation of a complex modulus 40

Figure 4.3 Aggregate gradations of four asphalt mixtures 42

Figure 4.4 Schematic of dynamic modulus test 44

Figure 4.5 Relaxation modulus and master curve for SMA mix (log-log scale) 51

Figure 4.6 Relaxation modulus and master curve for ODOT442 mix (log-log scale) 52

Figure 4.7 Relaxation modulus and master curve for ODOT302 mix (log-log scale) 52

Figure 4.8 Relaxation modulus and master curve for FRL mix (log-log scale) 53

Figure 4.9 Comparison of the measured and calculated for FRL mix 56

Figure 4.10 Comparison of the measured and calculated $g(t)$ for SMA mix 57

Figure 4.11 Comparison of the measured and calculated $g(t)$ for ODOT442 mix 57

Figure 4.12 Comparison of the measured and calculated $g(t)$ for ODOT302 mix 58

Figure 4.13 Sigmoidal approximation of relaxation modulus (log-log scale) 60

Figure 4.14 Comparison of temperature dependency of asphalt mixtures 62

Figure 4.15 Typical deformation and load curves from resilient modulus tests (after LTPP P07, 2001) 65

Figure 4.16 Instantaneous and total resilient deformations (after LTPP P07, 2001) 66

Figure 4.17 Resilient modulus test results 68

Figure 4.18 Typical result of resilient modulus test 71

Figure 4.19 Resilient moduli of subgrade soils at different moisture contents 72

Figure 4.20 Variation of resilient modulus with moisture content 73

Figure 5.1 U.S 30 project map (courtesy of ODOT) 76

Figure 5.2 Instrumentation plan of test section 664 (courtesy of Khoury) 80

Figure 5.3 The variation of moisture content of the subgrade for section 664 82

Figure 5.4 Hourly variations of pavement temperature 84

Figure 5.5 Single axle configuration used for CLV tests (not to scale) 85

Figure 5.6 Typical strain response at the bottom of the FRL layer 86

Figure 5.7 Developed 3-D FEM model and refined mesh for the loading area 87

Figure 5.8 Three mesh schemes: (left) coarse mesh; (center) medium mesh; (right) fine mesh 89

Figure 5.9 Sketch of moving traffic loading and representation of load waveform 92

Figure 5.10 Partitioned pavement surface for applying moving traffic loads 92

Figure 5.11 Comparison of the measured and the calculated longitudinal tensile strains 95

Figure 5.12 Comparison of the measured and the calculated transverse tensile strains ... 96

Figure 5.13 Comparison of the measured and the calculated vertical stresses 97

Figure 5.14 Comparison of the measured and the calculated deflections 98

Figure 5.15 Comparison between the measured and the calculated maximum tensile strains 102

Figure 5.16 Comparison between the measured and calculated maximum vertical stresses 102

Figure 5.17 Comparison between the measured and the calculated maximum deflections 103

Figure 5.18 Temperature dependency curves used in linear elastic FE model after calibration 105

Figure 5.19 Comparison between the measured and the calculated maximum tensile strains 107

Figure 5.20 Comparison between the measured and the calculated maximum vertical stresses 107

Figure 5.21 Comparison between the measured and the calculated maximum deflections 108

Figure 6.1 The effect of thickness variation on maximum tensile strain 112

Figure 6.2 Results of PerRoad analysis 114

Figure 6.3 Variation of maximum tensile strain with pavement temperature and layer thickness 121

Figure 6.4 Effect of load level on maximum tensile strain 124

Figure 6.5 Effect of vehicle speed on maximum tensile strain 125

Figure 7.1 FWD loading and magnitude curve 130

Figure 7.2 FWD deflection vs. load 135

1 INTRODUCTION

1.1 Research Objectives and Approach

Traditionally, hot-mix-asphalt (HMA) materials in mechanistic analyses for flexible asphalt pavements have been treated as pure elastic solids, though they behave like viscoelastic materials in nature. The application of the theory of linear viscoelasticity to design and analysis of flexible asphalt pavements has not been dominant to date, though it is conceptually old in origin.

Unlike elastic solids, the behavior of HMA materials is strongly contingent on temperature and loading frequency. They behave more like elastic solids at low temperature and high loading frequency whereas at high temperature and low loading frequency their behavior is more like that of a viscous fluid. At medium temperatures and loading frequencies they behave like viscoelastic materials that normally exhibit a significant level of elastic solid stiffness while dissipate energy by frictional resistance as viscous fluids.

The principal goal of the research presented herein consisted of incorporating laboratory-determined viscoelastic material properties into a three-dimensional finite element (FE) model to accurately simulate the behavior of a pavement structure to traffic loading at different temperatures and vehicular speeds. This FE model was applied to the U.S. 30 perpetual pavement constructed in Wayne County, Ohio, and to develop design nomographs for practical use. Importantly, results of this research significantly improve the accuracy of current design and analysis methods which are widely used in predicting

pavement responses and to provide practical guidelines for perpetual pavement design and analysis. The specific objectives and approach of this research include:

- *Characterization of viscoelastic properties of HMA materials*. Implementing an advanced viscoelastic constitutive model is limited by the ability to obtain viscoelastic material properties and its accuracy. In this research, dynamic modulus test was chosen as a measure of the complex modulus of HMA materials. Using HMA mixtures provided by the Ohio Department of Transportation (ODOT), HMA specimens were compacted and tested following procedures described in Appendix A in NCHRP Report 465 (2002).
- *Development of a three-dimensional viscoelastic FE model*. Although the theory of linear viscoelasticity is old in origin, its application to design and analysis of flexible asphalt pavements has not been prevalent to date. In this research, the generalized Maxwell model was selected to represent the behavior of HMA materials which are mechanically approximated by a 5-term Prony series. The model was constructed using ABAQUS Version 6.6-3 (User's Manual, 2006), which is extensively used in the FE modeling for pavement design and analysis. The developed viscoelastic FE model improves the accuracy of current design and analysis methods in predicting the behavior of flexible asphalt pavements under different temperatures and traffic speeds.
- *Calibration of the developed viscoelastic FE model*. It has been a conventional way to calibrate the developed FE model to either strains and

stresses, or pavement deflections. No model has been calibrated to strains, stresses, and deflections simultaneously. In this study, the developed viscoelastic FE model was calibrated to all three variables at the same time to assure the model simulate well not only the strain and stress but also the deflection.

- *Parametric studies of the FE model.* The effects of layer thickness, layer modulus, axle load, traffic speed, and pavement temperature were parametrically studied. A comparative study of the thickness design between PerRoad and the developed viscoelastic FE model was conducted as well. A regression model relating the maximum tensile strain to the pavement temperature at different thicknesses of the ODOT302 and base layers was also established.
- *Development of statistical models to predict pavement response from Falling Weight Deflectometer (FWD) tests.* Upon the completion of the pavement, the FWD is normally used to assess the quality of the pavement structure or detect weak areas within the pavement structure. To this end, statistical models were developed relating FWD deflection to pavement response (the maximum tensile strain at the bottom of the fatigue resistance layer and the maximum vertical compressive strain on top of the subgrade) under selected pavement conditions.

1.2 Outline of the Research Presented

In Chapter 2, the evolution of mechanistic analysis for flexible asphalt pavements is briefly reviewed, which is divided into three stages. Chapter 3 presents the background of the theory of linear viscoelasticity and thus its mechanical representation.

Chapter 4 is dedicated to the mechanistic characterization of HMA materials and unbound granular materials. The dynamic modulus test is used to determine the complex modulus of HMA materials. Resilient moduli of HMA material and unbound granular materials are tested following procedures generally accepted for the resilient modulus testing of pavement.

In Chapter 5, the U.S. 30 perpetual pavement project is first introduced, along with its instrumentation plan, controlled load vehicle tests and the background on perpetual pavement design. Next, a viscoelastic FE model is built in ABAQUS. The developed FE model is validated by and calibrated to field-measured pavement response. Finally, a comparative study between the linear elastic FE model and the viscoelastic FE model is conducted to compare their relative abilities to predict pavement response.

Chapter 6 focuses on parametric studies of the developed viscoelastic FE model. The effects of layer thickness, layer modulus, axle load, vehicular speed, and pavement temperature are discussed. This chapter also explores the difference in thickness design between the PerRoad and the viscoelastic FE model developed in this research.

In Chapter 7, a FWD FE model is developed to predict pavement response. Statistical models are developed to predict pavement response from FWD deflections

under selected pavement conditions. These models are important in practice to assess pavement quality using the FWD upon the completion of pavement construction.

Finally a summary of findings and recommendations for future study are given in Chapter 8.

2 LITERATURE REVIEW

Asphalt pavement design has evolved through three stages since the construction of the first asphalt roadway laid by Professor E.J. DeSmedt in 1870 in Newark, New Jersey (Abraham, 1929):

1. Empirical design. Prior to the early 1920s, pavement thickness was determined completely from hands-on experience (Huang, 2004). No sound concepts of mechanics of materials were applied to designs.
2. Elastic mechanistic-empirical (M-E) design. This stage ended in the early 1990s. The most important achievement during this stage was that the design and analysis of pavement structure was based on the mechanics of materials, although assumptions needed to be made.
3. Viscoelastic M-E design. To date, this stage is characterized by the consideration of advanced material constitutive models and advanced material characterization methods. Application of the viscoelastic theory is one of most important accomplishments.

In the following sections of this chapter, literature reviews were only undertaken for the second and third stages. It is as well noted that the review is focused on mechanical analyses for pavement designs.

In the mechanical analysis, there are several critical locations worthy of attention as shown in Figure 2.1. Pavement response at each of these critical locations control

specific distress. For example, the horizontal tensile strain at the bottom of the HMA layer(s) is used to predict the fatigue life of the pavement structure while the vertical compressive strain at top of subgrade is used to estimate rutting of the pavement as a result of the permanent deformation of the subgrade.

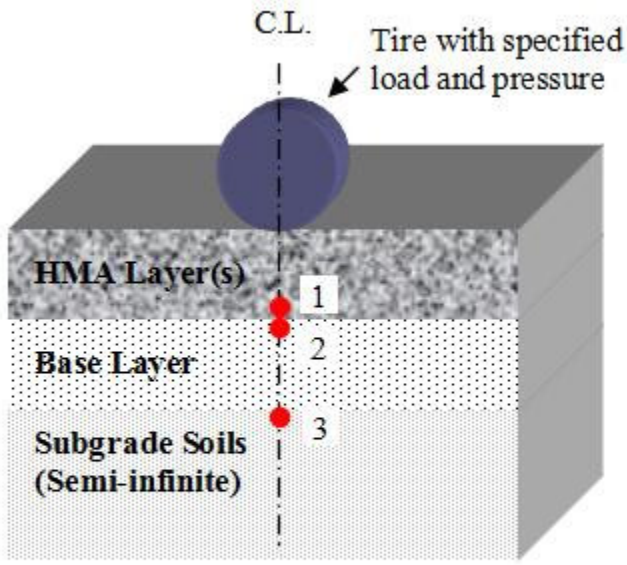

1. Horizontal tensile strain at the bottom of HMA layer(s)
2. Vertical compressive strain at top of base
3. Vertical compressive strain at top of subgrade

Figure 2.1 Critical analysis locations in a pavement structure

2.1 Elastic M-E Design

Some early theories made it possible for a pavement structure to be analyzed mechanistically. Barber (1946) utilized Terzaghi's ultimate bearing capacity theory to estimate the pavement thickness needed to limit the shear failure of the pavement. Boussinesq's equation was modified by the Kansas State Highway Commission (1947) to calculate subgrade deflection and limit it to $2.54\,mm$ $(0.1\,in.)$.

Burmister's elastic layered theory was the first analysis theory extensively accepted (Burmister, 1943, 1945) (Figure 2.2). This theory assumes that the HMA and unbound materials are homogeneous and isotropic linearly elastic solids. Material properties required for each layer include the modulus of elasticity and Poisson's ratio. The material is assumed to be weightless and infinite in areal extent, while a uniformly distributed static circular vehicular loading is assumed.

Layered elastic solutions were first developed by Burmister (1943) for a two-layer pavement system and these were later extended to a three-layer pavement system (Burmister, 1945). Subsequently, with the help of computers, various computer programs were developed, based on this theory or its modification, to apply to a multi-layer pavement system.

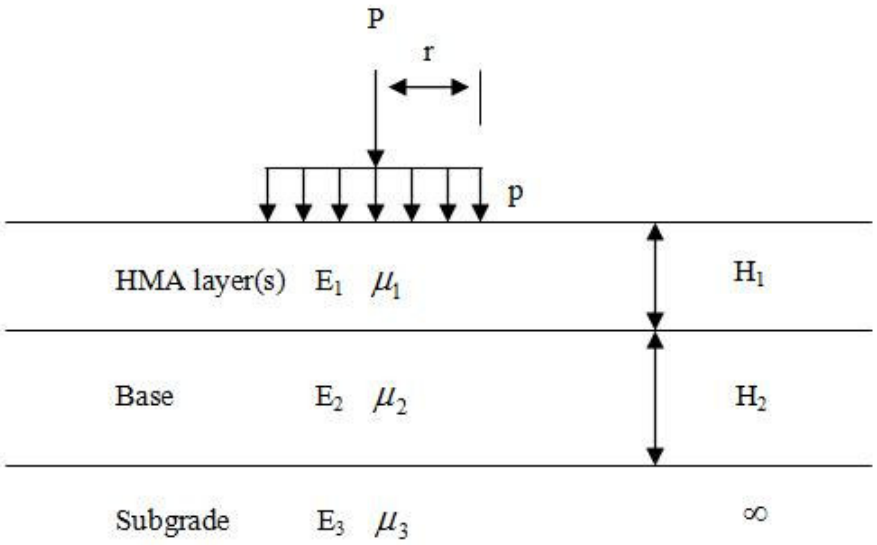

Figure 2.2 Elastic layered theory and its inputs

The CHEV program was the earliest one developed by the Chevron Research Company (Warren and Dieckmann, 1963). Later on, the elastic layered theory was modified by the Asphalt Institute (Hwang and Witczak, 1979) to include the non-linear elasticity of granular materials and used to develop the DAMA program. A well-publicized program, BISAR, was developed by the Shell (De Jong et al., 1973) to consider not only the vertical loading but also horizontal loading. In order to analyze multiple wheel loads, Kopperman et al. (1986) developed the program ELSYM5 for elastic five-layer pavement systems.

With the application of finite elements method to pavement analysis first by Duncan et al. (1968), two earliest and best known programs, ILLI-PAVE (Raad and Figueroa, 1980) and MICH-PAVE (Harichandran et al., 1989), were developed. In

comparison with non finite element programs, the latter could handle non-linearity better for stress-dependent materials, such as aggregates and soils.

The inherent disadvantages of the elastic (multi-) layered theory are that (1) the consideration of HMA materials as pure elastic solids is a significant simplification; and (2) the treatment of vehicular loading as static is a major deficiency.

2.2 Viscoelastic M-E Design

It is in general recognized that the mechanistic analysis of pavements depends on two major factors (Sousa et al., 1991): the material characterization method and its accuracy, and the accuracy of mechanistic models to simulate pavement response. The most important accomplishment in this stage is the application of viscoelasticity theory to HMA materials, which in nature behave viscoelastically but not purely elastically as assumed in the second stage.

Though the concept of viscoelasticity is old in origin, its application to pavement design and analysis has not been dominant to date. The earliest application may be dated back to the early 1960s. Sector and Monismith (1961) applied viscoelastic theory to predict the behavior of asphalt concrete specimens used in triaxial compression tests.

In recent years, researchers have successfully applied linear viscoelastic theory to describe the behavior of HMA materials. Elseifi et al. (2006 a) conducted a comparative study between the elastic FE model and the linear viscoelastic FE model and concluded that it is imperative to incorporate a viscoelastic constitutive model into pavement design methods for improved accuracy. The elastic theory grossly underestimated pavement

responses, which is not conservative and may lead to the premature failure of flexible asphalt pavements. In later research by Elseifi et al. (2006 b), a viscoelastic constitutive model was applied to predict the behavior of bituminous sealants at low temperatures. They found that measured and calculated deflections matched very well at low service temperatures of -28$^{\circ}C$ (-33.3$^{\circ}F$) to -40$^{\circ}C$ (-40$^{\circ}F$). To evaluate the pavement damage caused by dual and wide-base tires, Elseifi et al. (2005) applied the generalized Kelvin model into an FE program to simulate pavement responses. In these three papers, they all concluded that it is imperative in the mechanical analysis to include the viscoelastic properties of HMA materials.

More recently, the theory of viscoelastoplasticity has also been extensively used to analyze HMA materials. Chehab (2002) developed an advanced material characterization procedure including the theoretical models and its supporting experimental testing protocols necessary for predicting the response of asphaltic mixtures subjected to tension loading. The model encompasses the elastic, viscoelastic, plastic and viscoplastic components of asphalt concrete behavior. In contrast, Zhao (2002) developed similar procedures for predicting the response of asphaltic mixtures subjected to compression loading. Wen (2001) applied a viscoelastic model to characterize asphalt concrete in indirect tensile testing. To study the failure mechanism of fatigue cracking in asphalt pavements, Mun (2003) utilized a viscoelastic continuum damage model to investigate the initiation and growth of bottom-up and top-down fatigue cracks. Lee (2003) included viscoelastic material properties in a continuum damage model to predict the fatigue life of asphaltic mixtures and presented a more simplified fatigue model.

Weissman et al. (1998) incorporated viscoelastic parameters in the FE method to help define appropriate specimen size and shape for laboratory tests, to check stress and strain distribution in laboratory test specimens, and to predict stresses and strains in a pavement structure loaded by the Heavy Vehicle Simulator.

To study the effect of vehicle-pavement interaction on pavement response, Mikhail and Mamlouk (1997) incorporated viscoelastic material parameters into an FE model to simulate pavement responses. A G-ratio was used to represent the time-dependent property of HMA materials.

Pirabarooban et al. (2003) successfully developed a visco-elasto-plastic creep model representing the time-dependency of asphalt mixtures to evaluate their rutting potential and to identify factors having a significant effect. The creep model parameters were derived from Asphalt Pavement Analyzer test results.

In comparison with the elastic M-E design, the most important characteristic of the viscoelastic M-E design is the recognition and application of viscoelastic behavior of HMA materials in mechanical analysis. The inclusion of a viscoelastic constitutive model into an FE program to simulate pavement response for pavement structures is getting more dominant, which will overcome inherent shortcomings of the elastic layered theory that was extensively used in the elastic M-E design stage.

It is also of interest that the plastic and viscoplastic behaviors have been incorporated into FE programs at the North Carolina State University in comparison with other studies where mainly focused on simulating linear viscoelastic behavior. One has

to acknowledge that this was a significant advancement representing the direction of future studies in this area.

For the time being, however, linear viscoelastic theory has its own advantages and is more promising to be accepted for both theoretical researches and routine designs and analyses for asphalt pavements: (1) current studies demonstrated that the behavior of asphalt materials can be successfully simulated using linear viscoelastic theory; (2) plastic behavior is not a significant part for asphalt materials under normal traffic loads and normal pavement temperatures; (3) the performance of the viscoelastoplastic model is more prone to be affected by material property parameters that have to be measured in the laboratory since it demands more advanced material properties; (4) the availability on FE software to implement the viscoelastoplastic model is challenging for most researchers and engineers currently. Considering these four facts aforementioned, linear elastic theory is the best choice currently for the fact that the linear viscoelastic theory provides not only sufficient accuracy to simulate the behavior of asphalt materials but also the simplicity for the purpose of researches and routine designs and analyses.

3 VISCOELASTIC MODELING OF HMA MATERIALS

It is commonly practiced that a flexible asphalt pavement consists of HMA layer(s), aggregate base layer, and infinite subgrade layer. Each layer structurally contributes its function to form the so-called pavement structure supporting vehicular loading. In the design and analysis of flexible asphalt pavements, one of the key components is to model the viscoelastic behavior of HMA materials. In this Chapter, the background of the theory of linear viscoelasticity and its mechanical model representation are introduced. The introduction to the modeling of unbound granular materials will be briefly presented in Chapter 4, along with their mechanical characterization.

3.1 Theory of Linear Viscoelasticity

Traditionally, HMA materials were treated as pure elastic solids, although they behave viscoelastically in nature. The application of viscoelastic theory to design and analysis of asphalt pavements has not been prevalent to date, although the concept is old in origin. Unlike elastic solids, the behavior of HMA materials depends strongly on temperature and loading frequency, the latter of which means that their response is a function of the current as well as past input. At low temperature and high loading frequency they behave more like elastic solids whereas at high temperature and low loading frequency their behavior is more like that of a viscous fluid. In between, they are

viscoelastic materials that exhibit a significant level of elastic solid stiffness while dissipate energy by frictional resistance as viscous fluids.

Figure 3.1 graphically illustrates the distinction between an elastic material and a viscoelastic material from the perspective of the stress-strain behavior during a loading and unloading cycle, where σ is the applied stress and ε is the resulted strain. The red hysteretic loop represents either time-dependent viscoelastic behavior (strain accumulation due to viscoelasticity only) or, if the damage occurred, the amount of energy loss due to frictional resistance, whereas there is no hysteretic loop (energy loss) when a load is applied to a pure elastic solid and then removed.

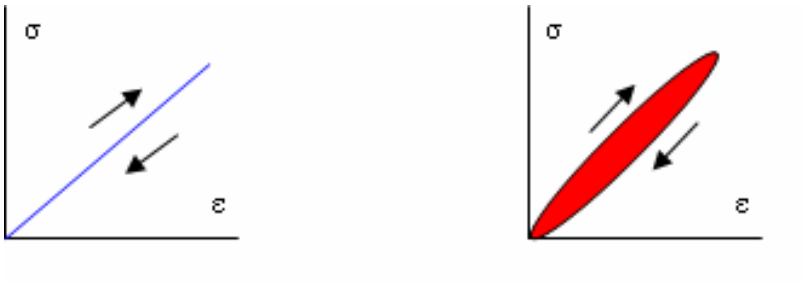

Figure 3.1 Stress-strain behavior between elastic (left) and viscoelastic materials (right)

To differentiate which causes a hysteric loop for viscoelastic materials, time-dependent viscoelasticity or accumulated damage, Shapery (1984) proposed the concept of pseudo strains defined as:

$$\varepsilon^R = \frac{1}{E_R}\int_0^t E(t-\tau)\frac{d\varepsilon}{d\tau}d\tau . \qquad (3 - 1)$$

Where, ε = uniaxial strain,

E_R = a reference modulus set as an arbitrary constant,

$E(t)$ = uniaxial relaxation modulus,

t = time,

τ = an integration constant.

In what follows, these variables will be remained the same unless otherwise noted. Figure 3.2 presents the stress-strain behavior of a linear viscoelastic material (no damage). Left plot in Figure 3.2 shows the conventional stress-strain behavior. The hysteric loop was caused by accumulated strain due to viscoelasticity (time-dependency) because there was no damage induced within linear viscoelasticity. Right plot illustrates the same stress plotted against the pseudo strain calculated using equation (3 – 1). As it can be seen, all hysteric loops disappear and these curves are similar to linear elastic behavior. In this research, because asphaltic materials are assumed to be linear viscoelastic and no damage is allowed, all strains are expressed as conventional ones.

According to Park and Schapery (1999), "The uniaxial, nonaging, isothermal stress-strain equation for a linear viscoelastic material can be represented by a Boltzmann superposition integral":

$$\sigma(t) = \int_0^t E\left(t-\tau\right)\frac{d\varepsilon(\tau)}{d\tau}d\tau . \qquad (3 - 2)$$

Or rewritten as,

$$\varepsilon(t) = \int_0^t D(t-\tau)\frac{d\sigma(\tau)}{d\tau}d\tau . \qquad (3 - 3)$$

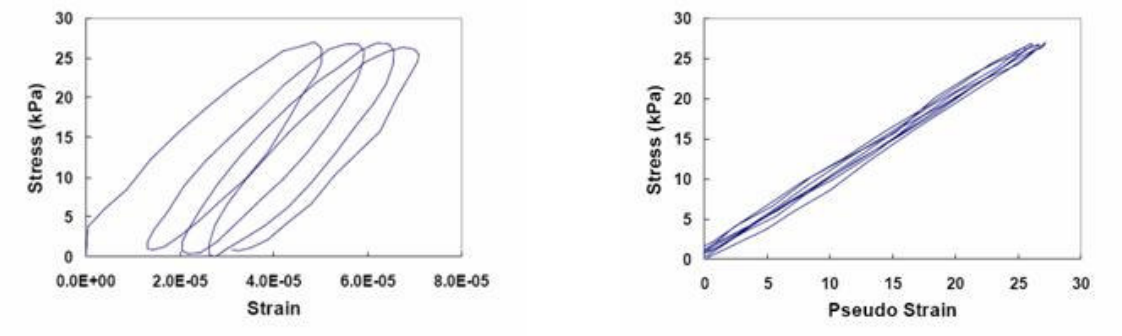

Figure 3.2 Stress-strain behavior under linear viscoelastic cyclic loading against strain (left) and pseudo strain (right) (after Daniel, 2001)

Where, $E(t)$ is the relaxation modulus and $D(t)$ is the creep compliance; the relationship between which is (Ferry, 1980):

$$\int_0^t E(t-\tau)D(\tau)d\tau = t \qquad \text{for t} > 0. \qquad (3 - 4)$$

The relaxation modulus $E(t)$ is independent of the strain level, while the creep compliance $D(t)$ is free of stress level and they are functions of time alone within linear viscoelasticity.

A linear viscoelastic material is assumed to be a thermorheologically-simple material, meaning that the time-temperature superposition principle can be applied.

Thus, the behavior at low temperature is identical to that at high loading frequency, and that at high temperature is identical to that at low loading frequency.

The implication of time-temperature superposition principle to laboratory testing is that the long-time behavior of viscoelastic materials can be predicted by the behavior at elevated temperature without having to test the materials actually over a long time. Vice versa, the short-time behavior can be simulated by that at low temperature. Thus, laboratory tests are only conducted at relatively narrow bands of temperatures and loading frequencies to sufficiently define a material function without having to define it over the complete range of its domain. As such, the range of a material function is expanded by combining the responses at different temperatures and loading frequencies.

3.2 Mechanical Model Representing Linear Viscoelastic Behavior

In order to predict the behavior of HMA materials, it is necessary to model their stress-strain relationship. The stress-strain behavior of linear viscoelastic materials can be simulated by the behavior of a mechanical model consisting of elastic (spring) elements and viscous (dashpot) elements. Various models constructed of these two basic elements are employed to describe the viscoelastic response of asphalt materials to vehicular loading for mechanistic analysis of asphalt pavements.

The simplest mechanical model imitating linear viscoelastic behavior is one spring combined with one dashpot, either in series (the Maxwell model Figure 3.3 (left) or in parallel (the Voigt model or Kelvin model (Figure 3.3 (right)). A relaxation

modulus E is assigned to the spring element while a friction resistance η is assigned to the viscous dashpot. These two models are generally too over simplified to describe real linear viscoelastic behavior (Ferry, 1980). The Maxwell model cannot simulate creep behavior well, and the Voigt model does not account for relaxation behavior. More useful mechanical models are built of these two models.

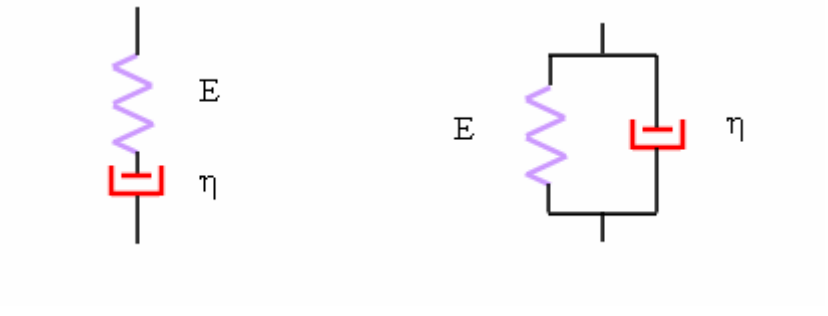

Figure 3.3 The Maxwell model (left) and the Kelvin model (right)

Generally, there are two more complicated mechanical models that have been very successful in simulating the behavior of asphalt materials: the Generalized Maxwell Model and the Generalized Kelvin model. In this study, the Generalized Maxwell model is selected to describe the behavior of HMA materials subjected to dynamic moving traffic loads. Compared to the Generalized Kelvin model describing the creep behavior well, the Generalized Maxwell model more properly simulates the relaxation behavior of HMA materials under traffic loading.

The Generalized Maxwell model, also called the Wiechert model, is composed of a spring and m Maxwell elements connected in parallel as shown in Figure 3.4. In this model, each spring element is assigned a relaxation modulus E_m, and each dashpot is assigned a frictional resistance η_m. When the model is subjected to a constant strain, the force on each spring-dashpot pair relaxes exponentially. Since the stresses are additive in the generalized Maxwell model, the relaxation modulus $E_m(t)$ for pair m is given by

$$E_m(t) = E_m e^{-tE_m/\eta_m} = E_m e^{-t/\tau_m} . \qquad (3-5)$$

In which the time constant τ_m, the relaxation time, is defined as η_m / E_m. Then

$$E(t) = \sum_{i=1}^{m} E_i e^{-t/\tau_i} . \qquad (3-6)$$

To consider the relaxation modulus at equilibrium deformation, when time approaches infinity, a single spring is added to Maxwell pairs in parallel. Finally, the relaxation modulus describing the Generalized Maxwell model in Figure 3.4 is given as follows:

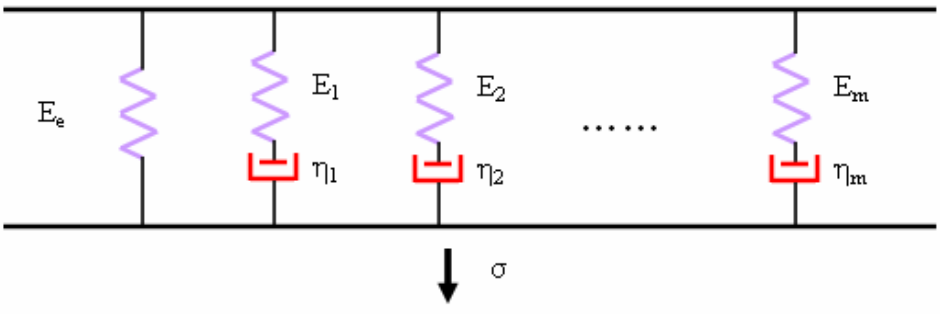

Figure 3.4 The Generalized Maxwell model

$$E(t) = E_e + \sum_{i=1}^{m} E_i e^{-(t/\tau_i)} . \qquad (3-7)$$

Where, E_e (equilibrium modulus), E_i (relaxation strength), and τ_i (relaxation time) are all positive constants. As seen in equation (3 – 7), the relaxation modulus approaches the equilibrium modulus when the time is infinite. Equation (3 – 7) is also known as a Prony or a Dirichlet series expansion.

Mathematically, equation (3 – 7) may be rewritten as

$$E(t) = E_0 - \sum_{i=1}^{m} E_i (1 - e^{-(t/\tau_i)}) . \qquad (3-8)$$

Where, E_0 is initial (instantaneous) modulus, while the relationship between E_e and E_0 is

$$E_e = E_0 - \sum_{i=1}^{m} E_i . \qquad (3-9)$$

3.3 Summary

The background of the theory of linear viscoelasticity is presented in this chapter. Two basic viscoelastic models are reviewed. The Generalized Maxwell model is the most general form of the linear viscoelasticity for simulating the linear viscoelastic behavior of asphaltic materials compared with basic models each consisting of one spring and one dashpot only. Also, the Generalized Maxwell model more properly simulates the relaxation behavior of HMA materials under dynamic moving traffic loads. A Prony

series is further introduced to express the stress-strain relationship, which is used in finite element modeling in this research.

4 MATERIAL CHARACTERIZATION

It is in general recognized that the mechanistic analysis of a pavement depends on two major factors (Sousa et al., 1991): the material characterization method and its accuracy, and the accuracy of mechanistic models to simulate pavement responses. It is required by the new AASHTO 2002 Pavement Design Guide (on level 1) that pavement materials be characterized mechanistically such that the pavement response (stress, strain, and deflection) due to traffic loading and environmental factors can be analyzed based on sound mechanical theories.

The U.S. 30 perpetual pavement consists of six layers of paving materials which are from top to bottom: (1) Stone Mastic Asphalt (SMA); (2) Superpave Asphalt Concrete (ODOT442); (3) Intermediate Asphalt Concrete (ODOT302); (4) Fatigue Resistant Layer (FRL); (5) Aggregate Base (ODOT304); (6) the Subgrade. More details about the U.S. 30 perpetual pavement and its paving materials will be later introduced in Chapter 5.

Because the viscoelastic properties of HMA materials are key to the viscoelastic FE model used in this research, the characterization of viscoelastic properties of HMA materials are introduced in more detail prior to the discussion of resilient modulus testing of HMA and unbound granular materials.

4.1 Dynamic Modulus Testing and Results

Typically, two types of testing methods are used to characterize the viscoelastic properties of HMA materials: dynamic modulus testing and static creep testing. In this research, dynamic modulus testing was chosen as the measure of the complex modulus of HMA materials. Viscoelastic material parameters were calculated from complex modulus to incorporate into the FE model. Prior to presenting the dynamic modulus testing, the background on the complex modulus, dynamics modulus, and phase angle is introduced in the following section.

4.1.1 Complex Modulus, Dynamic Modulus, and Phase Angle

Simply stated, the complex modulus, E^*, is the modulus of a viscoelastic material subjected to sinusoidal loading. The complex modulus relates stresses to strains in the frequency domain for a linear viscoelastic material under continuously applied sinusoidal loading (compression only). Mathematically, the complex modulus is defined as the ratio of the amplitude of the sinusoidal stress at any given time and frequency to the sinusoidal strain at the same time and frequency.

The dynamic modulus is defined as the absolute value of the complex modulus, which is represented by the ratio of peak stress to peak strain. Due to the nature of viscoelasticity, there is a time lag between the sinusoidal stress and sinusoidal strain, which is called the phase angle.

Summarily, the complex modulus, dynamic modulus, and phase angle can be graphically depicted as shown in Figure 4.1.

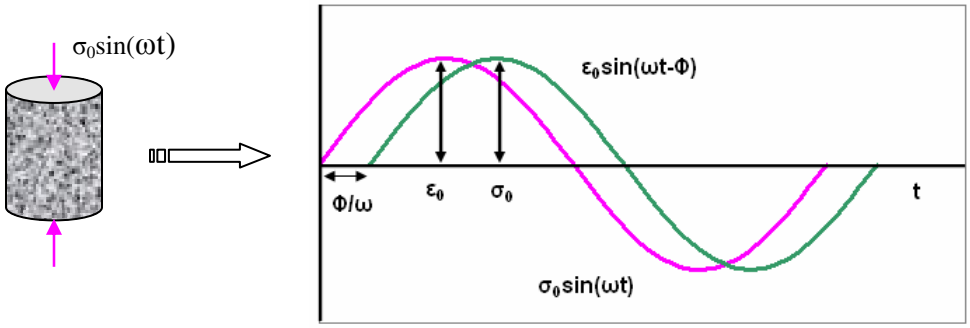

Figure 4.1 Typical dynamic modulus test curves (no tension force applied)

As shown in Figure 4.1, a sinusoidal stress $\sigma(t) = \sigma_0 \sin(\omega t)$ is applied to the asphalt mix specimen (without tension applied actually, although a full curve including compression and tension is shown), the resulting strain is given as $\varepsilon(t) = \varepsilon_0 \sin(\omega t - \varphi)$, which is also sinusoidal with a time lag of φ / ω. According to the definitions of the complex modulus and dynamic modulus, they can be expressed as:

$$\text{Complex modulus: } E^* = \frac{\sigma_0 e^{i\omega t}}{\varepsilon_0 e^{i(\omega t - \varphi)}} \qquad (4-1)$$

Where, E^* = relaxation modulus,

σ_0 = peak stress,

ε_0 = peak strain,

ω = angular velocity,

φ = phase angle,

t = time,

i = unit complex number, $\sqrt{-1}$.

Dynamic Modulus: $|E^*| = \frac{\sigma_0}{\varepsilon_0}$. (4 – 2)

As a result of the time lag between stress and strain, the complex modulus can be treated as a complex number:

$E^* = E' + iE''$. (4 – 3)

Where, E' is the storage modulus or elastic component, and E'' is the loss modulus or viscous component. The relationship among E^*, E', and E'' may also be graphically represented by Figure 4.2.

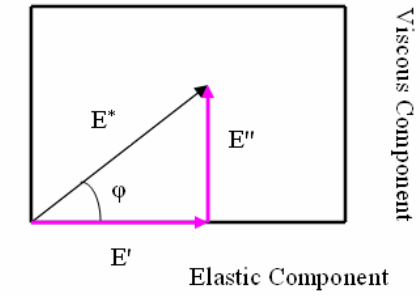

Figure 4.2 Complex representation of a complex modulus

As can be seen, for a pure elastic material, $\varphi = 0^\circ$, and $E^* = E'$; for a pure viscous material, $\varphi = 90^\circ$, and $E^* = E''$. Between two limits, the larger the phase

angle, the more viscous the material. It is noted that this complex representation will be used in converting dynamic modulus data to relaxation modulus data.

4.1.2 Experiments and Results

Asphalt Mixtures

Four different types of asphalt mixtures were designed to resist specific distresses for the U.S. 30 perpetual pavement. The surface layer is 12.5 *mm* (0.5 *in.*) thick and is composed of Stone Mastic Asphalt with PG 76-22M binder. Second layer is 19 *mm* thick and consists of type A Superpave asphalt concrete with PG 76-22M binder. For better rutting performance, polymer modified high grade binder was selected for both of the two top layers. It was demonstrated that the use of PG 76-22M binder improved rutting resistance dramatically (Liao et al., 2005) compared with the normal use of PG 64-22 binder.

The asphalt base layer consists of a large stone base mix with PG 64-22 binder. And it is intended to provide high stiffness for the pavement structure. As for the fatigue resistance layer, it is a special large stone base mix with a rich binder content of 4.6 percent to improve the fatigue resistance.

The chart shown in Figure 4.3 summarizes the gradation distributions of these four mixes. The ODOT302 mix is the coarsest among these mixes, and the ODOT442 is the finest. The SMA mix mainly consists of coarse aggregates to form a stone-on-stone contact skeleton structure primarily for better rutting performance.

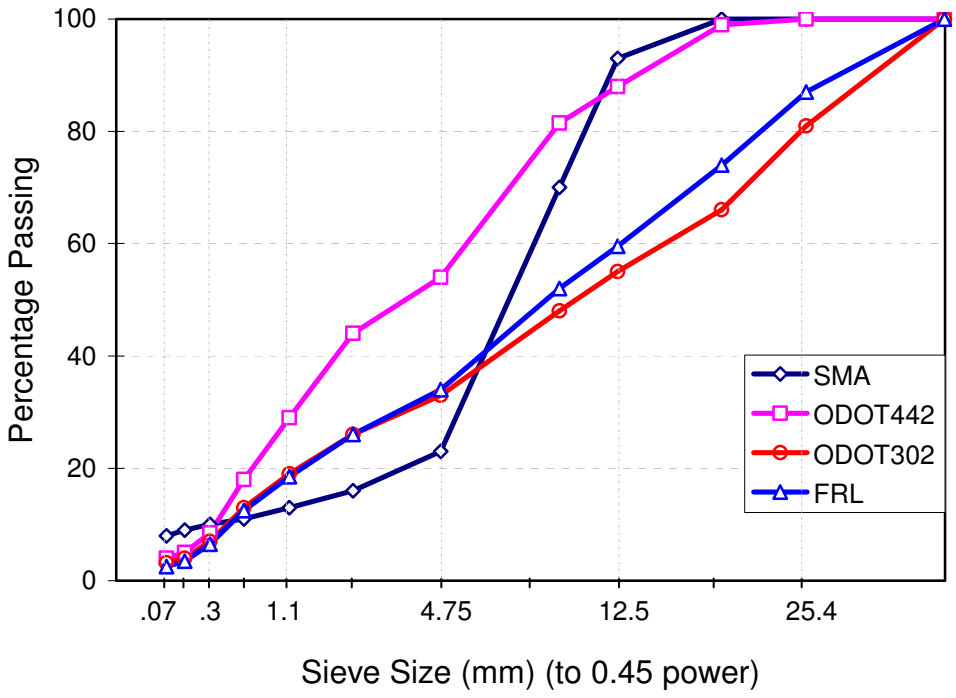

Figure 4.3 Aggregate gradations of four asphalt mixtures

Asphalt Mixture Specimens

Following the procedures in the *Test Method for Dynamic Modulus of Asphalt Concrete Mixtures for Permanent Deformation* contained in NCHRP Report 465 (NCHRP, 2002), four specimens for each mix type with dimensions of 100 *mm* (4 *in.*) diameter by 150 *mm* (6 *in.*) high were cored and cut out from Superpave Gyratory compacted specimens in the laboratory. The ends of all specimens were cut perpendicular to their axis and were made as smooth as possible and with as little disturbance as possible. The measured air void content on average was 7.5 percent for the SMA mix, 9.5 percent for the ODOT442 mix, 7.8 percent for the ODOT302 mix, and

7.3 percent for the FRL mix. The air void content of each specimen was as close to the as-constructed air void content for the mixes used in the in U.S 30 project as possible.

Test Configuration

As shown in Figure 4.4, a materials testing machine was used to continuously apply a sinusoidal force on the test specimens. The sinusoidal force can be applied over a range of frequencies from 0.5 Hz to 25 Hz. An environmental chamber (which is not depicted in Figure 4.4) was required to control the test specimen at the desired test temperature with an accuracy of $\pm 0.2\ ^{\circ}C$ ($\pm 0.1\ ^{\circ}F$) over a range of the test temperatures from -10 $^{\circ}C$ (14 $^{\circ}F$) to 54.4 $^{\circ}C$ (130 $^{\circ}F$). Two extensometers positioned 180 degrees apart were used to measure the resulting sinusoidal axial strain.

Prior to each test, the specimen was placed into the environmental chamber to allow it to reach the desired test temperature, as prescribed by the test specifications. A contact load equal to 5 percent of the dynamic load was applied to the specimen prior to the application of the dynamic load. A dynamic load was selected to generate an axial strain between 50 and 150 microstrains, and the specimen was first preconditioned with 200 cycles at 25 Hz. After the initial preconditioning, the selected dynamic load was applied to the specimen and the axial deformation measured by the extensometers was recorded at frequencies of 25, 10, 5, 1, 0.5, and 0.1 Hz. Each specimen was tested at temperatures of -10 $^{\circ}C$ (14 $^{\circ}F$), 4.4 $^{\circ}C$ (40 $^{\circ}F$), 21.1 $^{\circ}C$ (70 $^{\circ}F$), 37.8 $^{\circ}C$ (100 $^{\circ}F$), and 54.4 $^{\circ}C$ (130 $^{\circ}F$), respectively. If excessive permanent deformation greater than 1000

microstrains was observed, the specimen should be discarded and the maximum dynamic load should be reduced to half.

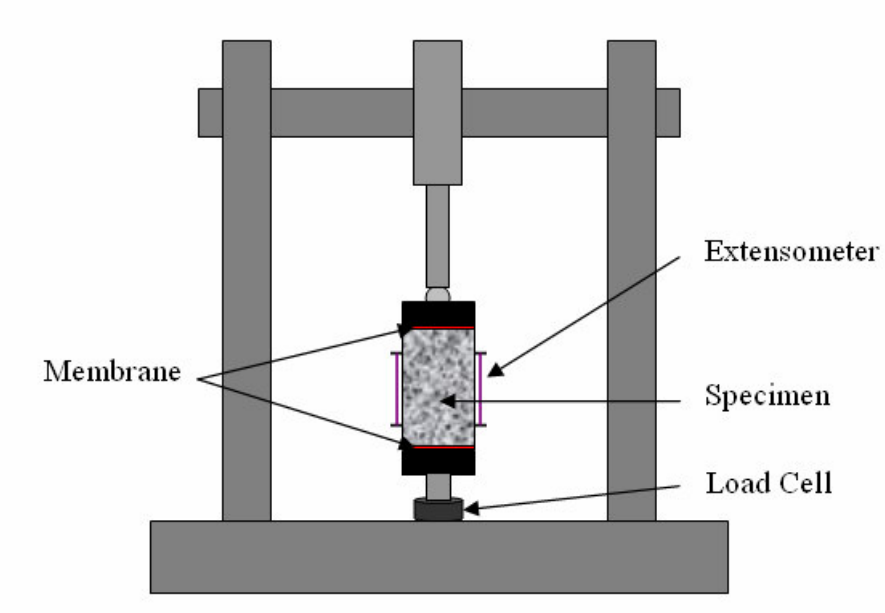

Figure 4.4 Schematic of dynamic modulus test

Test Results

To obtain the dynamic modulus and the phase angle, the following procedures were undertaken for each test (NCHRP, 2002):

- Collect and save data from the last 6 full cycles of loading and deformation data. Compute the average amplitude of the sinusoidal load and deformation from each extensometer over the first full 5 cycles.

- Determine the average time lag between the maximum load and the maximum deformation over the full 5 cycles.
- Calculate the loading stress, σ_0 as $\sigma_0 = \frac{\overline{P}}{A}$, where A is the area of the specimen, and $\overline{P}$ is the average load amplitude.
- Calculate the recoverable axial strain, ε_0 as $\varepsilon_0 = \frac{\overline{\Delta}}{GL}$, where $\overline{\Delta}$ the average deformation amplitude, and GL is the gauge length.
- Calculate the dynamic modulus, $|E^*|$ as $|E^*| = \frac{\sigma_\circ}{\varepsilon_\circ}$.
- Calculate the phase angle as $\varphi = \frac{t_i}{t_p} \times 360$, where t_i is the average time lag between a cycle of stress and strain, and t_p is the average time for a stress cycle.
- Repeat all of above steps for each frequency.
- Repeat all of above steps for each test temperature.

Results of dynamic modulus testing are presented in Tables 4.1 through 4.4 for the SMA, ODOT442, ODOT302, and FRL mixes, respectively.

Table 4.1 Dynamic Moduli and Phase Angles for SMA Mix

f (1/sec)	-10ºC		4.4ºC		21.1ºC		37.8ºC		54.4ºC	
	$\|E^*\|$, GPa	φ(º)	$\|E^*\|$, GPa	φ(º)	$\|E^*\|$, GPa	φ(º)	$\|E^*\|$, GPa	φ(º)	$\|E^*\|$, GPa	φ(º)
25	12.571	3.9	9.981	7.0	5.575	14.2	2.972	22.9	1.206	28.6
10	12.802	3.9	9.366	6.5	4.974	13.7	2.492	22.3	0.878	21.2
5	12.506	3.8	8.981	7.5	4.376	14.5	2.062	22.8	0.614	26.7
1	11.628	4.9	7.856	8.6	3.322	17.4	1.237	23.8	0.306	25.8
0.5	11.224	5.3	7.381	8.6	2.914	18.5	0.978	25.7	0.234	26.0
0.1	10.285	6.1	6.227	11.6	1.991	20.3	0.634	25.2	0.146	28.7

Table 4.2 Dynamic Moduli and Phase Angles for ODOT442 Mix

f (1/sec)	-10ºC		4.4ºC		21.1ºC		37.8ºC		54.4ºC	
	$\|E^*\|$, GPa	φ(º)	$\|E^*\|$, GPa	φ(º)	$\|E^*\|$, GPa	φ(º)	$\|E^*\|$, GPa	φ(º)	$\|E^*\|$, GPa	φ(º)
25	10.330	8	7.125	17.3	4.020	16.9	1.940	22	0.689	26.5
10	10.488	6.2	6.737	10.1	3.385	16.9	1.492	23.1	0.469	23.3
5	10.049	8.1	6.304	12.2	2.965	17.8	1.216	22	0.311	28.4
1	8.915	9.5	5.147	14.9	1.962	21.3	0.670	24.5	0.131	27.2
0.5	8.458	10.1	4.682	15.7	1.646	22.6	0.516	25.4	0.095	27.8
0.1	7.336	11.7	3.664	18.3	1.114	23.8	0.319	24.3	0.574	28.9

Table 4.3 Dynamic Moduli and Phase Angles for ODOT302 Mix

f (1/sec)	-10ºC		4.4ºC		21.1ºC		37.8ºC		54.4ºC	
	$\|E^*\|$, GPa	φ(º)	$\|E^*\|$, GPa	φ(º)	$\|E^*\|$, GPa	φ(º)	$\|E^*\|$, GPa	φ(º)	$\|E^*\|$, GPa	φ(º)
25	16.594	3.7	13.571	3.6	8.862	16.2	5.273	20.4	1.754	32.2
10	17.049	2.7	13.012	5.6	8.005	14.6	3.978	25.6	1.122	27.6
5	16.818	3	13.093	5.8	7.324	15.1	3.300	24.4	0.782	31.9
1	15.875	3.9	11.675	6.7	5.618	17.3	2.018	26.9	0.366	34.0
0.5	15.511	4.5	11.149	7.4	4.905	18.4	1.576	28.9	0.261	36.2
0.1	14.620	4.7	9.641	9.4	3.545	23.6	0.928	28.9	0.130	33.0

Table 4.4 Dynamic Moduli and Phase Angles for FRL Mix

f (1/sec)	-10ºC		4.4ºC		21.1ºC		37.8ºC		54.4ºC	
	$\|E^*\|$, GPa	φ(º)	$\|E^*\|$, GPa	φ(º)	$\|E^*\|$, GPa	φ(º)	$\|E^*\|$, GPa	φ(º)	$\|E^*\|$, GPa	φ(º)
25	19.110	4.9	9.981	6.6	11.317	10.5	5.609	24.6	2.047	35.3
10	19.699	2.3	9.366	4.8	10.111	9.4	4.441	24.5	1.242	26.8
5	19.404	3.1	8.981	5.7	9.272	13.1	3.708	24.5	0.834	34.0
1	18.513	3.5	7.856	6.7	7.298	15.7	2.221	27.9	0.339	39.7
0.5	18.095	3.7	7.381	6.6	6.462	17.9	1.705	30.1	0.215	40.4
0.1	16.835	3.9	6.227	9.0	4.665	22.6	0.935	30.6	0.092	37.5

As can be seen, there is a general trend of increased dynamic modulus with an increase in the loading frequency and a decrease in temperature. An opposite trend, however, was observed for the phase angle in which an increased phase angle was measured at increased temperatures and decreased loading frequencies. This is attributed to the viscoelastic behavior of asphalt mixtures.

4.1.3 Conversion between Dynamic Modulus and Relaxation Modulus

The dynamic modulus, $\left|E^*\right|$, in the frequency domain can be converted to the relaxation modulus, $E(t)$, in the time domain. In what follows, the symbols of t and f for time (sec.) and frequency ($1/\text{sec.}$), respectively, are used. An approximation method proposed by Schapery and Park (1999) was adopted in this research with the basic steps summarized as follows:

- Calculate the storage modulus, $E^{'}(f)$, based on the dynamic modulus, $\left|E^{*}\right|$, and the phase angle, φ, by the relationship $E^{'}(f) = \left|E^{*}\right| \cdot \cos(\varphi)$.
- Regress $E^{'}(f)$ and compute the local log-log slope, n, at every measured frequency by the relationship $n = {d \log(E^{'}(f))}/{d \log(f)}$.
- Calculate the adjustment function $\lambda^{'} = \Gamma(1-n) \cdot \cos(n\pi/2)$, where $\Gamma(1-n)$ is the gamma function.
- Calculate $E(t) = {E^{'}(f)}/{\lambda^{'}}$, where $t = {1}/{f}$.

As concluded by Schapery and Park (1999), compared to the method proposed by Christensen (1982), this very simple approximation approach significantly enhances the accuracy by employing the slope of the storage modulus function on logarithmic scales without the loss of any simplicity. All calculated relaxation moduli are presented in Tables 4.5 through 4.8.

Up to the present, relaxation modulus data has been converted from dynamic modulus data determined by dynamic modulus tests. The time dependency and temperature dependency of HMA mixtures were explored in the following sections such that the necessary viscoelastic material parameters for ABAQUS analyses can be prepared.

Table 4.5 Relaxation Moduli of SMA Mix

t (sec)	-10 ºC	4.4 ºC	21.1 ºC	37.8 ºC	54.4 ºC
	E(t), GPa	E(t), GPa	E(t), GPa	E(t), GPa	E(t), GPa
0.04	12.498	9.598	5.014	2.399	0.842
0.1	12.646	8.968	4.457	2.015	0.659
0.2	12.295	8.548	3.893	1.656	0.445
1	11.291	7.388	2.894	0.988	0.229
2	10.842	6.916	2.520	0.761	0.176
10	9.816	5.734	1.796	0.498	0.110

Table 4.6 Relaxation Moduli of ODOT442 Mix

t (sec)	-10 ºC	4.4 ºC	21.1 ºC	37.8 ºC	54.4 ºC
	E(t), GPa	E(t), GPa	E(t), GPa	E(t), GPa	E(t), GPa
0.04	10.109	6.579	3.459	1.527	0.471
0.1	10.212	6.343	2.901	1.166	0.335
0.2	9.681	5.843	2.519	0.959	0.215
1	8.428	4.627	1.639	0.519	0.094
2	7.932	4.161	1.368	0.397	0.069
10	6.748	3.155	0.911	0.248	0.043

Table 4.7 Relaxation Moduli of ODOT302 Mix

t (sec)	-10 ºC	4.4 ºC	21.1 ºC	37.8 ºC	54.4 ºC
	E(t), GPa	E(t), GPa	E(t), GPa	E(t), GPa	E(t), GPa
0.04	17.065	13.387	8.063	4.387	1.164
0.1	16.804	12.698	7.249	3.625	0.786
0.2	16.541	12.698	6.555	3.066	0.508
1	15.536	11.152	4.869	1.748	0.245
2	15.148	10.575	4.189	1.348	0.171
10	14.205	8.981	2.866	0.792	0.090

Table 4.8 Relaxation Moduli of FRL Mix

t (sec)	-10 ºC	4.4 ºC	21.1 ºC	37.8 ºC	54.4 ºC
	E(t), GPa	E(t), GPa	E(t), GPa	E(t), GPa	E(t), GPa
0.04	19.134	15.832	10.473	4.505	1.273
0.1	19.655	15.187	9.307	3.526	0.849
0.2	19.257	14.619	8.370	2.917	0.531
1	18.166	13.107	6.417	1.661	0.202
2	17.672	12.438	5.581	1.238	0.127
10	16.409	10.659	3.977	0.661	0.059

4.1.4 Master Curve of Relaxation Modulus

For thermorheologically-simple asphaltic materials, the effects of time and temperature can be expressed through one parameter, the shift factor. As such, one master curve of relaxation moduli may be constructed and determined at different loading frequencies and temperatures. The shift factor is defined as follows:

$$aT = \frac{t}{\xi}. \qquad (4-4)$$

Where, aT = time-temperature shift factor at the reference temperature, T_{ref},

t = time before shifting at a test temperature, T,

ξ = reduced time at the reference temperature, T_{ref}, after shifting,

Thus, the relaxation modulus at each test temperature can be expressed by the master curve of relaxation moduli at the same reference temperature as:

$$E(\xi, T_{ref}) = E(t, T). \qquad (4-5)$$

Where, $E(\xi, T_{ref})$ = relaxation modulus at the reduced time and reference temperature, T_{ref},

$E(t,T)$ = relaxation modulus at test time, t, and test temperature, T.

Figures 4.5 through 4.8 present laboratory-determined relaxation moduli and the corresponding master curve for each mix. The reference temperature for all master curves has been taken as $21.1^{\circ}C$. The temperature-dependency curves can be obtained with the help of these master curves, as it will be shown later in this chapter.

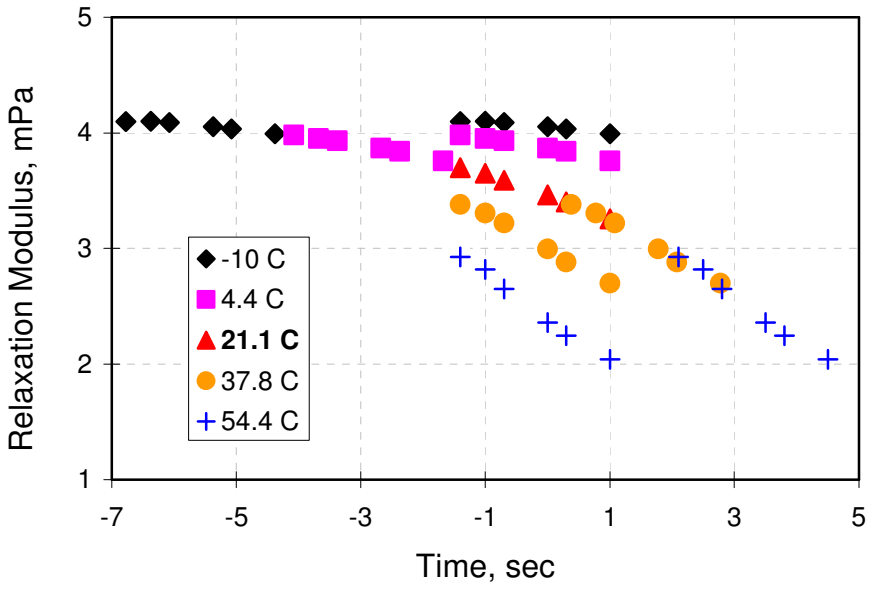

Figure 4.5 Relaxation modulus and master curve for SMA mix (log-log scale)

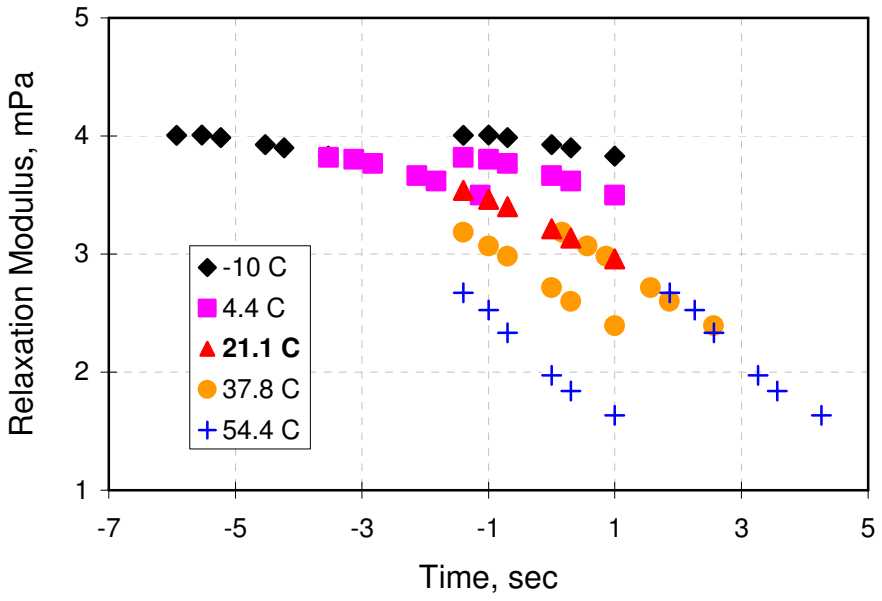

Figure 4.6 Relaxation modulus and master curve for ODOT442 mix (log-log scale)

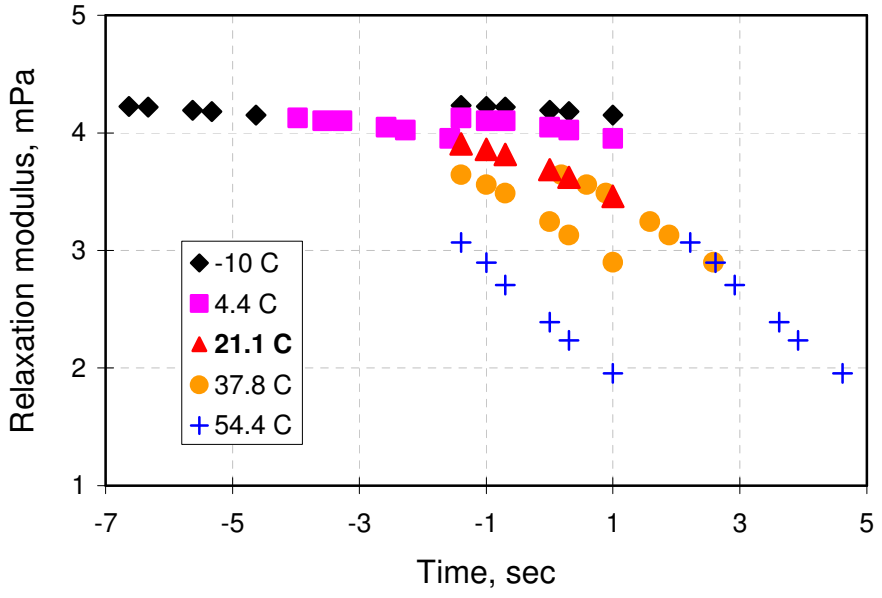

Figure 4.7 Relaxation modulus and master curve for ODOT302 mix (log-log scale)

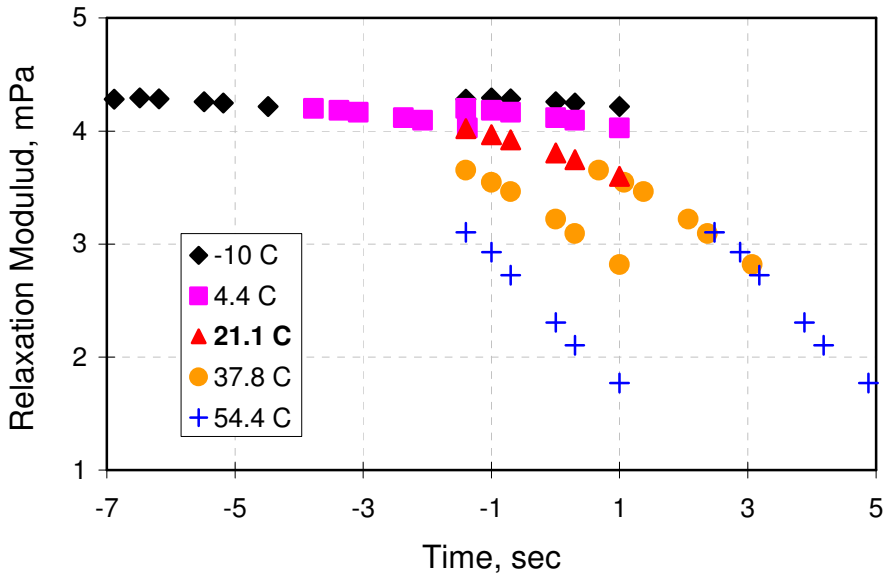

Figure 4.8 Relaxation modulus and master curve for FRL mix (log-log scale)

4.1.5 Time Dependency and Prony Series

In ABAQUS, the time dependency can be represented by using Prony series in the form of shear moduli. The shear modulus $G(t)$ is calculated from the relaxation modulus $E(t)$ by the traditional relationship:

$$G(t) = \frac{E(t)}{2(1+\nu)}. \qquad (4-6)$$

Where, $G(t)$ = shear modulus,

$E(t)$ = relaxation modulus,

ν = Poisson's ratio.

The Poisson's ratio of all mixes was assumed to be 0.35 over the range of test temperatures and loading frequencies used in this research. Once $G(t)$ is obtained, the $G(t)$ ratio represented by $\tilde{g}(t)$ is computed by normalizing $G(t)$ by $G_i(t)$, the instantaneous shear modulus. In ABAQUS (Theory Manual, 2006), $g(t)$ is expressed by:

$$g(t) = 1 - \sum_{i=1}^{N} g_i (1 - e^{(-t/\tau_i)}) \qquad (4-7)$$

Where, N = the number of Prony series terms,

g_i = material constants,

τ_i = retardation time.

Each exponential term in equation (4-7) is called a Prony series term. ABAQUS can internally calculate N, g_i, and τ_i based on the specified maximum number of terms N and the root-mean-square error (RMSE), where the latter is defined as:

$$RMSE = \sqrt{\frac{1}{N} \sum_{i=1}^{N} \left[g_i(t) - \tilde{g}_i(t) \right]^2} \; . \qquad (4-8)$$

Where, N is the number of the Prony series terms; $g(t)$ is the calculated shear modulus ratio and $\tilde{g}(t)$ is the measured shear modulus ratio.

In general, it is believed that at least 4 Prony series terms are needed to obtain a sufficiently accurate approximation to the laboratory-determined data $\tilde{g}(t)$. As it will be shown later in Figure 4.9, a Prony series with 5-terms approximate the measured shear modulus ratio curve very well with a root-mean-square error of only 0.01. The RMSR

reduced from 0.1 to 0.01 when N increased from 2 to 5. Therefore, it was decided that a 5-term Prony series was employed to approximate the measured shear modulus ratios. Table 4.9 summarizes the calculated parameters for equation (4 – 7) for each asphaltic mix.

Figure 4.9 shows the comparison between the measured and the calculated $g(t)$ for different N for the FRL mix. The calculated $\tilde{g}(t)$ was obtained from equation (4 – 7) based on constants listed in Table 4.9 while the measured $g(t)$ was determined by measured modulus data in the laboratory.

Table 4.9 Constants of Prony Series

Constant	SMA	ODOT442	ODOT302	FRL
g_1	0.2301	0.2570	0.1053	0.1747
g_2	0.2847	0.2545	0.2287	0.2293
g_3	0.2432	0.2075	0.2377	0.2597
g_4	0.1566	0.1754	0.2416	0.2313
g_5	7.03E-02	9.06E-02	1.61E-01	9.44E-02
τ_1	9.66E-06	3.23E-05	5.76E-07	2.07E-03
τ_2	2.37E-03	1.33E-03	2.74E-04	5.28E-03
τ_3	1.58E-01	3.94E-02	3.17E-02	2.38E-01
τ_4	8.479	1.130	1.362	11.894
τ_5	470.5	55.7	75.8	631.0

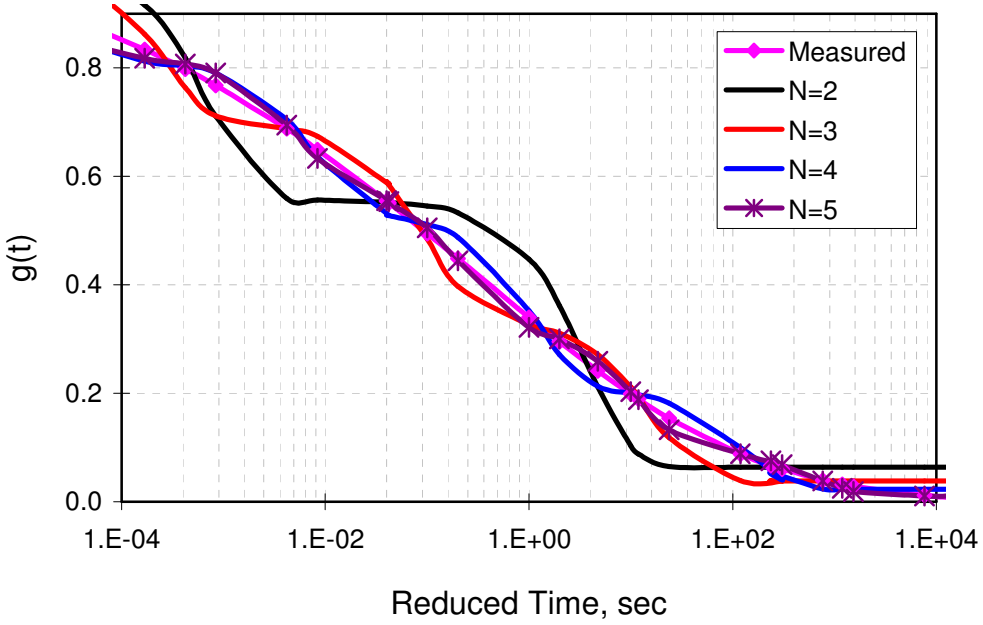

Figure 4.9 Comparison of the measured and calculated for FRL mix

Figures 4.10 through 4.12 illustrate the approximation of $g(t)$ when $N = 5$ for the remaining asphaltic mixes. It was found that an approximation with 5 Prony series terms matches the measured $g(t)$ very closely for the remaining asphaltic mixtures too. As previously indicated the Prony series approximation also defines the time dependency of a viscoelastic material in ABAQUS. By employing the time-temperature supposition principle, the function of the shear modulus ratio is extended to an unlimited time domain from a limited time duration measured in the laboratory.

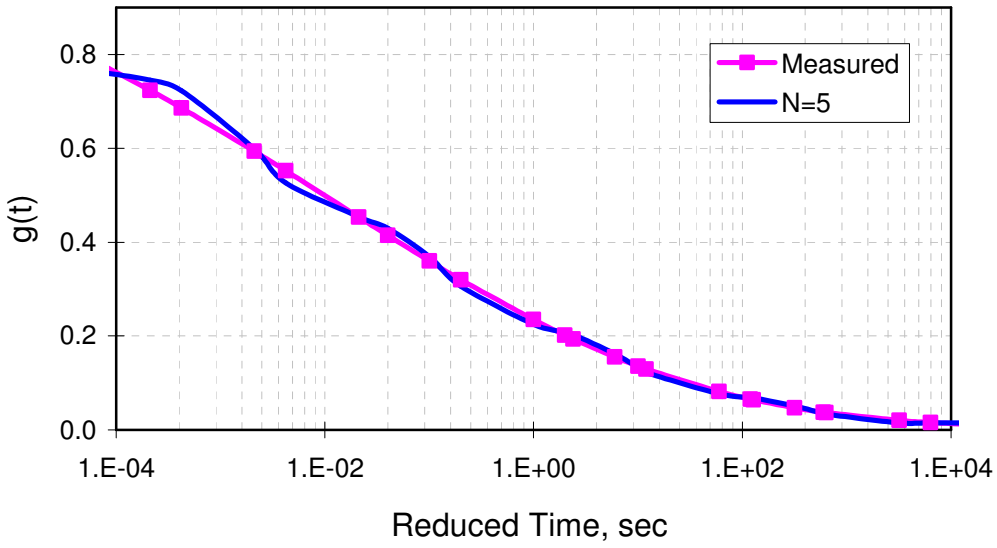

Figure 4.10 Comparison of the measured and calculated $g(t)$ for SMA mix

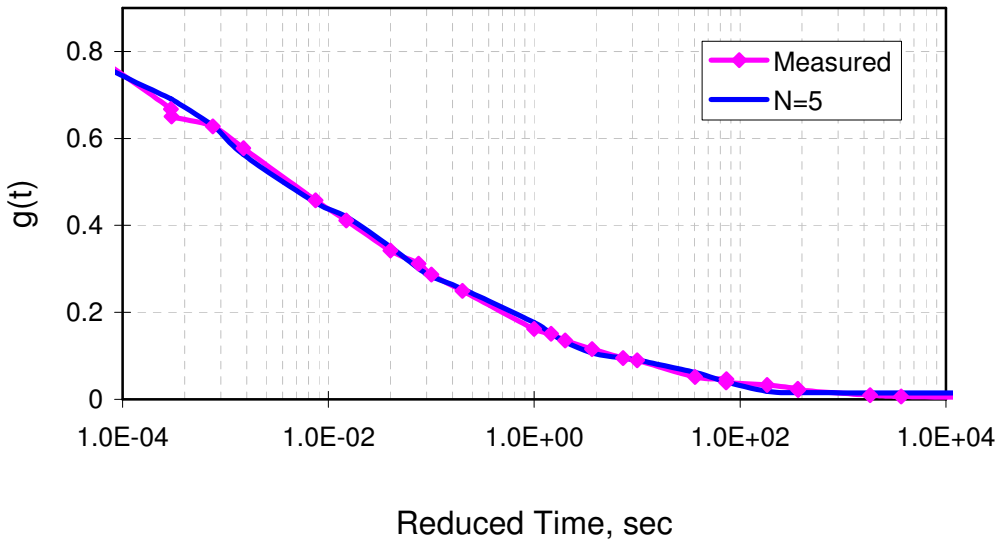

Figure 4.11 Comparison of the measured and calculated $g(t)$ for ODOT442 mix

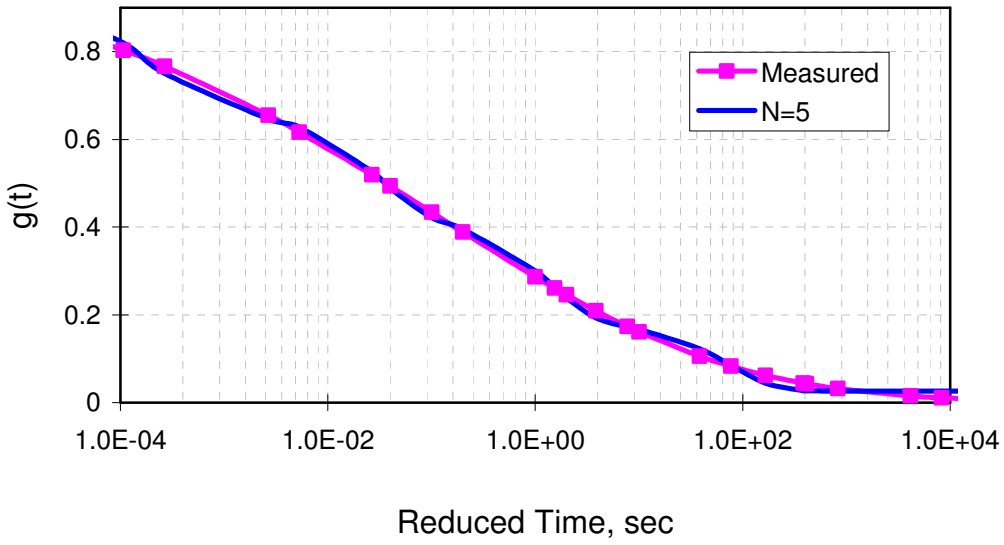

Figure 4.12 Comparison of the measured and calculated $g(t)$ for ODOT302 mix

4.1.6 Temperature Dependency and WLF Equation

In addition to the need to define the time dependency, the temperature dependency has to be defined in ABAQUS as well. This is implemented by using the Williams-Landel-Ferry (WLF) equation (Williams et al., 1955) in the form of:

$$\log(aT) = \frac{-C_1(T - T_{ref})}{C_2 + (T - T_{ref})}. \qquad (4-9)$$

Where, aT = the time-temperature shift factor,

C_1, C_2 = regression coefficients,

T_{ref} = the reference temperature, $^{\circ}C$,

T = Test Temperature, $^{\circ}C$.

Constants C_1 and C_2 are dependent on the reference temperature for a given asphalt mix. To obtain the constants, the relaxation modulus data was first fitted to a sigmoid function, introduced in the AASHTO 2002 Pavement Design Guide, in the form of:

$$\log(E(\xi)) = \delta + \frac{\alpha}{1+\exp(\beta+\gamma\log(\xi))}. \qquad (4-10)$$

Where, $\alpha, \beta, \gamma, \delta$ = regression coefficients,

ξ = reduced time.

Figure 4.13 presents the comparison of the sigmoidal functions fitting for the four asphalt mixtures. In comparison to the remaining three asphalt mixtures, the FRL mixture is more sensitive to time at low loading frequency. Similarly, the FRL mix is expected to be more sensitive to high temperature. At high temperatures and/or low loading frequencies, the SMA mix is expected to be less dependent on temperature and loading rate.

By fitting the relaxation modulus to a sigmoidal function, the time dependency is determined at a selected reference temperature. One shift factor was obtained at each test temperature.

Constants C_1 and C_2 in equation (4 – 9) were obtained by fitting the WLF equation to these shift factors for each mix as shown in Table 4.10. At the same time, comparisons are made between the calculated and the measured shift factors as presented in Table 4.11.The calculated shift factor was obtained from the WLF equation whereas

the measured shift factor was obtained by fitting the relaxation modulus data to the sigmoidal function.

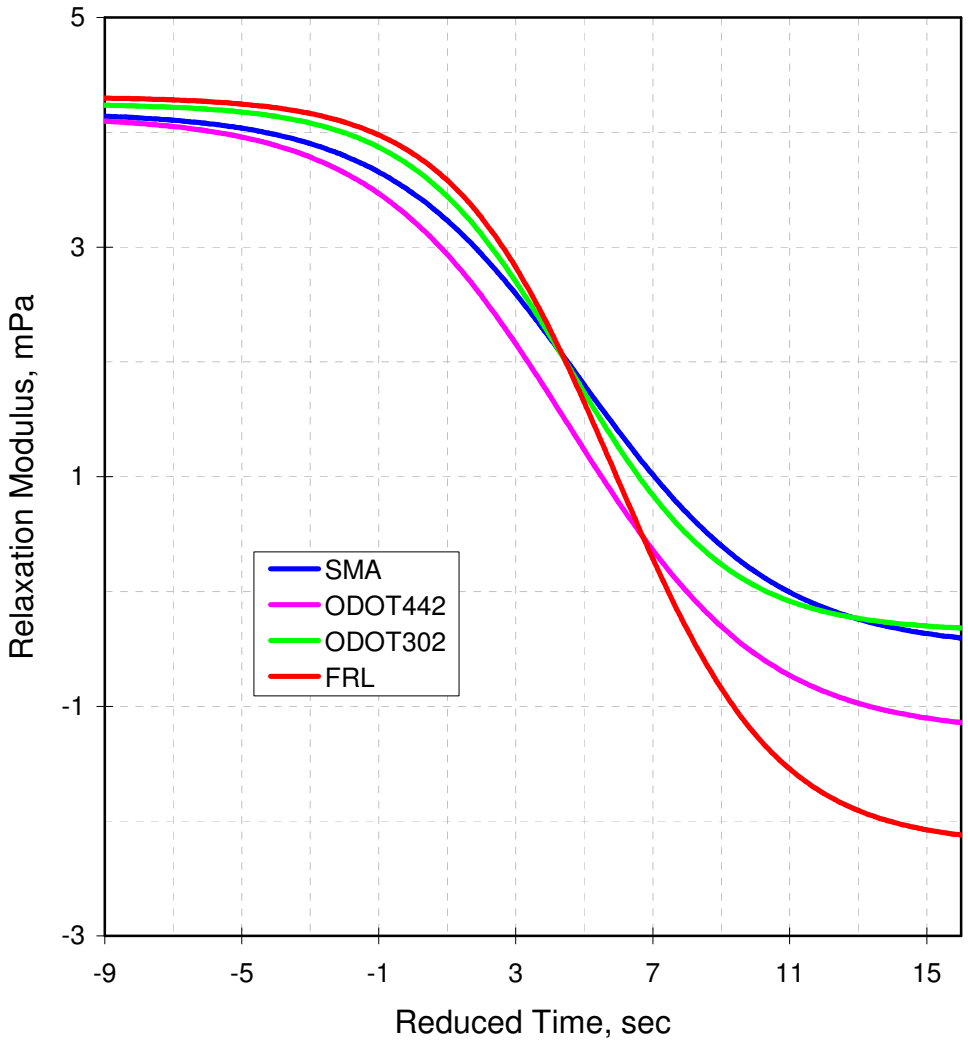

Figure 4.13 Sigmoidal approximation of relaxation modulus (log-log scale)

Table 4.10 WLF Equation Constants

Mix	C_1	C_2
SMA	16.648	126.760
ODOT442	17.947	155.030
ODOT302	15.675	118.111
FRL	21.914	157.396

Table 4.11 Measured and Calculated Shift Factors

Temp.	Shift Factor (log scale)							
	SMA		ODOT442		ODOT302		FRL	
	Meas.	Calc.	Meas.	Calc.	Meas.	Calc.	Meas.	Calc.
-10	5.38	5.41	4.53	4.50	5.63	5.60	5.47	5.40
4.4	2.68	2.53	2.13	2.17	2.57	2.58	2.38	2.60
21.1†	0.00	0.00	0.00	0.00	0.00	0.00	0.00	0.00
37.8	-1.78	-1.94	-1.56	-1.75	-1.59	-1.94	-2.08	-2.10
54.4	-3.50	-3.46	-3.26	-3.17	-3.62	-3.45	-3.88	-3.83

†Reference Temperature

With the calculated constants C_1 and C_2, a comparison of WLF-based temperature dependency for four asphalt mixtures is shown in Figure 4.14.

From Figure 4.14, it is expected that ODOT442 mix is more temperature-dependent at low temperatures but the FRL mix is more temperature-dependent at high temperatures, which agrees well with the findings from the time dependency as shown in Figure 4.13.

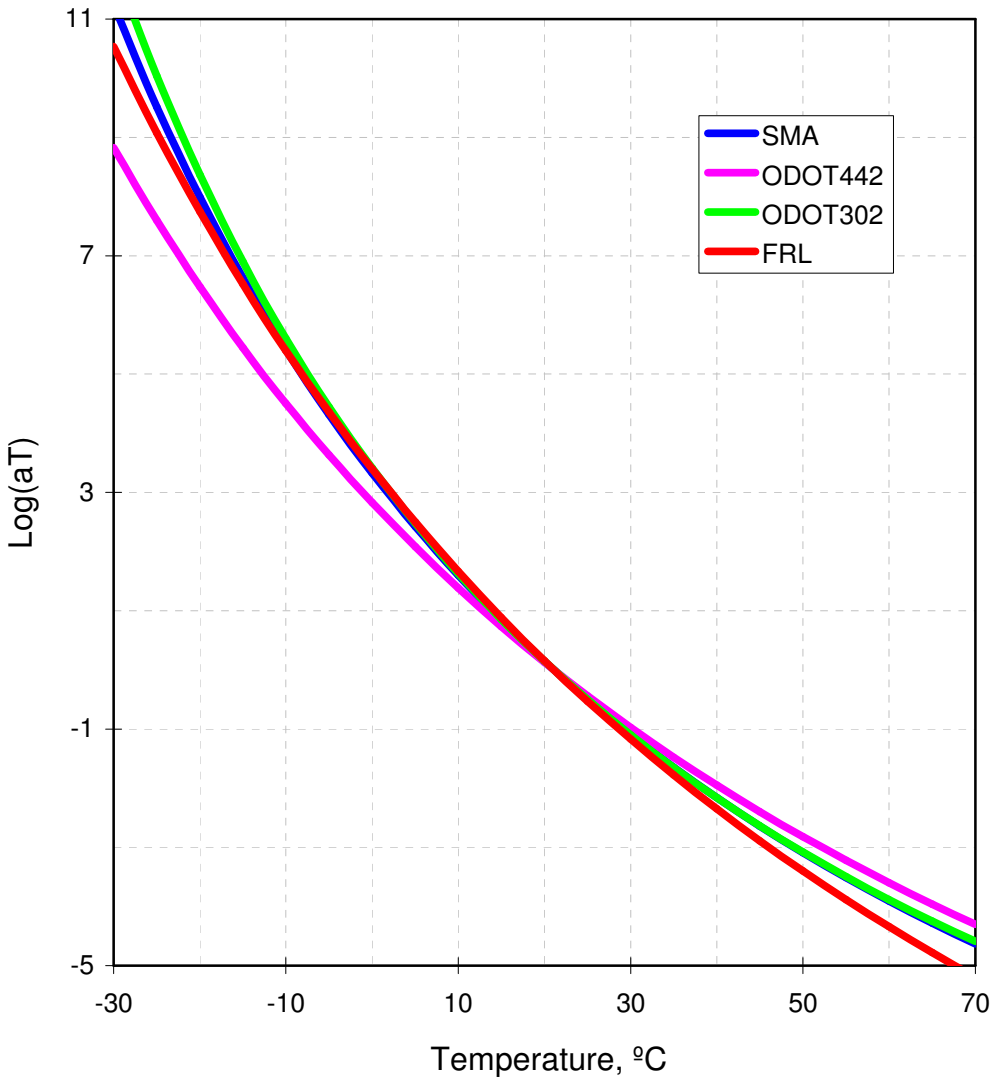

Figure 4.14 Comparison of temperature dependency of asphalt mixtures

4.2 Resilient Modulus Testing and Results

The terminology of resilient modulus is extensively used in the design and analysis of asphalt pavements. It represents a measure of the modulus of elasticity of paving materials but with an appreciable distinction. Both of them are obtained by dividing the stress by the strain. However, the modulus of elasticity is used for tests where a static load is applied whereas the resilient modulus is employed for tests where a rapid (cyclic) load is applied, e.g., traffic load. The two traditional resilient modulus laboratory tests are:

1. Repeated-load indirect tension resilient modulus test. It is typically used on HMA samples.
2. Triaxial resilient modulus test. It is typically used on unbound granular materials such as aggregate base and subgrade soils.

Resilient modulus test results on HMA mixtures are presented in the following sections prior to the introduction of similar results for unbound aggregates and soils.

4.2.1 HMA mixtures

For each HMA mixture, 2 specimens (150 *mm* (6 *in.*) in diameter and 38.1 to 76.2 *mm* (1.5 to 3 *in.*) in thickness) were compacted in the laboratory using the Superpave Gyratory Compactor. The measured air void content on average was 7.5 percent for the SMA mix, 9.5 percent for the ODOT442 mix, 7.8 percent for the

ODOT302 mix, and 7.3 percent for the FRL mix. The air void content of each specimen was as close to the as-constructed air void content for the mixes used in the in U.S 30 project as possible. All specimens had a diameter of $150\,mm$ $(6\,in.)$ and a thickness of around $53\,mm$ $(2.1\,in.)$.

The determination of resilient modulus of each mixture was conducted following the procedures contained in Appendix 1 in the NCHRP, *Recommended Standard Test Method for Determining the Resilient Modulus of Bituminous Mixtures by Indirect Tension* (NCHRP, 1997). Where the resilient modulus is determined following this approach it is regarded as a measure of the elastic modulus of the asphalt mixture recognizing certain nonlinear characteristics under rapidly applied cyclic load.

A repeatedly applied haversine load of fixed magnitude with a duration of 0.1 seconds followed by a rest period of 0.9 seconds was applied to test specimens. During testing, the specimen was subjected to a dynamic cyclic load (equal to 95 percent of the total load) and a constant load (equal to 5 percent of the total load). A .total load corresponding to a load level of 30, 15, and 5 percent of the indirect tensile strength measured at $25^{\circ}C\,(77^{\circ}F)$, were used at temperatures of $5^{\circ}C\,(41^{\circ}F)$, $25^{\circ}C\,(77^{\circ}F)$, and $40^{\circ}C\,(104^{\circ}F)$.

If vertical deformation greater than 25 microstrains could not be achieved using the aforementioned load level at the corresponding temperature, the total load was increased such that an adequate deformation could be recorded. Nevertheless, if the total vertical deformation greater than $0.76\,mm$ $(0.03\,in.)$ was monitored, the total load was

reduced to the minimum value possible while retaining an adequate deformation for good resolution.

During testing, two vertical deformation response curves were monitored to ensure that the acceptable vertical deformation ratio between two maximum vertical deformations was within 2.0 such that the specimen was applied with an acceptable symmetrical load. If a deformation ratio greater than 2.0 was obtained, the test was stopped and the specimen was realigned toward the large deformation side.

An environmental chamber was used to control specimen temperature at $5^{\circ}C\,(41^{\circ}F)$, $25^{\circ}C\,(77^{\circ}F)$, and $40^{\circ}C\,(104^{\circ}F)$, respectively. A specific temperature was kept within $0.5^{\circ}C\ (0.3^{\circ}F)$. Typical deformation and load curves obtained from the resilient modulus test are shown in Figure 4.15.

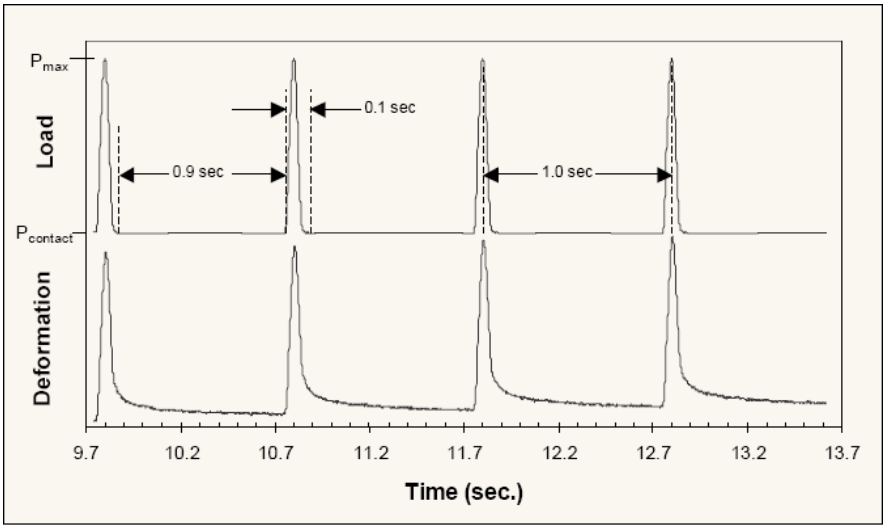

Figure 4.15 Typical deformation and load curves from resilient modulus tests (after LTPP P07, 2001)

Figure 4.16 represents the method to determine the total recoverable horizontal deformation. This value includes both the instantaneous recoverable deformation and the time-dependent continuing recoverable deformation during the rest-period portion of a complete cycle.

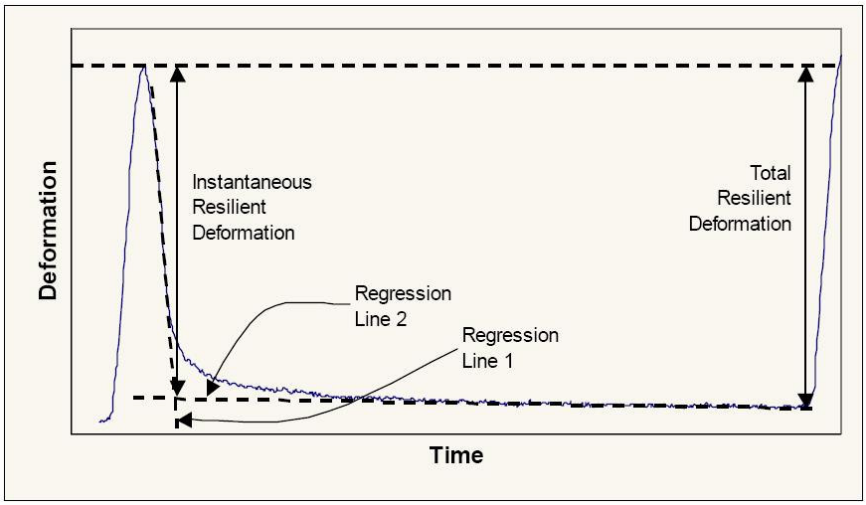

Figure 4.16 Instantaneous and total resilient deformations (after LTPP P07, 2001)

Regression line 1 in Figure 4.16 is drawn based on all data points after the maximum deformation occurs and before the specimen has rebounded by 75 percent of the total deformation. Regression line 2 is determined based on all data points in the last 0.75 seconds of each cycle up to the initiation of the next load cycle (LTPP P07, 2001).

The total resilient modulus was calculated as follows:

$$Mr = P \text{ x } \frac{\mu_r + 0.27}{t \times \Delta H_t}. \qquad (4-11)$$

Where, P = repeated maximum load, kN,

μ_r = Poisson's ratio, assumed to be 0.35 in this research,

t = thickness of specimen, m,

ΔH_t = total recoverable horizontal deformation, m.

A summary of resilient moduli for all mixtures is shown in Figure 4.17. Summarily, the results of the resilient modulus test are in good agreement with that of the dynamic modulus test. FRL mix is the stiffest whereas ODOT442 mix is the least stiff among four mixes.

4.2.2 Subgrade Soils

The resilient modulus of subgrade soils is one of the essential material properties that are required for the mechanical analysis for a flexible pavement system. In this research, disturbed subgrade soil samples obtained at the U.S. 30 test site were taken to the laboratory for soil classification and resilient modulus testing.

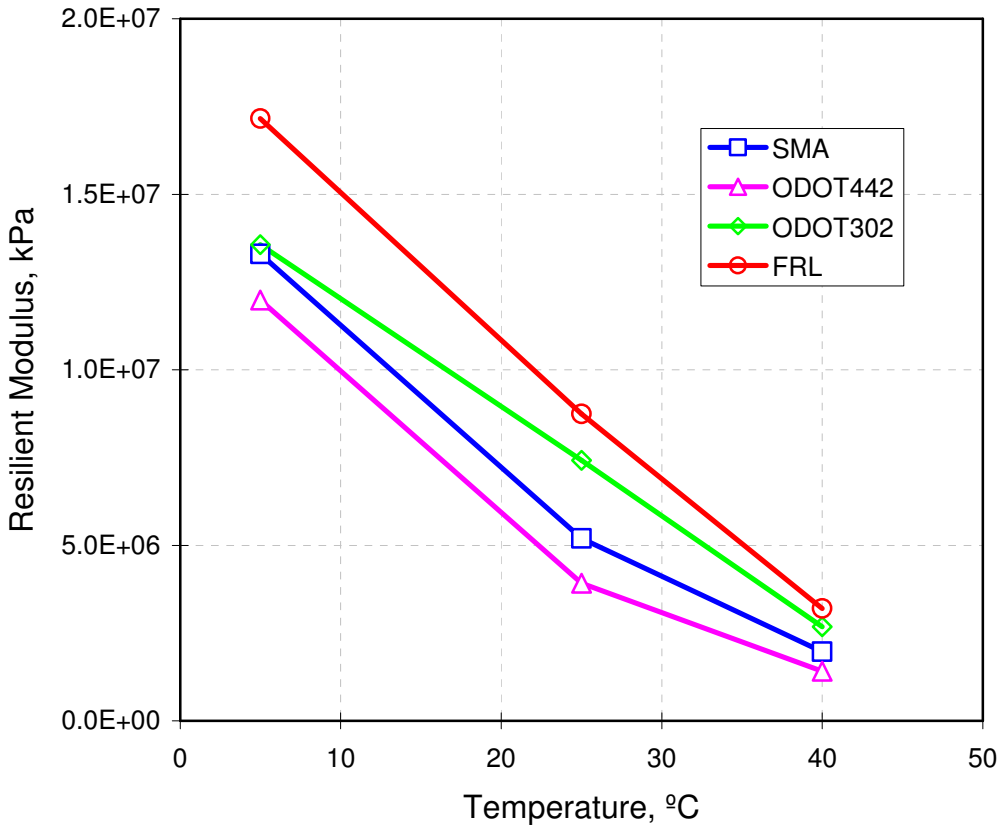

Figure 4.17 Resilient modulus test results

Soil Classification

In the laboratory, sieve analysis, Atterberg's limits tests, and compaction tests were performed. The test results are shown in Table 4.12, where the soil classification was given according to the AASHTO and ODOT systems, respectively. All were grouped within the same categories: A-4 (AASHTO) and A-4-a (ODOT).

Table 4.12 Atterberg Limits and Soil Classification

Specimen	Liquid Limit (%)	Plastic Limit (%)	Plastic Index (%)	% Passing #200	Classification		OMC* (%)	$(\gamma_d)_{max}$ (kN/m^3)
					AASHTO	ODOT		
WB Sta 885+00	26.94	17.04	9.90	46.9	A-4	A-4-a	12.10	18.82
EB Sta 876+60	26.66	17.23	9.43	38.2	A-4	A-4-a	12.80	18.90
WB Sta 876+60	25.90	17.67	8.23	39.3	A-4	A-4-a	14.40	18.82
EB RS Sta 884+00	25.99	18.72	7.27	41.7	A-4	A-4-a	14.50	18.58
EB LS Sta 884+00	24.44	16.49	7.95	48.9	A-4	A-4-a	13.30	18.82
EB Sta 663+50	23.28	17.20	6.15	41.0	A-4	A-4-a	11.80	19.38

* Optimum moisture content.

Experiments and Results

Five resilient modulus tests were performed at different moisture contents. Each soil sample was dried, pulverized, and then re-compacted inside a split mold, using a static compaction method to form the test specimen.

The test specimens were compacted at their maximum dry unit weights but at different moisture contents following the procedures contained in AASHTO T 294-92 specification, *Resilient modulus of unbound granular base/subbase materials and subgrade soils* (AASHTO, 1992), in order to investigate any effect that the moisture content has on the resilient modulus of subgrade soils. Based on the target maximum dry unit weight and the target moisture content, the mass of soils required to fill the compaction mold was calculated. Then five layers of equal mass were used to form the specimens to the desired specimen height under a static load. All specimens were compacted at a diameter of $101.6\,mm$ $(4\,in.)$ and a height of $203.2\,mm$ $(8\,in.)$.

The resilient modulus testing was conducted following the same procedures as in AASHTO T 294-92. The test equipment and configuration used for resilient modulus

tests is essentially the same as that used for the conventional triaxial compression test. The only difference between them is that the axial load is applied as a series of 1 Hz pulse loads during resilient modulus tests, while it is increased monotonically during triaxial compression tests. The load sequences for each test are listed in Table 4.13.

Table 4.13 Load Sequences Applied during Resilient Modulus Tests

σ_c, *kPa*	Seq. No.	σ_d, *kPa*	No. of Cycles
41.4	0	27.6	<500*
41.4	1	13.8	100
	2	27.6	100
	3	41.4	100
	4	55.2	100
	5	69.0	100
20.7	6	13.8	100
	7	27.6	100
	8	41.4	100
	9	55.2	100
	10	69.0	100
0.0	11	13.8	100
	12	27.6	100
	13	41.4	100
	14	55.2	100
	15	69.0	100

*Initial conditioning load cycles.

Typical resilient modulus test results are plotted in Figure 4.18 corresponding to one test. A summary of resilient modulus tests is shown in Figure 4.19, which indicates that the resilient modulus initially decreased with an increase in the deviator stress but it remains essentially constant beyond a certain deviator stress value. The bilinear nature of the relationship between the resilient modulus and the deviatoric stress is well defined.

This bilinear relationship occurs because of the fact that the soil specimen was somewhat overconsolidated during its preparation stage, and the maximum compressive load applied to the soil during compaction closely matches the breakpoint deviatoric stress for each test specimen. This indicates that the breakpoint deviatoric stress is essentially the pre-consolidation pressure. More discussions can be found in the paper by Masada et al. (2006).

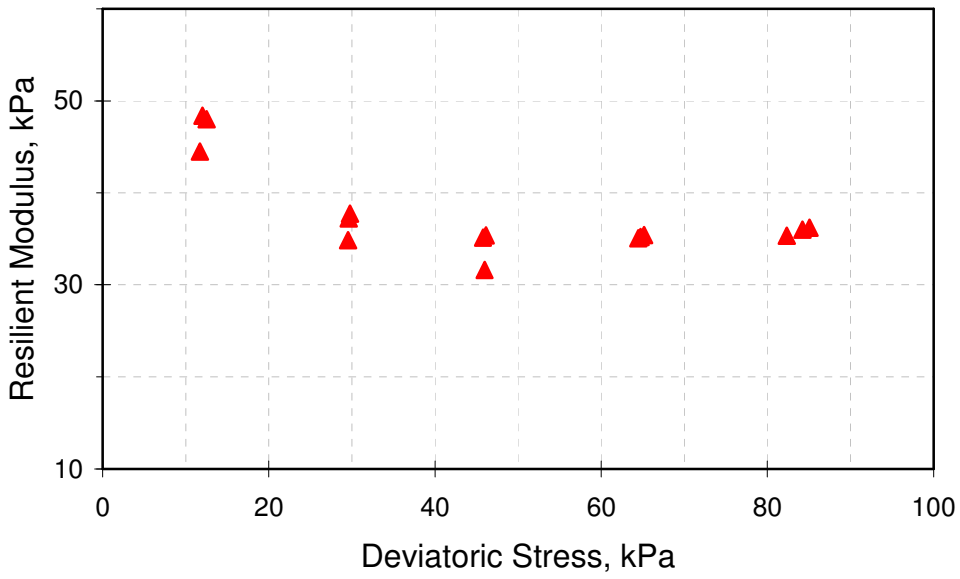

Figure 4.18 Typical result of resilient modulus test

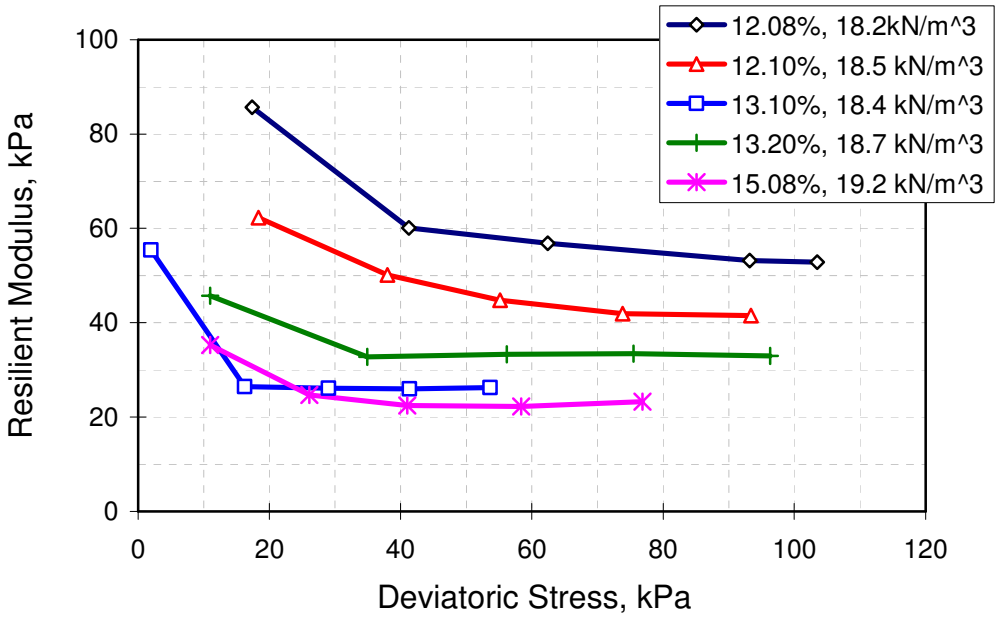

Figure 4.19 Resilient moduli of subgrade soils at different moisture contents

A summary of resilient modulus variation versus moisture content at different levels of the deviatoric stress is shown in Figure 4.20. As can be seen from Figure 4.20, the resilient modulus decreased as the moisture content increased, even though the dry unit weight remained unchanged. The resilient modulus decreased by approximately 55 percent under the deviator stress levels considered and the curves became flatter as the moisture content increased.

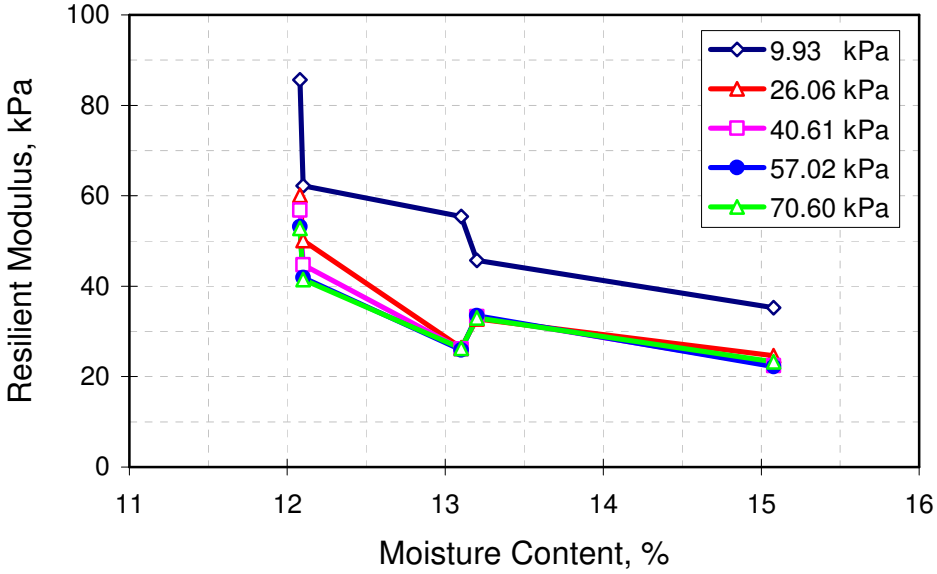

Figure 4.20 Variation of resilient modulus with moisture content

It should be noted that the resilient modulus increased when the moisture content changed from 13.1 percent to 13.2 percent as shown in Figures 4.19 and 4.20. This might be caused by the maximum dry unit weight that counteracted the effect of the moisture content.

4.2.3 Aggregates

Unlike subgrade soils, the resilient modulus of the aggregates was not tested in the laboratory. Since the same type of aggregate base, ODOT304, has been extensively tested in the SHRP project (Masada, 2001), a resilient modulus of 137.9 kPa (20 ksi) was adopted in this research.

4.3 Summary

This chapter is dedicated to the mechanical characterization of HMA materials and unbound granular materials used at the U.S. 30 perpetual pavement project. The viscoelastic properties of HMA materials were measured using the dynamic modulus tests. These laboratory-determined dynamic moduli were converted into shear modulus ratios to be incorporated into the ABAQUS program. The temperature and time dependency was explored in obtaining the dynamic moduli.

In addition to the dynamic moduli, resilient moduli were also determined in the laboratory for HMA materials and unbound granular materials. Nevertheless, a resilient modulus of $137.9\,kpa$ $(20\,ksi)$ was adopted instead of testing aggregates.

5 FE MODELING OF U.S. 30 PERPETUAL PAVEMENT

5.1 U.S. 30 Perpetual Pavement Project

5.1.1 Project Overview

This demonstration project exclusively designed to validate the concept of perpetual pavement which was constructed in two westbound lanes is a four-lane divided rural freeway U.S. 30 (with a current ADT of 17720 vehicles) in Wayne County, Ohio. The project borders on the west by State Route 83 and on the east by Kansas Road near State Route 57 (Figure 5.1) with a total length of approximately 12.87 *km* (8 miles) (Sargand et al., 2006).

Mechanistic analyses were performed by a task force led by Dr. Sang-soo Kim (FPO, 2004) to determine the total thickness of HMA layers with aiming at limiting the tensile strain at the bottom of the FRL layer to less than 70 microstrains which is taken as the endurance limit that will prevent bottom-up fatigue cracking from initiating (Carpenter et al., 2003). These analyses were performed using 1.2 times of the legal load and concluded that the goal would be achieved if using 412.75 *mm* (16.25 *in.*) thick HMA materials. Typical ODOT specification materials were used for two bottom layers but premium courses with polymer-modified asphalt binder were used for two surface layers. The distribution of sub-layers within HMA materials of 412.75 *mm* (16.25 *in.*) is shown in Table 5.1, together with mix properties and design air void contents.

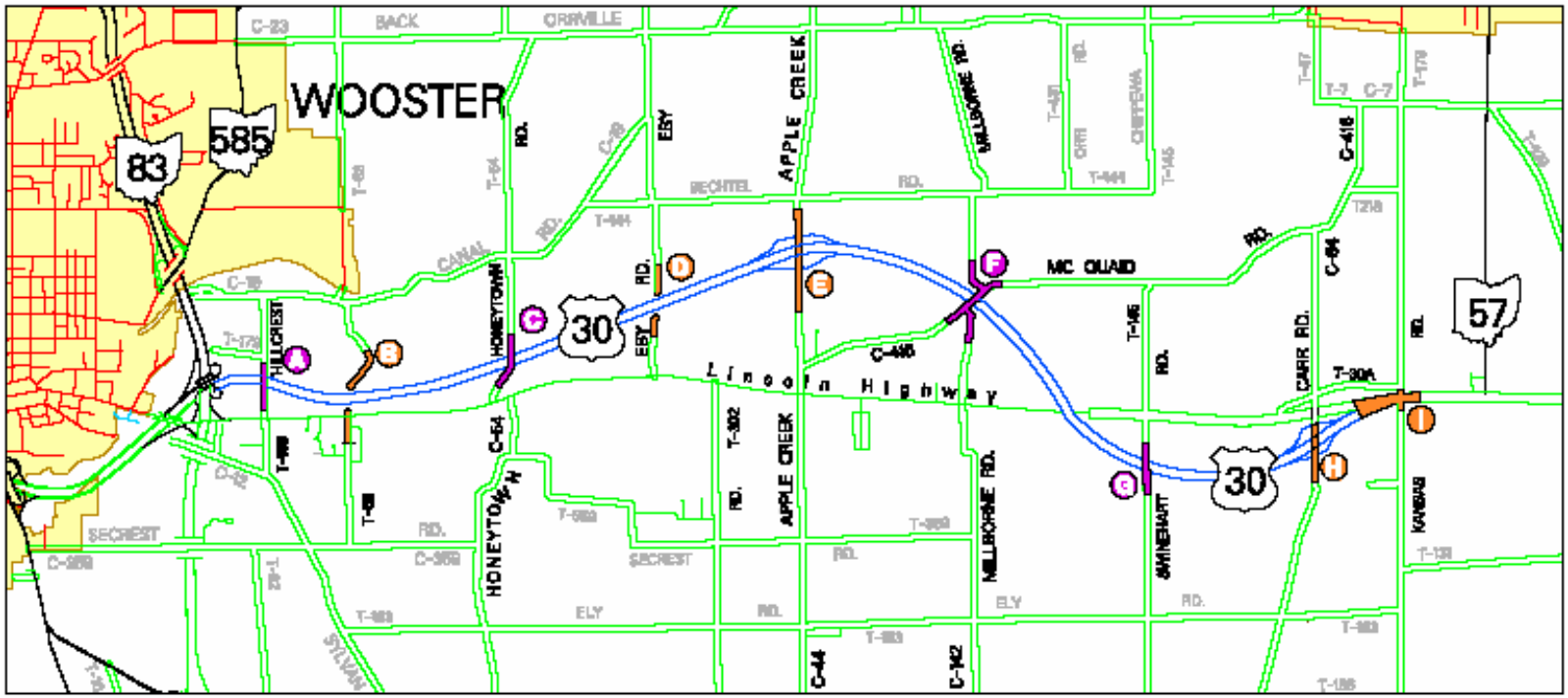

Figure 5.1 U.S 30 project map (courtesy of ODOT)

Table 5.1 Perpetual Pavement Build-Up

Course	Thickness (mm)	ODOT Item No.	Description	Design Air Void Content (%)
Surface	38.1	856	Stone Mastic Asphalt (SMA), 12.5 mm, PG 76-22M. 93% ~ 97% target density.	3.5
Intermediate	44.5	442	Superpave Asphalt Concrete, type A, 19 mm, PG 76-22M. 93% ~ 97% target density.	4
Asphalt Base	228.6	302	ODOT's large stone base mix, PG 64-22. This is a high modulus layer. 93% ~ 96% target density	4.5
Fatigue resistant layer	101.6	Special (302)	ODOT's large stone base mix with rich binder, 3% air void, 94% ~ 97% target density	3
Aggregate Base	152.4	304	Highly crushed densely graded granular base with under drain	---

5.1.2 Brief Introduction to Perpetual Pavement

According to APA (2002), "A perpetual pavement is designed and built to last longer than 50 years without requiring major structural rehabilitation or reconstruction, and needing only periodic surface renewal in response to distresses confined to the top of pavement layers". Since the 1960s, great efforts have been made to build full-depth and deep-strength asphalt pavements in the United States and service lives of those well-designed and well-built have been greatly increased.

Each layer of a perpetual pavement is designed to resist specific distress by the material selection and HMA mix design. A brief summary of HMA considerations is presented in the following paragraphs. More details on HMA considerations of a perpetual pavement may be referred to a synthesis by APA (2002).

A fatigue resistant layer on highly-crushed and densely-graded aggregate base is especially designed to resist bottom-up fatigue cracking resulting from repeatedly applied traffic loads. From the perspective of mix design, a higher asphalt binder content is used to produce a lower air void content and thus a higher volume of binder in the voids in

mineral aggregate (VMA), which lead to better durability and flexibility. Also, a higher asphalt binder content enhances the mixture's resistance to moisture-induced damage. In addition, from the perspective of the thickness design, the initiation of fatigue cracking could be completely prevented by limiting the tensile strain to less than the endurance limit of 70 microstrains.

The intermediate layer intends to provide good stability and durability to the pavement structure with a characteristically high modulus to carry most of the traffic load. A stone-on-stone contact skeleton structure is desired to provide good stability in this layer. The wearing surface course must combine the qualities of resistance to rutting, surface cracking, good friction, mitigation of splash and spray, and minimization of tire-pavement noise. An SMA mix with a polymer-modified and higher grade asphalt binder normally satisfies these considerations.

Nevertheless, the most significant characteristic of a perpetual pavement is that its mechanistic design process is conceptually more focused on a design for the maximum tensile strain than a design for incremental damage (APA, 2002). It means that bottom-up fatigue cracking will never occur if the HMA mixes are sufficiently thick to keep the maximum tensile strain less than 70 microstrains throughout the service life of the perpetual pavement.

5.1.3 Instrumentation Plan

A comprehensive instrumentation plan was developed to monitor environmental conditions and the structural response of the pavement under vehicular loading (Sargand

et al., 2006). Three test sections were constructed and instrumented with two adjacent test sections constructed at Station 876+60 and designated as sections 876A and 876B. The third test section designated as section 664 was constructed at Station 664+00. In this research, only instrumentation data collected at section 664 with the instrumentation plan shown in Figure 5.2 is to be utilized. In the succeeding paragraphs, a brief summary on instrumentation is presented and more details can be referred to the paper by Sargand et al. (2006).

Strain gages were embedded at the bottom of varying HMA layers to measure strain response. The longitudinal tensile strain at the bottom of the FRL layer was measured to evaluate the potential of fatigue cracking resulting from repeat traffic loads, which is a primary concern for the perpetual pavement. In addition, both the longitudinal and transverse tensile strains were measured at the bottom of ODOT302 layer. There was no strain gages placed at the bottom of the ODOT442 layer for section 664.

Besides, vertical compressive stresses on top of the subgrade were monitored with two pressure cells for section 664. These stresses are used to evaluate the rutting potential of the subgrade, the rutting of which could contribute to the majority of total pavement rutting (Liao et al., 2007). Four Linear Variable Displacement Transducers (LVDTs) were bedded to measure the vertical displacement of the pavement with two shallow referenced LVDTs measuring deflection above the subgrade and the remaining two deep referenced LVDTs measuring total deflection of the pavement. The displacement of the subgrade can be calculated from the difference between these two measurements.

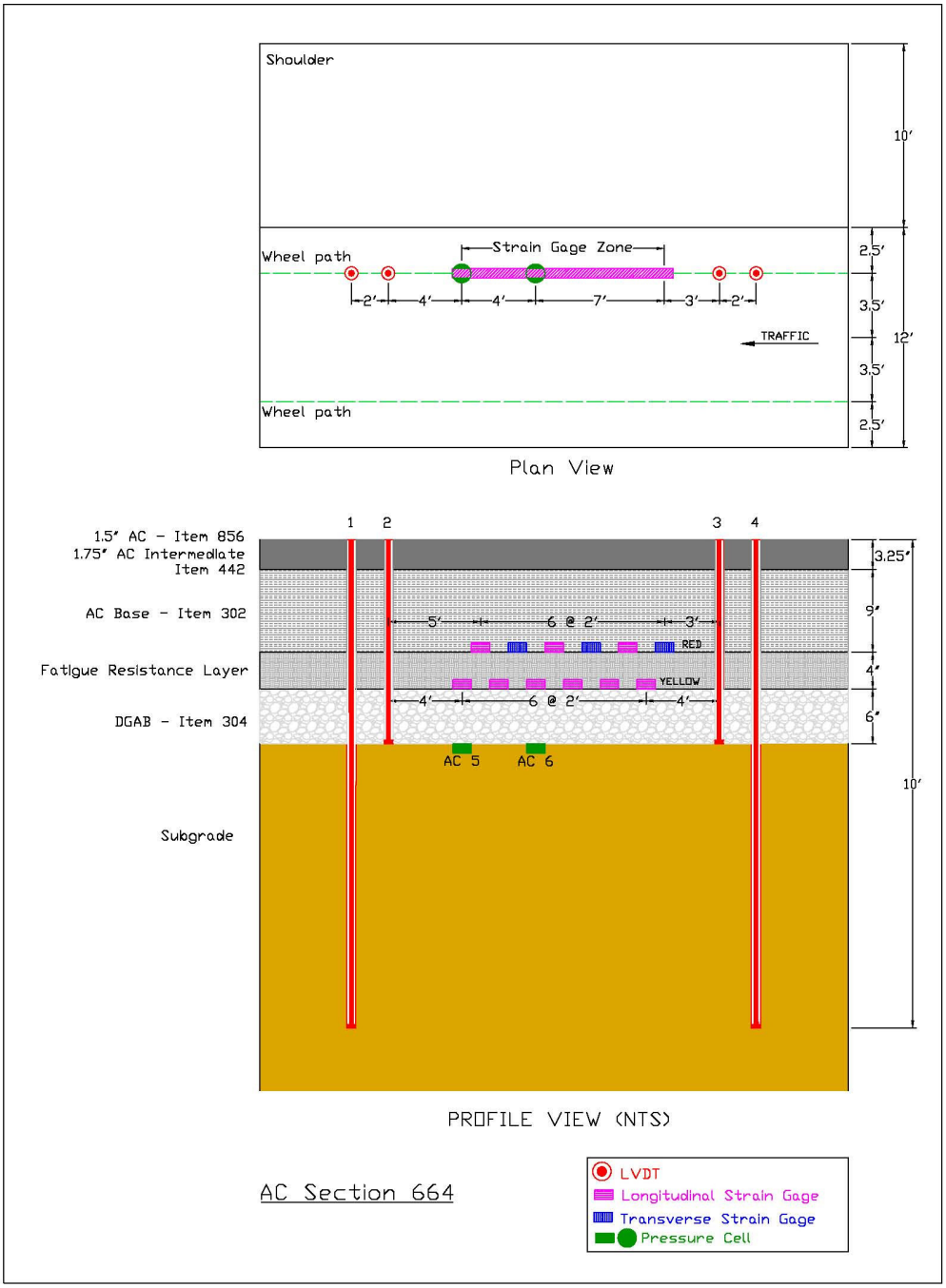

Figure 5.2 Instrumentation plan of test section 664 (courtesy of Khoury)

The seasonal instrumentation mainly including thermistor probes and Time-Domain-Reflectometry (TDR) was intended to monitor pavement temperature as well as volumetric moisture content of the subgrade and the base. A summary of these instruments is listed in Table 5.2. In the following sections, collected moisture content, pavement temperature, and controlled load vehicle (CLV) test data at the time of CLV tests are to be introduced in more detail.

Table 5.2 Load Response and Seasonal Instrumentation Details

Measurement	Manufacturer	Sensor
Deflection	Macro Sensors	HSD 750 – 500
Strain	Dynatest Consulting Inc.	Dynatest PAST II-AC SG
Stress	Geokon Inc.	Geokon 3500 PC
Temperature	Measurement Research Cor.	MRC Thermistor
Moisture	Campbell Scientific Inc.	CS – TDR Probe
Groundwater Table	-	Open Wells

5.1.4 Moisture Content

The moisture content plays an important role in determining the resilient modulus of fine-grained subgrade thereby significantly affecting the dynamic response of the pavement. A total of ten TDR probes were installed to monitor volumetric moisture content within the subgrade and the base with the first probe installed at a depth of $463.55\,mm$ $(18.25\,in.)$ down from the pavement surface. The top eight TDR probes near the surface were spaced with depth at intervals of $152.4\,mm$ $(6\,in.)$ whereas the remaining two were at intervals of $304.8\,mm$ $(12\,in.)$. The last one extended to $1574.8\,mm$ $(62\,in.)$ below the top of the subgrade.

Figure 5.3 shows the variation of the moisture content of the subgrade at the time the controlled load vehicle testing was conducted for section 664. As seen in Figure 5.3, there is an abrupt jump from about 13 percent to averagely 30 percent in moisture content at a depth of about 1219.2 *mm* (48 *in.*) down from the pavement surface. The resilient modulus of subgrade soils is then determined, along with laboratory resilient modulus test results, from field-measured moisture content.

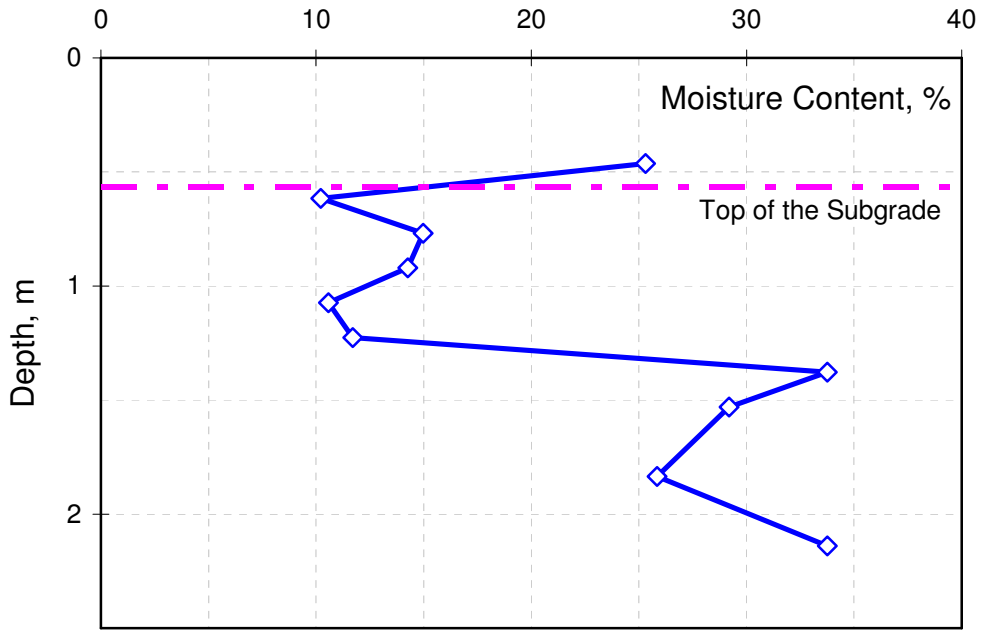

Figure 5.3 The variation of moisture content of the subgrade for section 664

5.1.5 Temperature

Temperature has a key impact on the behavior of HMA materials. To study the effect of temperature on pavement behavior, a total of five depths within the pavement were monitored for temperature variations with MRC thermistor probes. The probes were intended to measure temperature gradients throughout HMA layers, base, and the subgrade and data was collected hourly. The CLV tests were conducted from 8:00 AM to 1:00 PM. The daily peak temperature of the pavement occurred at about 4:00 PM, with hourly variations of pavement temperature presented in Figure 5.4. Peak temperature is important to consider in the possible development of the maximum tensile strain at the bottom of the FRL layer.

5.1.6 Controlled Load Vehicle Testing

The CLV testing conducted on July 19, 2006 was used to collect the dynamic structural response of the pavement to truck loading using a conventional ODOT single axle trucks with the configuration shown in Figure 5.5. CLV tests were conducted at four speeds of $8\,km/h$ ($5\,mph$), $40.2\,km/h$ ($25\,mph$), $72.4\,km/h$ ($45\,mph$), and $88.5\,km/h$ ($55\,mph$) with 4 runs per speed.

The single axle truck has a clearance between dual tires of $0.124\,m$ ($4.88\,in.$). The axle/tire clearance is $1.295\,m$ ($51\,in.$). The center-to-center axle spacing between the front axle and real axle is $4.506\,m$ ($177.4\,in.$). The width of each tire footprint is $212.8\,mm$ ($8.38\,in.$) measured in the field. The vertical tire pressure and tire weight for

each tire tread were measured during CLV testing and made available in this study. The tire weight may vary significantly from one tire imprint to another.

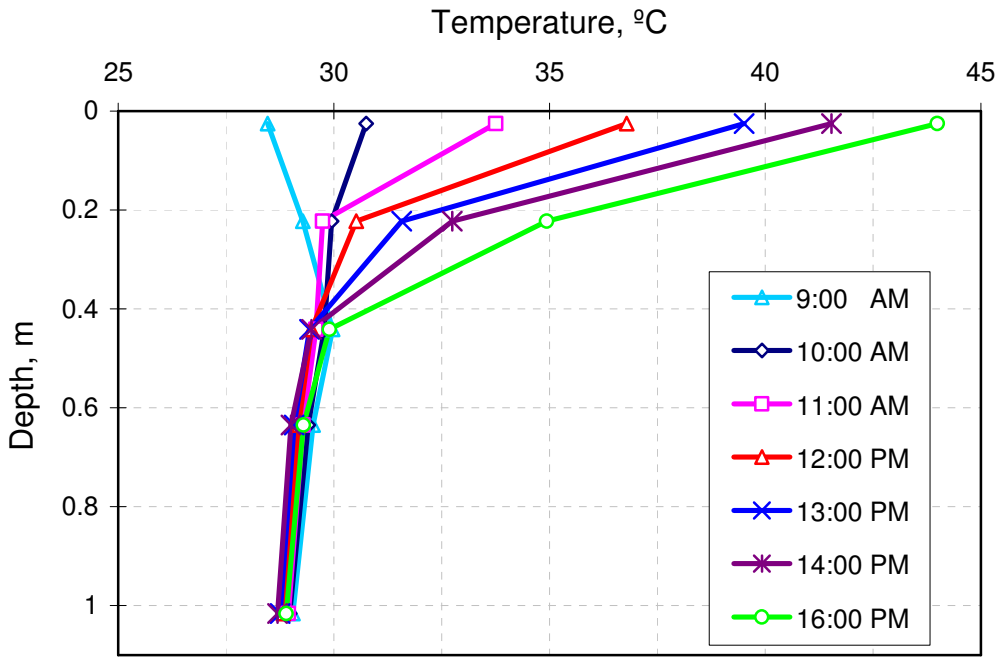

Figure 5.4 Hourly variations of pavement temperature

During CLV tests, pavement structural response in the form of deflection, strain, and vertical stress were measured. One example of the longitudinal tensile strain collected at the bottom of the FRL layer at a traffic speed of 88.5 km/h (55 mph) is plotted in Figure 5.6. Ideally, traffic loading is symmetrically applied if the instrumentation axis is right below the center of dual tires as indicated in Figure 5.5.

However, it was impossible in practice to have such a perfect driver. Then the concept of offset relative to two deep-referenced LVDTs was adopted to indicate how much the outermost edge of the outer tire was away from the instrumentation axis. For an ideal test, the offset value should be 274.8 *mm* (10.82 *in.*). The offset is important for calibration of the viscoelastic model in later sections.

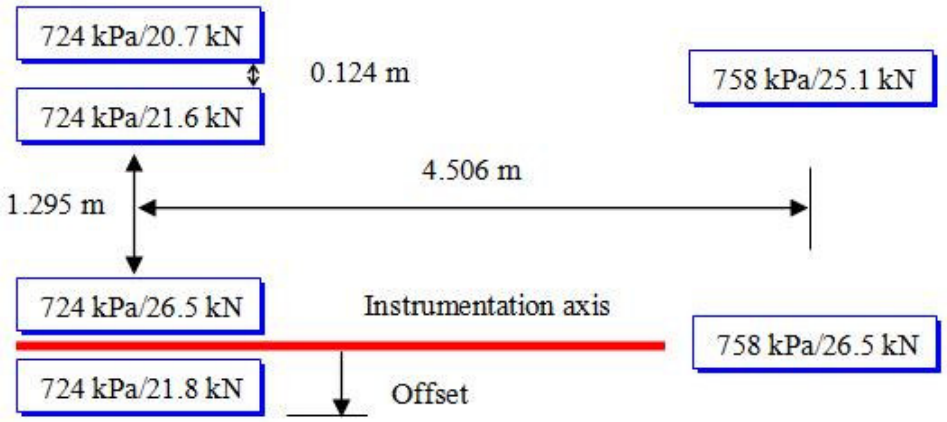

Figure 5.5 Single axle configuration used for CLV tests (not to scale)

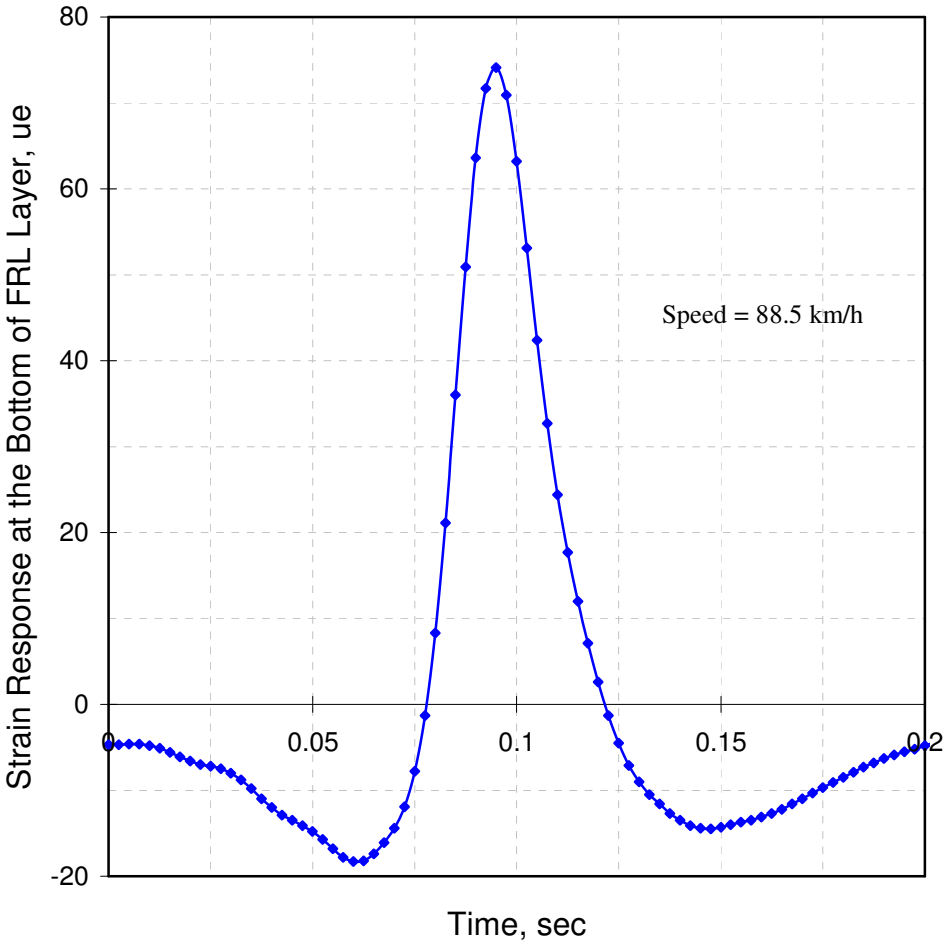

Figure 5.6 Typical strain response at the bottom of the FRL layer

5.2 Viscoelastic FE Model Formulation

5.2.1 Model Idealization

A three-dimensional FE model was developed using ABAQUS Version 6.6-3 (User's Manual, 2006) to represent the pavement structure corresponding to section 664

at the U.S. 30 perpetual pavement. Figure 5.7 shows the snapshot of the developed FE model. The convention on coordinate system was defined so that the positive X axis coincides with the direction of traffic. The positive Z axis directs down to the subgrade from the pavement surface. The traffic moves from negative X axis to positive X axis as indicated in Figure 5.7 by the black arrow.

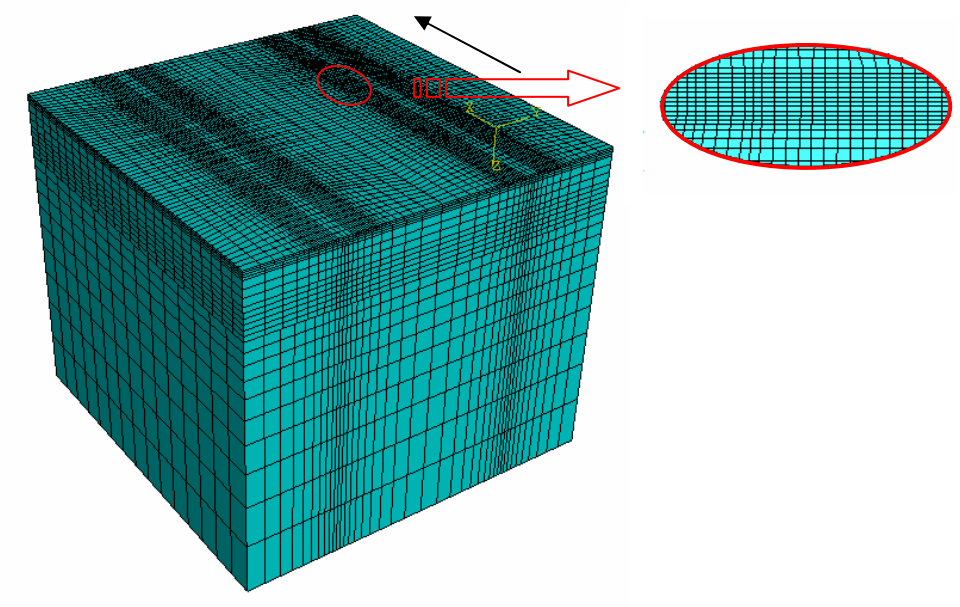

Figure 5.7 Developed 3-D FEM model and refined mesh for the loading area

The model has a dimension of $3.658\,m$ $(144\,in)$ along the direction of traffic and $3.658\,m$ $(144\,in.)$ along the transverse direction (the width of one lane) and is $3.048\,m$ $(120\,in.)$ in depth. A model of such size was used to minimize the edge effect, especially on the longitudinal tensile strain. Also, the model length of $3.658\,m$ $(144\,in.)$ in the

direction of traffic was selected such that one full passage of the truck on the pavement can be achieved to obtain a complete longitudinal tensile strain response curve including the expected compression-tension-compression sequence.

It was also assumed that there is no vertical or horizontal movement at the bottom of the FE model, thus the bottom of the model was completely restrained. Horizontal movement perpendicular to the perimeters was also restrained whereas the remaining two directions were considered free (thus there were two degrees of freedom). Since the pavement is new, the interface between different layers is assumed to be tied together without any relative movement.

The model was idealized with 8-node linear brick reduced integration elements (C3DR8). The FE mesh includes a fine mesh close to the loading area and a coarse mesh away from it (Figure 5.7). To ensure the accuracy of the FE model and the convergence of the mesh idealization, a sensitivity analysis was undertaken with three mesh schemes (Figure 5.8). The red rectangular represents the exact size of the tire imprint. The smallest element dimension, total number of elements for the complete FE model, strain response, and run time required to complete one analysis are summarized in Table 5.3.

The predicted longitudinal maximum tensile strains between the medium mesh model and the fine mesh model agree very well while the coarse mesh model underestimates the strain response by 7.4 percent. It is believed that the longitudinal strain converges to 78 microstrains based on the results of the mesh sensitivity analysis. The medium mesh and fine mesh models have the same accuracy of predictability; however, the fine mesh model requires twice the computational time as compared to the

medium mesh model. Taking both accuracy and required computation time into consideration, the medium mesh model is selected as the most advantageous option with less run time and without any loss of accuracy.

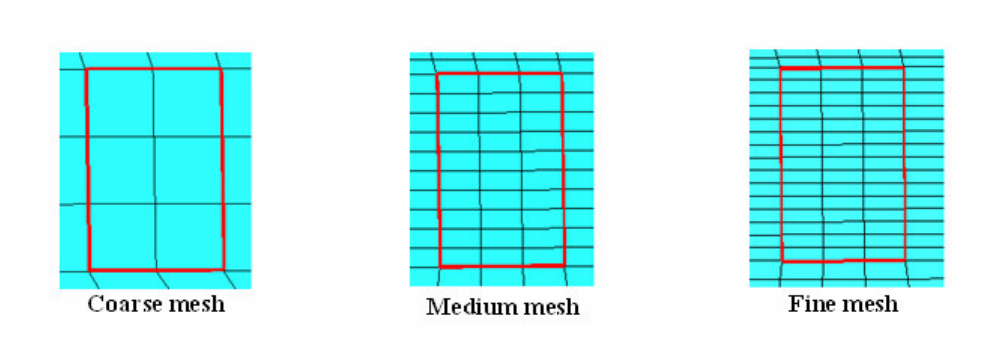

Figure 5.8 Three mesh schemes: (left) coarse mesh; (center) medium mesh; (right) fine mesh

Table 5.3 Results of Sensitive Analysis to Mesh Size

Mesh Case	Smallest Element Length (mm)	Total No. Elements	Strain* (με)	Run Time (min.)
Coarse	63.5	10,036	72.4	55
Medium	20.3	27,492	77.9	90
Fine	11.4	41,604	78.0	180

* It represents the longitudinal maximum tensile strain calculated at the bottom of the FRL layer

To determine whether it is worth considering full axle loading or not, two cases were analyzed: case 1 with only two tire weights right on top of target sensors (half

loading); case 2 with full axle loading (full loading). Comparisons of the calculated strain, stress, and deflection responses are summarized in Table 5.4.

Table 5.4 Comparison of Loading Cases 1 and 2

Case	Strain* (με)	Stress† (kPa)	Deflection# (mm)
Half Loading	72.4	22.1	0.287
Full Loading	78.7	24.5	0.219

*Maximum tensile strain at the bottom of the FRL layer.
†Maximum vertical stress on top of the subgrade.
#Maximum pavement deflection on top of the pavement surface.

The difference in the predicted peak longitudinal strains at the bottom of the FRL layer between the two cases is about 7.4 percent, 10.3 percent in the predicted peak vertical stress on top of the subgrade, and 31 percent in the predicted peak deflection on top of pavement surface. It was then concluded that the full axle loading should be considered in the FE model, indicating that no symmetry on the truck axle loading was considered.

5.2.2 Traffic Loading Simulation

In nature, traffic vehicles apply moving dynamic loads to the pavement structure, thus traffic loading should be considered as a dynamic moving load in the FE model.

To simulate the movement of traffic loading, the load area of each tire footprint was gradually shifted along the wheelpath in the direction of traffic. For each load area,

the amplitude of the traffic load waveform was represented by a haversine function defined in ABAQUS by using a smooth step function (Figure 5.9). The load time was determined by dividing the length of each load area by the traffic speed and. In total, eleven increments (locations of the load) were used to achieve one full passage of the axle over the entire model (Figure 5.9). The clearance between each two increments is small as the truck is on top of the target sensor whereas it is large as the truck moves away from the top of the target sensor. The location of the target sensor is where the pavement response is calculated. A snapshot of partitioned pavement surface for applying truck loads is shown in Figure 5.10. The bold line indicates the location of the instrumentation axis relative to the FE model.

The width of each tire footprint was accurately measured in the field along with the tire pressure and was assumed to be uniformly distributed at a measured magnitude of $724\,kPa$ ($105\,psi$). In contrast, the length of each tire tread was back-calculated from its measured tire pressure and width.

Although the tire pressure is assumed to be distributed uniformly, the tire weight varies from one tire to another. Compared to most currently used mechanistic analysis software, this FE model can handle unequal tire weights.

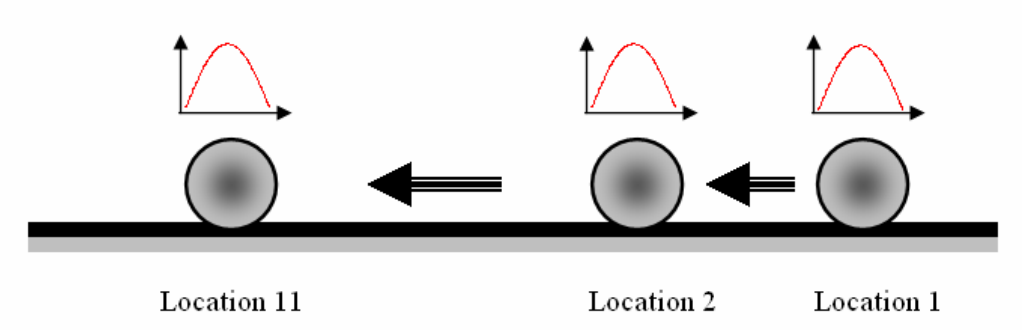

Figure 5.9 Sketch of moving traffic loading and representation of load waveform

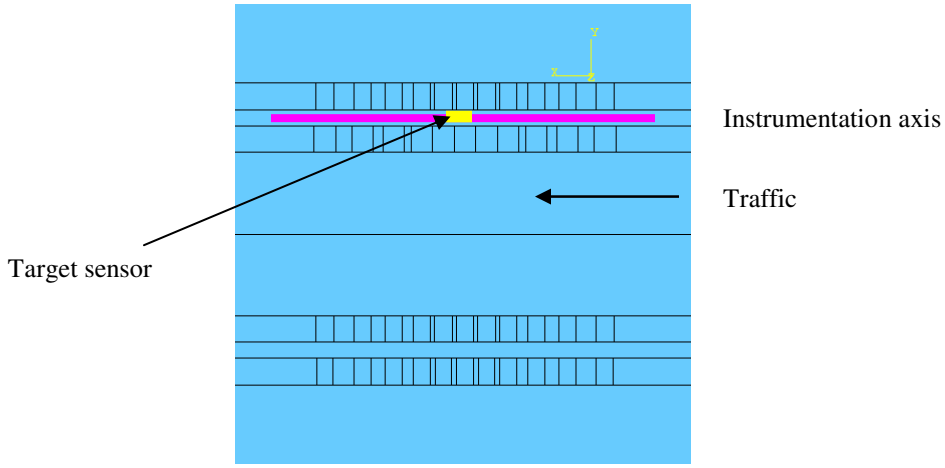

Figure 5.10 Partitioned pavement surface for applying moving traffic loads

5.3 Calibration of Viscoelastic FE Model

After the FE Model was formulated, it needed to be verified by and calibrated to the field-measured pavement response to guarantee its applicability and accuracy to

predict pavement response. The basic principle was to make a fine adjustment to the laboratory-determined instantaneous elastic modulus for each mix such that the predicted response agrees closely with the field-measured response. The concept of the instantaneous elastic modulus was used in ABAQUS to represent the elastic modulus of HMA materials at a high loading frequency and at the reference temperature and it physically represents the initial response of HMA materials at the reference temperature. It was assumed to be the relaxation modulus at a loading frequency of 25 Hz and at the reference temperature of 21.1 $^{\circ}C$ (70 $^{\circ}F$) in this research. Both HMA and unbound granular materials were assumed to be isotropic and homogeneous and the Poisson's ratio does not change with the loading rate and temperature.

For the constructed U.S. 30 perpetual pavement, most traffic is supposed to travel at about 88.5 km/h (55 mph), thus the model was calibrated to the field-measured pavement response at this traffic speed. The pavement temperature was set to that when the CLV test at 88.5 km/h (55 mph) was performed. To calibrate the developed viscoelastic FE model, the calculated maximum longitudinal tensile strain at the bottom of the FRL layer, the maximum transverse tensile strain at the bottom of the FRL layer, the maximum vertical stress on top of the subgrade, and the maximum deflection on top of pavement surface were selected for comparison. Hereinafter, it is understood that the maximum longitudinal tensile strain, the maximum transverse tensile strain, the maximum vertical stress, and the maximum deflection represent the corresponding maximum longitudinal tensile strain at the bottom of the FRL layer, the maximum transverse tensile strain at the bottom of the FRL layer, the maximum vertical

compressive stress on top of the subgrade, and the maximum deflection on top of the pavement surface.

Maximum Longitudinal Tensile Strain Comparison

Figure 5.11 shows the comparison of the measured and the calculated maximum tensile strains. The peak values match very well, a measured figure of 77.9 microstrains versus a calculated value of 78.7 microstrains. In terms of curve shapes, the measured loading duration is shorter than the calculated. However, as it is seen, the two curves agree well. These curves also reveal that the sensor was subjected to a compressive strain when the truck approached. As the truck traveled on top of the target sensor, it generated tension. However, as the truck moved away, the sensor was under compression again. The calculated and the field-measured strains showed that the locations of compression and tension are in good agreement as well.

It is concluded that the developed viscoelastic FE model successfully simulated the time delay of strain response as indicated by the discrepancy between the first compression valley and the second compression valley. The delayed recovery due to the viscosity led to a smaller compression valley after the peak tension in Figure 5.11.

It is of interest to note that the asymmetric strain response observed by Elseifi et al. (2006 a) was not observed in this study and although a delayed recovery existed, the compression area was still pronounced as the truck moved away.

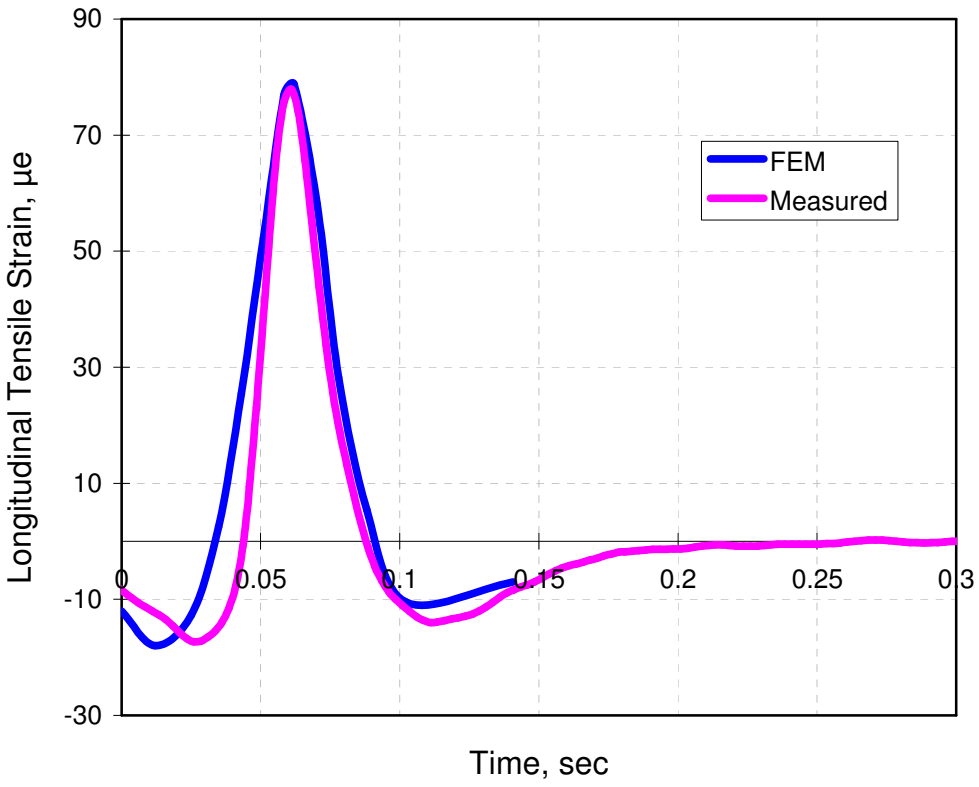

Figure 5.11 Comparison of the measured and the calculated longitudinal tensile strains

Maximum Transverse Tensile Strain Comparison

The calculated and the measured maximum transverse tensile strains are compared in Figure 5.12. As it can be seen, the viscoelastic FE model predicted the maximum transverse tensile strain less accurately in comparison with the prediction of the maximum longitudinal tensile strain. It is not possible to calibrate the FE model to the field-measured longitudinal and transverse strains simultaneously with the same accuracy because of the fact that the pavement has different stiffness values in two

directions which are neglected in the FE model. Similar findings were documented by Mateos and Snyder (2002).

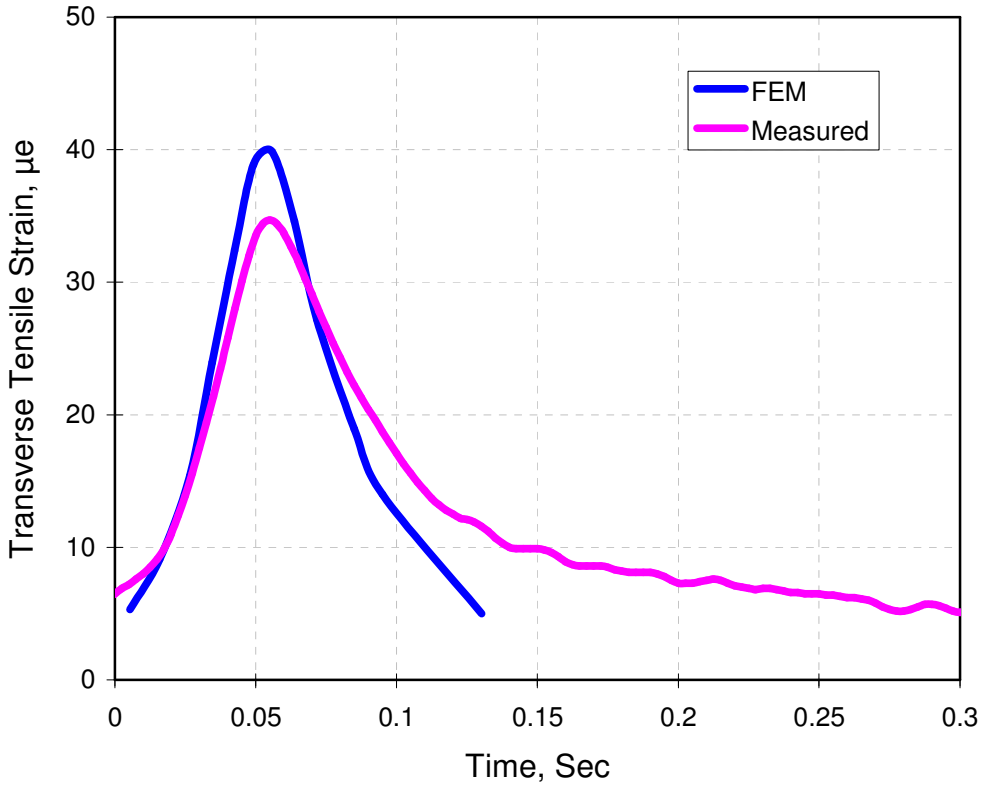

Figure 5.12 Comparison of the measured and the calculated transverse tensile strains

Maximum Vertical Stress Comparison

Figure 5.13 presents the comparison between the measured and the calculated maximum vertical stresses on top of the subgrade. As it can be seen, the two curves are in good agreement.

Maximum Deflection Comparison

The measured and the calculated maximum deflections are shown in Figure 5.14. As indicated by peak response, a percentage difference of 13.4 percent is seen, which is larger than that on the maximum tensile strain and the maximum vertical stress. This discrepancy between calibrations for the strain, stress, and deflection is discussed in more detail later in this section.

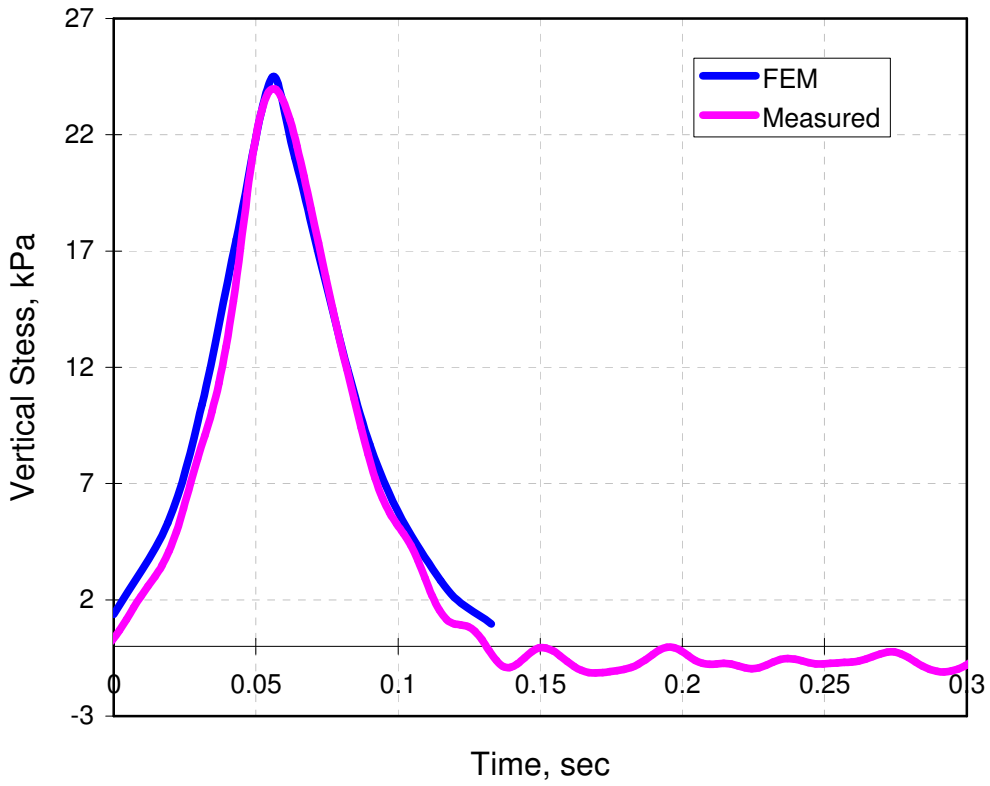

Figure 5.13 Comparison of the measured and the calculated vertical stresses

As it can be seen from the above comparisons, the good agreement between the calculated and the measured maximum tensile strain and the maximum vertical stress suggests that the constitutive behavior of HMA materials may adequately be described by a Prony series with 5 terms.

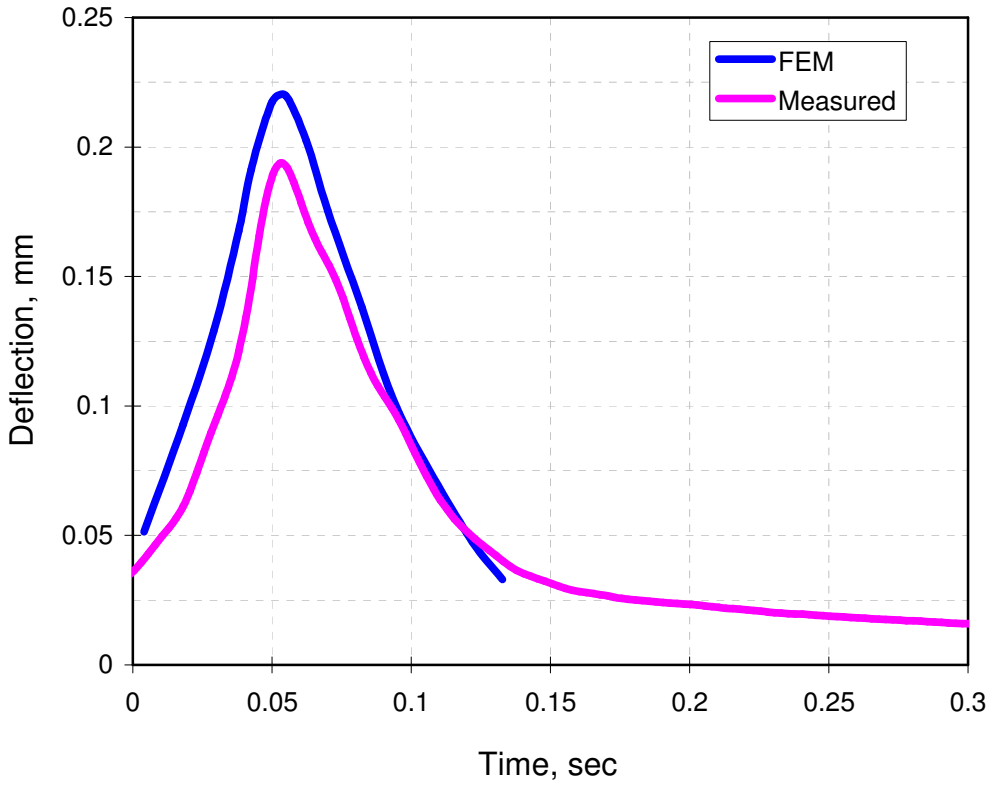

Figure 5.14 Comparison of the measured and the calculated deflections

As for the comparison between the calculated and the measured pavement deflections, the agreement was not as good as that for the maximum tensile strain and the

maximum vertical stress. This is believed to be caused by the non-linearity of the subgrade soils. Huang (1969) found that the non-linearity of soils has a large impact on vertical deflection while a very small effect on vertical stress.

To further examine the effect of the non-linearity of subgrade soils on pavement response, a case study was performed simply considering different resilient moduli of subgrade soils at three levels: 38.6 *mPa* (5.6 *ksi*), 55.2 *mPa* (8 *ksi*), and 71.7 *mPa* (10.4 *ksi*). With each resilient modulus of subgrade soils, one FE analysis was conducted to calculated pavement responses including maximum tensile strain, maximum vertical stress, and maximum deflection and results are shown in Table 5.5. As it can be seen, the variation of the resilient modulus of subgrade soils had the most significant effect on the maximum deflection, the least impact on the maximum tensile strain, and an intermediate influence on the maximum vertical stress. The resilient modulus used in calibration of the viscoelastic FE model was 55.2 *mPa* (8 *ksi*) that most likely represent the resilient modulus of subgrade soils within a couple of feet under the subgrade surface. It is expected that subgrade soils are normally stiffer as their depth increases. Therefore, the calculated maximum deflection would be closer to the measured maximum deflection if the non-linearity of subgrade soils is considered.

The Poisson's ratio of the subgrade was also slightly adjusted in order to achieve a good agreement between the calculated and measured maximum deflections. Although it did not significantly impact strain and stress responses, the Poisson's ratio of the subgrade played a moderate role on pavement deflection. The calibrated instantaneous elastic modulus and the laboratory-measured relaxation modulus for HMA mixes at a

loading frequency of 25 Hz and at a reference temperature of $21.1^{\circ}C\,(70^{\circ}F)$ are listed in Table 5.6, together with resilient moduli for aggregate base and the subgrade soils.

Table 5.5 Effect of Non-linearity of Subgrade soils

Resilient modulus of soils, mPa	Maximum Tensile Strain, με		Maximum Vertical Stress kPa		Maximum Deflection mm	
	Calculated	Percentage change	Calculated	Percentage change	Calculated	Percentage change
38.6	84.5	4.8	22.4	-9.7	0.27	20
55.2	80.6	0	24.8	0	0.22	0
71.7	77.4	4.0	27.0	-8.6	0.19	14.8

Table 5.6 Comparison of the Calibrated and Measured Moduli

Layer	Calibrated Instantaneous Elastic modulus (GPa)	Measured Relaxation Modulus (GPa)
SMA	4.87	5.01
ODOT442	3.65	3.46
ODOT302	7.71	8.06
FRL	8.11	10.47
Base	0.1379[$]	0.069 – 0.276[*$]
Subgrade	0.0552[$]	0.0517[$]

$ These are resilient moduli.
* This is the normal range for aggregates materials.

As shown in Table 5.6, it is reasonable to assume a laboratory-measured relaxation modulus at 25 Hz and at $21.1^{\circ}C\,(70^{\circ}F)$ to be physically equivalent to the initial response of HMA mixtures. The only exception is the FRL mix, where the calibrated instantaneous elastic modulus is $2.36\,GPa$ $(342\,ksi)$ less than the measured

relaxation modulus. As for the Poisson's ratio, it was assumed to be 0.35 for all HMA mixes, 0.40 for aggregates, and 0.48 for subgrade soils.

It is noted that, in what follows, the maximum tensile train solely represents the maximum longitudinal tensile strain at the bottom of the FRL layer, unless otherwise specified.

5.4 Predictability of Calibrated Viscoelastic FE Model

In the last section, the developed viscoelastic FE model was calibrated to the field-measured strain, stress, and deflection. The calibration results showed that the behavior of HMA materials can be well described by a 5-term Prony series. The calculated strains and stresses match the measured ones very well. In this section, the FE model is used to predict pavement responses at different traffic speeds and pavement temperatures to further evaluate its performance. This is then designated as the predictability of the developed viscoelastic FE model. To evaluate the predictability of the developed viscoelastic FE model, one set of pavement responses (maximum tensile strain, maximum vertical stress, and maximum deflection) was calculated at each traffic speed and the results are presented in Figures 5.15 through 5.17. As can be seen, the developed viscoelastic FE model performed consistently well in predicting pavement responses (maximum tensile strain, maximum vertical stress, and maximum deflection).

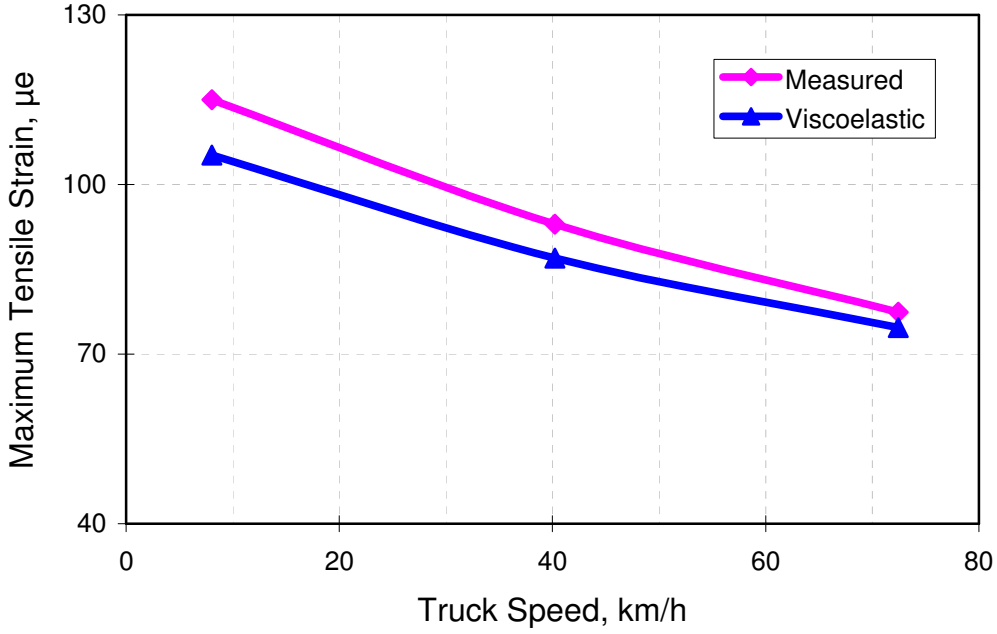

Figure 5.15 Comparison between the measured and the calculated maximum tensile strains

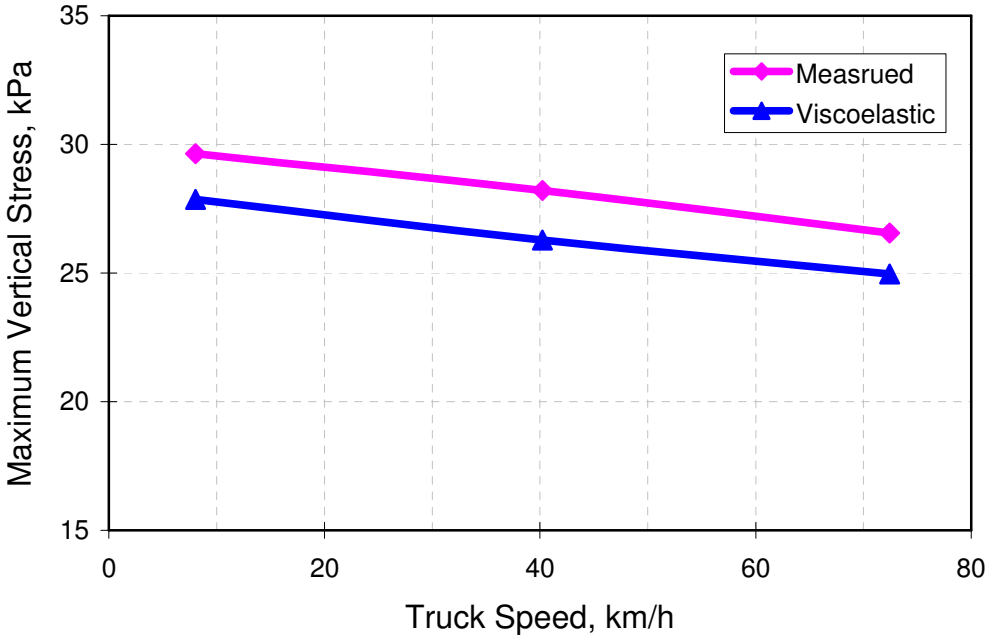

Figure 5.16 Comparison between the measured and calculated maximum vertical stresses

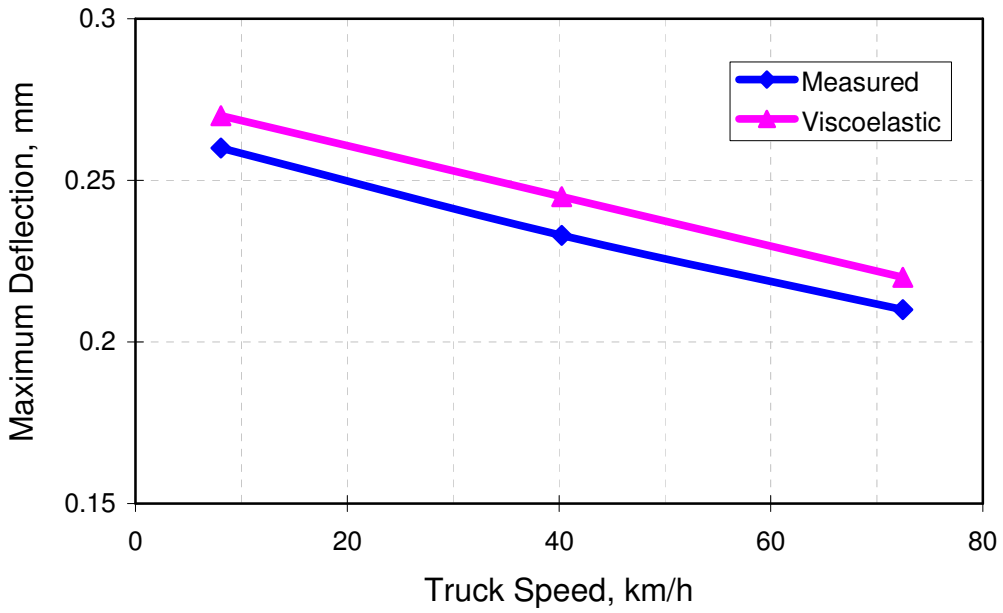

Figure 5.17 Comparison between the measured and the calculated maximum deflections

The calibration results presented in section 5.3 showed that Prony series can describe the behavior of the asphalt materials very well only at a traffic speed of $88.5\,km/h$ ($55\,mph$) and at a single profile of pavement temperature. The results of the predictability in this section indicated that the behavior of asphalt materials can be described over a range of traffic speeds from $8\,km/h$ ($5\,mph$) to $88.5\,km/h$ ($55\,mph$) and over a range of temperatures from $31^{\circ}C$ ($87.8^{\circ}F$) to $42^{\circ}C$ ($107.6^{\circ}F$). Thus this gives confidence that the developed viscoelastic FE model is capable of accurately predicting pavement response at intermediate and high temperatures and a relatively broad spectrum of traffic speeds.

5.5 Comparative Study between Linear Elastic FE and Viscoelastic FE Models

Traditionally, pavement responses were analyzed with elastic solutions in which each pavement layer was treated as an elastic material. However, HMA materials only behave elastically at low temperatures. At intermediate and high temperatures, the elastic theory cannot sufficiently capture the deformation characteristics of asphalt materials. Meanwhile, the effect of traffic speeds cannot be accounted for with the elastic theory, which is more pronounced at a low traffic speed.

In this section, a comparative study between the linear elastic FE and the linear viscoelastic FE models was initiated to evaluate their relative performance. The linear elastic FE model has the same characteristics as the viscoelastic FE model except for the constitutive model used for asphaltic materials. In the linear elastic FE model, the traditional Hook's law was used to describe the behavior of HMA materials while a Generalized Maxwell model was selected to describe the behavior of HMA materials in the viscoelastic FE model.

Although elastic behavior was assumed for asphaltic materials, the temperature dependency was still included in the linear elastic FE model. To consider the temperature dependency in the linear elastic FE model, resilient moduli were obtained at $5^{\circ}C\,(41^{\circ}F)$, $25^{\circ}C\,(77^{\circ}F)$, and $40^{\circ}C\,(104^{\circ}F)$ in the laboratory and were assumed to be changing exponentially with temperatures. Thus the resilient modulus at any temperature can be calculated from this exponential model, with the exponential temperature dependency curves for HMA materials shown in Figure 5.18. The linear elastic FE

model was calibrated with the field-measured pavement response at the same traffic speed and pavement temperatures as that used for calibrating the developed viscoelastic FE model before using it to predict pavement response at other traffic speeds and temperatures.

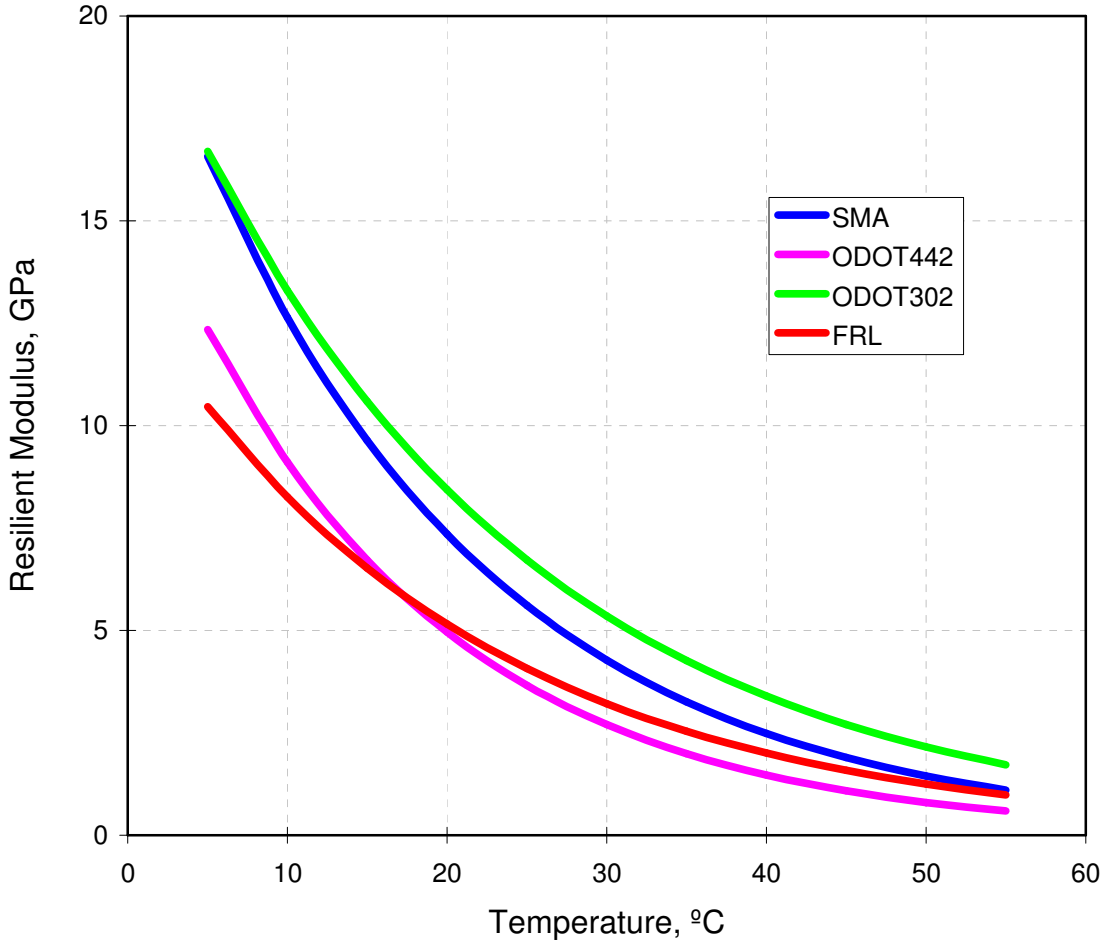

Figure 5.18 Temperature dependency curves used in linear elastic FE model after calibration

Since both the linear elastic FE and the viscoelastic FE models were calibrated to identical field-measured pavement response, it is reasonable to assume that they have identical accuracy in predicting responses at a traffic speed of 88.5 km/h (55 mph). To compare their relative predictability, one analysis was performed with each model at traffic speeds of 72.4 km/h (45 mph), 40.2 km/h (25 mph), and 8 km/h (5 mph), respectively. The results are shown in Figures 5.19 through 5.21. In these figures, the LEFEM represents results of the linear elastic FE model while the VEFEM presents results of the linear viscoelastic FE model.

As seen in these figures, the viscoelastic FE model performed better than the elastic FE model. Because the effect of loading rate was not included, the difference between the measured and the predicted pavement response increased when traffic speed decreased from 72.4 km/h (45 mph) to 8 km/h (5 mph), although the temperature dependency was accounted for. This showed that the behavior of HMA materials cannot be properly described without considering the time and temperature dependency at the same time.

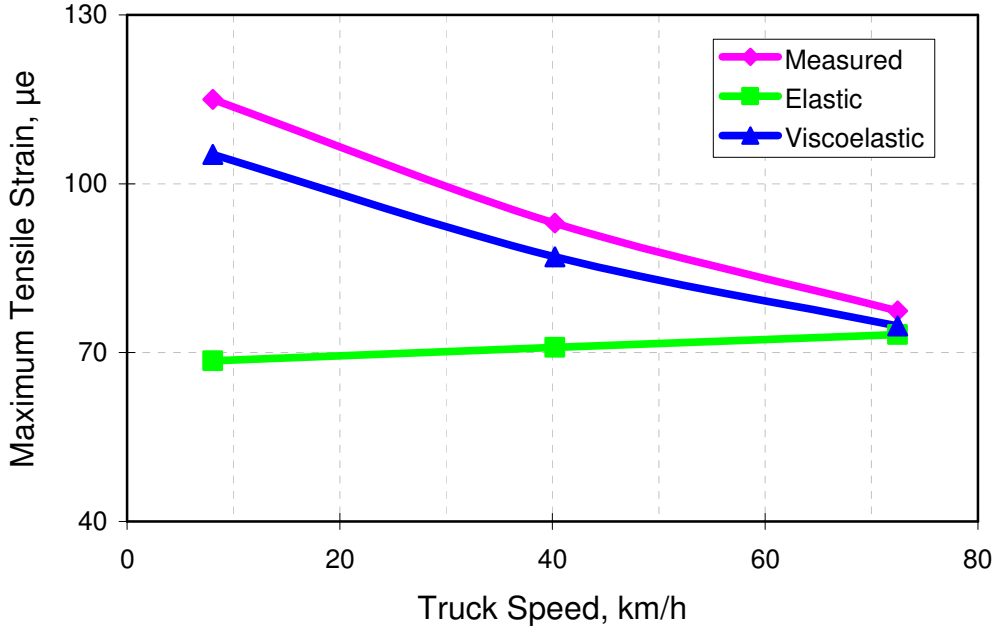

Figure 5.19 Comparison between the measured and the calculated maximum tensile strains

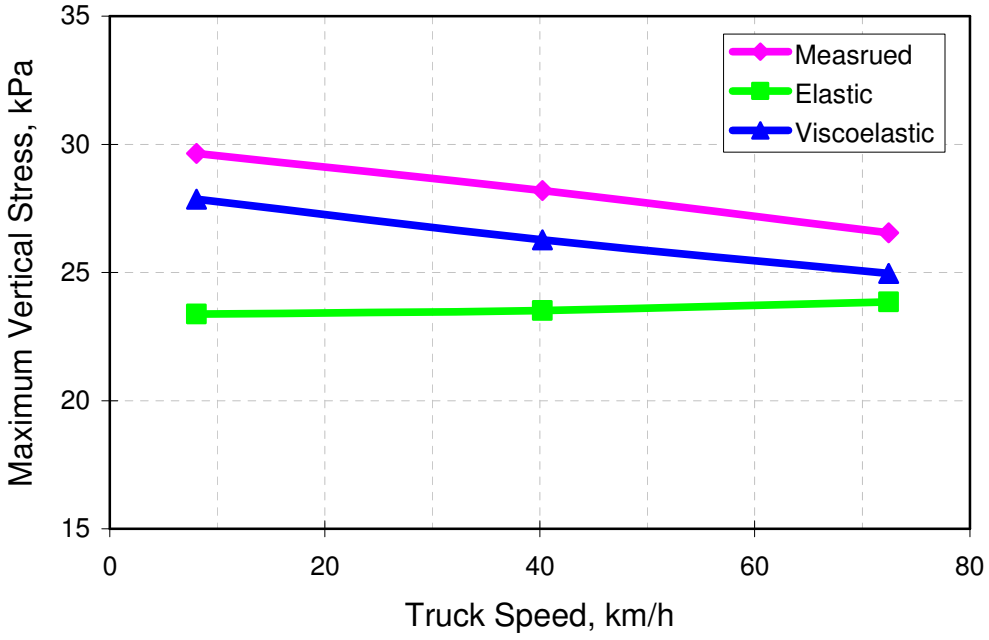

Figure 5.20 Comparison between the measured and the calculated maximum vertical stresses

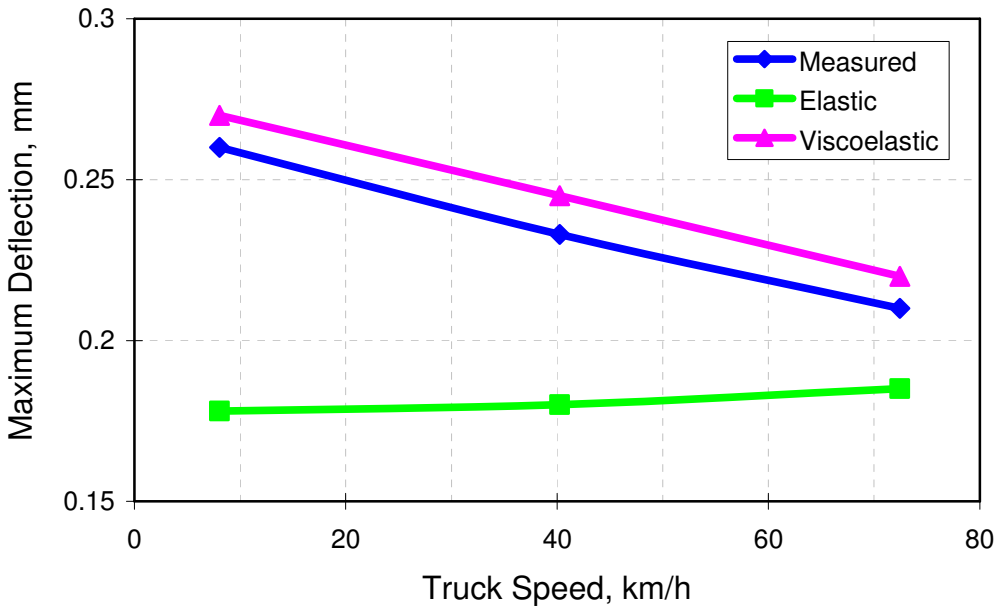

Figure 5.21 Comparison between the measured and the calculated maximum deflections

Conclusively, the viscoelastic FE model outperformed the elastic FE model. At different traffic speeds and pavement temperatures, the viscoelastic FE model performed consistently at about same level of accuracy. Together with the calibration results presented in section 5.3 and the predictability results shown in section 5.4, the following conclusions are drawn:

- The linear elastic FE model cannot accurately predict pavement response under a broad spectrum of traffic speeds and pavement temperatures. It underestimated pavement response, which is not conservative for design purposes and it might lead to premature pavement failure.

- The linear viscoelastic FE model including a 5-term Prony series is capable of accurately describing the behavior of HMA materials. It can accurately predict pavement response under a broad spectrum of traffic speeds and pavement temperatures. Thus, it should be able to replace the conventional elastic FE model for mechanic analyses in pavement design.

6 PARAMETRIC STUDY OF VISCOELASTIC FE MODEL

In this chapter, the developed viscoelastic FE model was used to perform parametric studies to examine the effects of design factors including layer thickness, layer modulus, pavement temperature, axle load, and vehicular speed, on the maximum tensile strain at the bottom of the FRL layer. In addition, a comparative study was conducted between PerRoad and the developed viscoelastic FE model to compare their relative abilities to predict pavement response.

6.1 The Effect of Layer Thickness

Since pavement thickness is of outmost concern in the design of perpetual pavements, the sensitivity of the maximum tensile strain at the bottom of the FRL layer to layer thickness is studied utilizing the developed viscoelastic FE model in this section. Furthermore, a comparative study is undertaken between the developed viscoelastic FE model and PerRoad, a specialized perpetual pavement design software (APA, 2004).

Sensitivity to Layer Thickness

It is important to ensure that the maximum tensile stain at the bottom of the fatigue resistant layer is less than the fatigue limit of 70 microstrains such that no fatigue cracking damage is generated, in the form of a bottom-up crack. Theoretically, the perpetual pavement will never fail by bottom-up fatigue cracking as long as the

maximum tensile strain remains at less than 70 microstrains throughout the lifetime of the perpetual pavement. To minimize the maximum tensile strain, the perpetual pavement must have sufficient thickness.

Because each HMA layer of a perpetual pavement is designed to resist specific distresses, especially the top and bottom HMA layers, only the thickness of the ODOT302 layer and the aggregate base layer were to be examined, considering that both the SMA and the ODOT442 layers serving as the wearing course which will be renewed periodically, while the FRL layer is a specific large stone asphalt mix with a rich asphalt binder and a low air void content to resist fatigue cracking damage.

For the ODOT302 and the base layers, two more thickness values were considered for each layer, in addition to the as-designed value. A total of five cases were analyzed as shown in Table 6.1. In each analysis case, all parameters used in the developed viscoelastic FE model were held constant except for the thickness value of the layer under consideration.

Table 6.1 Analysis Cases Used in Thickness Study

Layer	Case1 (mm)	Case 2 (mm)	Case 3 (mm)	Case 4 (mm)	Case 5 (mm)
ODOT302	228.6 (as-designed)	304.8	381	228.6	228.6
Base	152.4 (as-designed)	152.4	152.4	304.8	457.2

The developed viscoelastic FE model was used to obtain one maximum tensile strain at the bottom of the FRL layer for each case as shown in Table 6.1, and the results

are presented in Figure 6.1. The dotted horizontal line indicates the generally accepted limit of 70 microstrains on the maximum tensile strain. As can be seen in Figure 6.1:

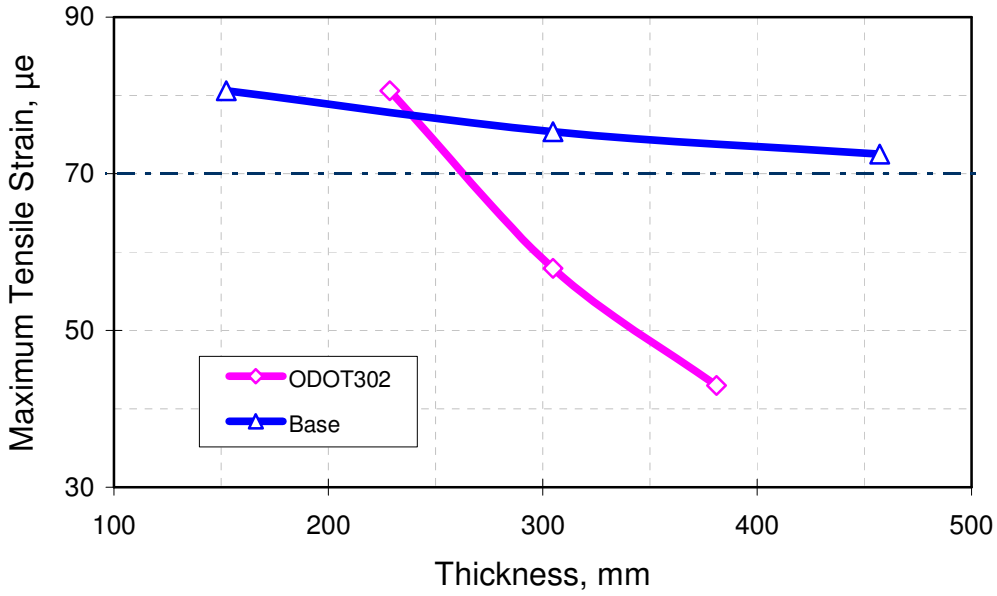

Figure 6.1 The effect of thickness variation on maximum tensile strain

- Increasing the thickness of the ODOT302 layer from 228.6 *mm* (9 *in.*) to 381 *mm* (15 *in.*) produces a decrease in the maximum tensile strain from 80.6 to 43.0 microstrains. The maximum tensile strain is about 70 microstrains when the ODOT302 layer is 261.6 *mm* (10.3 *in.*) thick.

- Increasing the thickness of the aggregate base did not reduce the maximum tensile strain as much as with an increase in ODOT302 layer due to the fact that aggregate base is a lot less stiff.
- The pavement deflection decreased when increasing the thickness of the ODOT302 layer. An opposite trend was observed when increasing the thickness of the aggregate base. For example, when the aggregate base increased from 152.4 *mm* (6 *in.*) to 457.2 *mm* (18 *in.*), the pavement deflection increased from 0.224 *mm* (8.801 *mil.*) to 0.230 *mm* (9.041 *mil.*).

Since the maximum tensile strain for the perpetual pavement was larger than 70 microstrains, one more separate case was analyzed including a 254 *mm* (10 *in.*) ODOT302 layer and a 304.8 *mm* (12 *in.*) aggregate base, yielding a maximum tensile strain of 67.3 microstrains. As such, one good alternative to limit the maximum tensile strain less than 70 microstrains may be achieved by increasing the thickness of the ODOT302 layer to 254 *mm* (10 *in.*) and the thickness of the aggregate base to 304.8 *mm* (12 *in.*) such that an economical design with less permanent deformation will be reached.

Comparative Study between the FE Model and PerRoad

PerRoad is a mechanistic-based and perpetual-pavement-design-oriented software developed by Dr. David Timm at Auburn University. The software makes use of the elastic layered theory to calculate pavement response at critical locations. Uncertainty associated with traffic loading, material properties, and construction can be considered by

using the Monte Carlo simulation technique. One snapshot of the analysis results screen is shown in Figure 6.2.

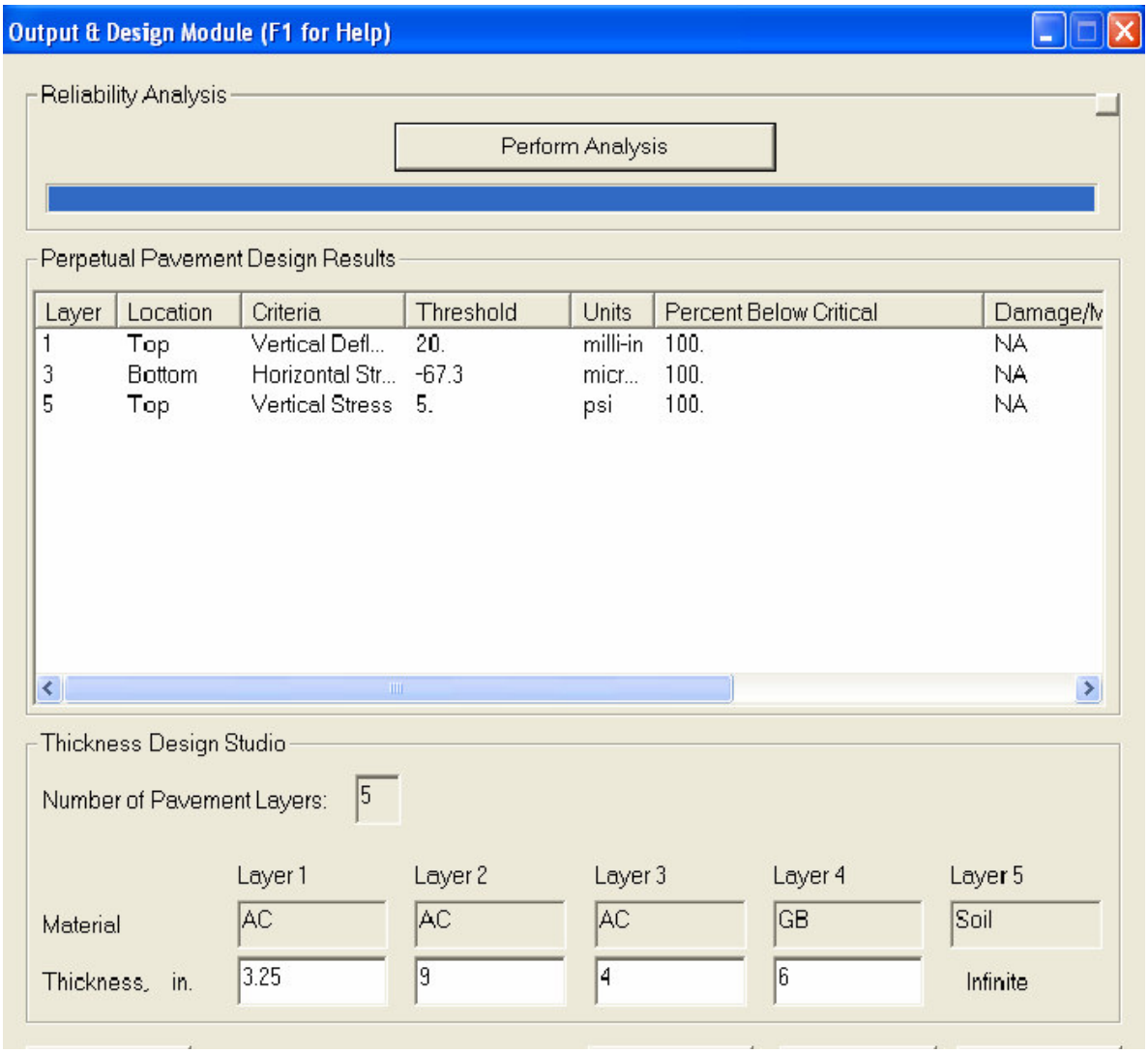

Figure 6.2 Results of PerRoad analysis

One of the advantages of PerRoad is that one can specify a threshold for a distress in its critical location. As in the examples indicated in Figure 6.2, a maximum vertical deflection limit of 0.508 *mm* (20 *mil.*) was specified on top of pavement surface. A maximum tensile strain of 67.3 microstrains was specified at the bottom of the FRL layer. Similarly, the maximum vertical compressive stress on top of the subgrade was limited to 34.5 *kPa* (5 *psi*). The column *Percent Below Critical* indicates the probability that a critical response will not exceed the specified threshold. A second convenient characteristic of PerRoad is the *Thickness Design Studio* in which with targeted threshold(s), the pavement thickness can be optimized.

To make a comparison of the thickness profile between PerRoad and the developed viscoelastic FE model, the elastic moduli inputted into PerRoad was first calibrated to the field-measured pavement responses using the developed viscoelastic FE model without considering viscoelasticity of HMA materials. An identical maximum tensile strain of 67.3 microstrains was specified in PerRoad. Because PerRoad can only handle up to five layers including the subgrade, the SMA and ODOT442 layers were combined into one layer. A thickness-weighted elastic modulus was calculated for the combined layer.

In total, two cases were analyzed respectively with PerRoad and the developed viscoelastic FE model. For each case, one thickness value for the ODOT302 layer was calculated depending on different thickness for aggregate base: 152.4 *mm* (6 *in.*) or 304.8 *mm* (12 *in.*). Analysis results are presented in Table 6.2.

Table 6.2 Comparison of Thickness Design

Layer	Thickness profile (mm)			
	By PerRoad	By Viscoelastic FEM	By PerRoad	By Viscoelastic FEM
SMA	38.1	38.1	38.1	38.1
ODOT442	44.45	44.45	44.45	44.45
ODOT302	*177.8*	*254.0*	*203.2*	*261.62*
FRL	101.6	101.6	101.6	101.6
Base	*304.8*	*304.8*	*152.4*	*152.4*

In comparison with the results computed by the developed viscoelastic FE model, PerRoad determined a thinner ODOT302 layer thickness by $54.8\,mm$ $(2.3\,in.)$ for the $152.4\,mm$ $(6\,in.)$ base and $76.2\,mm$ $(3\,in.)$ thinner for the $304.8\,mm$ $(12\,in.)$ base. Thus, PerRoad underestimated the maximum tensile strain. This can be attributed to the use of the elastic theory in PerRoad. It is also worth mentioning that traffic loading has to be equally applied at each tire in the PerRoad, which may lead to a smaller maximum tensile strain. From the thickness study presented in this section, two conclusions are drawn:

- The as-constructed perpetual pavement has insufficient pavement thickness to maintain the maximum tensile strain at the bottom of the FRL layer to less than 70 microstrains at the recorded high pavement temperatures under the normal traffic speed of $88.5\,km/h$ $(55\,mph)$. This was not intended in the original pavement design, since the methodology of perpetual pavement design included limiting the maximum tensile strain to less than 70 microstrains to prevent fatigue cracking damage in pavement structure.

- It is recognized that thickness designs by PerRoad may not be conservative, which could lead to premature failure of the pavement. The thickness design by PerRoad should be validated by other programs that include viscoelastic constitutive models, such as the one developed in this research.

6.2 The Effect of Layer Modulus

Layer Modulus is also one of two factors (thickness and modulus) playing a major role in developing the resistance of the pavement structure to distresses. Theoretically, a smaller thickness is required if higher modulus HMA materials are selected. The materials selection and mix designs were specified for each layer in the perpetual pavement structure. In this section, the effect of layer modulus on the maximum tensile strain is studied and the contribution of the modulus of each layer to the fatigue resistance is examined.

Three levels of layer modulus were considered as listed in Table 6.3. For HMA materials, they represent the instantaneous elastic modulus. In practice, these variations are generally associated with material testing, mix design, and construction.

To eliminate the thickness effect of each layer, the change of each response (strain, stress, and deflection) was normalized to the thickness of the corresponding layer. Then the sensitivity of the maximum tensile strain to the modulus variation can be evaluated based on the change per unit thickness. Since the subgrade is semi-infinite, normalization was not applied to this layer. The results are summarized in Table 6.4.

Table 6.3 Variations of Layer Modulus

Layer	Modulus (GPa)		
	-30 %	Measured	+30 %
SMA	5.792	8.274	10.756
ODOT442	4.344	6.206	8.067
ODOT302	9.170	13.101	17.031
FRL	9.653	13.790	17.927
Base	0.097	0.138	0.179
Subgrade	0.039	0.055	0.072

Table 6.4 Effect of Layer Modulus on Maximum Tensile Strain

Layer	Maximum Tensile Strain Change (με) per mm	
	-30%	+30%
SMA	2.99E-02	-2.72E-02
ODOT442	2.99E-02	-2.40E-02
ODOT302	2.72E-02	-2.09E-02
FRL	1.48E-01	-1.00E-01
Base	5.91E-03	-6.30E-03
Subgrade	3.86*	-3.25*

*These values are total changes without normalization to corresponding layer thickness.

From the table, it is found that the FRL layer played the most important role on the maximum tensile strain compared with other layers. When the FRL modulus increased by 30 percent, the maximum tensile strain decreased from 80.6 microstrains to 70.4 microstrains.

Nevertheless, it is not a good practice to increase the elastic modulus of the FRL layer to reduce the maximum tensile strain at the bottom of the FRL layer. The reason is two fold: (1) a small increase in the elastic modulus has a small effect on the maximum

tensile strain. (2) The fatigue life of the FRL mixes decreases as it becomes stiffer and less flexible.

6.3 The Effect of Pavement Temperature

Being viscoelastic materials in nature, the behavior of HMA mixtures strongly depends on pavement temperature. With increases in pavement temperature, the maximum tensile strain at the bottom of the FRL layer increases as well. Thus this raises a concern regarding the fatigue cracking damage of the pavement. For certain combinations of layer thickness, the highest pavement temperature at which the maximum tensile strain is less than 70 microstrains can be calculated utilizing the developed viscoelastic FE model, given the same material properties and traffic conditions.

This section is aimed at developing a relationship among the thicknesses of the ODOT302 and the aggregate base layers, pavement temperature, and maximum tensile strain. This relationship will be helpful in future perpetual pavement designs to determine the highest pavement temperature such that an acceptable limit of the maximum tensile strain of less than 70 microstrains is achieved for certain thicknesses of the ODOT302 and the aggregate base layers.

The pavement temperature profiles were retrieved from seasonal instrumentation. Five typical temperature profiles were chosen to calculate the maximum tensile strain with each at three thickness values of the ODOT302 layer and two thicknesses of the base layer. The selected five temperature profiles are shown in Table 6.5. A total of two

base thickness values were considered: 152.4 *mm* (6 *in.*) and 304.8 *mm* (12 *in.*), while three thicknesses of the ODOT302 layer were considered: (1) 228.6 *mm* (9 *in.*); (2) 254 *mm* (10 *in.*); and (3) 304.8 *mm* (12 *in.*).

Each pavement temperature profile is designated by the temperature at mid depth within the SMA layer (equal to 19.1 *mm* (0.75 *in.*)). For example, a pavement temperature of 40.2 $^{\circ}C$ (104 $^{\circ}F$) (Case No. 3) represents a temperature profile consisting of: (1) SMA at 40.2 $^{\circ}C$ (104 $^{\circ}F$); (2) ODOT442 at 36.5 $^{\circ}C$ (97.7 $^{\circ}F$); (3) ODOT302 at 32.8 $^{\circ}C$ (91 $^{\circ}F$); and (4) FRL at 30.8 $^{\circ}C$ (87.4 $^{\circ}F$).

Table 6.5 Selected Pavement Temperature Profiles

	Temperature ($^{\circ}C$)				
Case No.	1	2	3	4	5
SMA	27.2*	33.8*	40.2*	46.4*	52.4*
ODOT442	28.4	32.2	36.5	39.5	44.9
ODOT302	29.0	30.5	32.8	34.5	37.2
FRL	29.4	29.7	30.8	31.2	33.2

*These temperatures were used to develop curves in Figure 6.3.

To establish the aforementioned relationship, a total of 30 cases (5 temperature profiles x 6 thickness) were analyzed. For each combination of thickness of the ODOT302 layer, aggregate base, and pavement temperature, one maximum tensile strain was calculated and the results are shown in Figure 6.3.

As can be seen from this figure, given the same thickness of the ODOT302 layer and the aggregate base, the relationship between the maximum tensile strain and

pavement temperature is an exponential curve. There is also a general trend decreasing in the maximum tensile strain with an increase in the thickness of the ODOT302 layer and the aggregate base and with a decrease in pavement temperature. The following conclusions can be drawn from Figure 6.3:

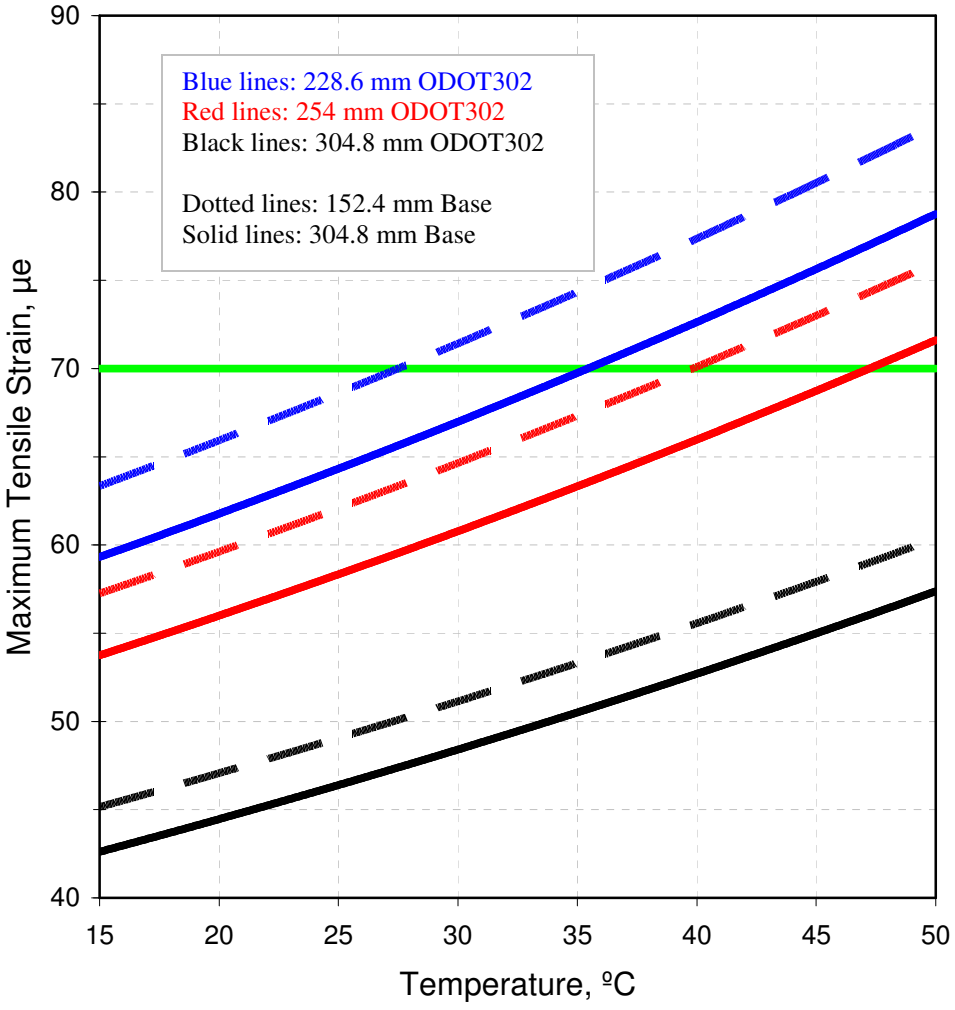

Figure 6.3 Variation of maximum tensile strain with pavement temperature and layer thickness

- Given the pavement temperature and the thicknesses of the ODOT302 layer and the base layer, the maximum tensile strain at the bottom of the FRL layer can be estimated exclusively.
- Provided that the maximum tensile strain has to be less than 70 microstrains, the highest pavement temperature can be estimated with given thickness of the ODOT302 and the base layers thicknesses.
- In the design of perpetual pavements considering a maximum tensile strain of less than 70 microstrains and the possible highest pavement temperature, the thicknesses of the ODOT302 and the base layers can be determined.
- Curves for different thicknesses of the ODOT302 and the base layers are not parallel to each other. The higher the pavement temperature, the more marked the effect of increasing the thickness of the ODOT302 and the base layers
- In order to limit the maximum tensile strain to less than 70 microstrains, the highest pavement temperature for the pavement including a 228.6 mm (9 $in.$) ODOT302 layer and 152.4 mm (6 $in.$) base layer should be about 27 $^{\circ}C$ (80.6 $^{\circ}F$). The as-constructed perpetual pavement will develop a maximum tensile strain larger than 70 microstrains where the pavement temperature exceeds 27 $^{\circ}C$ (80.6 $^{\circ}F$). This implies that, for most of the summer time, cumulative fatigue cracking damage will take place.

Figure 6.3 provides a very practical tool to guide in new perpetual pavement design with the aim at avoiding the generation of fatigue cracking at the bottom of fatigue

resistant layer. One has to be aware that the same HMA materials and the similar pavement structure were assumed while developing this figure.

6.4 The Effect of Load Level

Three load levels were considered to check the effect of axle load on the maximum tensile strain: 77.6 kN (17.4 $kips$), 90.5 kN (20.3 $kips$), and 103.5 kN (23.3 $kips$). The size of loading area was held constant whereas the loading pressure varied with the corresponding load magnitude. The pavement temperature varied from $15^{\circ}C$ ($59^{\circ}F$) to $35^{\circ}C$ ($95^{\circ}F$), which was measured at mid-depth of the ODOT302 layer (196.9 mm (7.75 $in.$)). The vehicle speed was taken as 88.5 km/h (55 mph) and the tire pressure was measured as 724 kPa (105 psi) that corresponds to an axle load of 90.5 kN (20.3 $kips$). The maximum tensile strain at the bottom of the FRL layer was normalized to the load magnitude and the results are presented in Figure 6.4.

The results revealed that the ratio maximum-tensile-strain/load is independent of the axle load magnitude, meaning that the calculated strain varies linearly with the load magnitude.

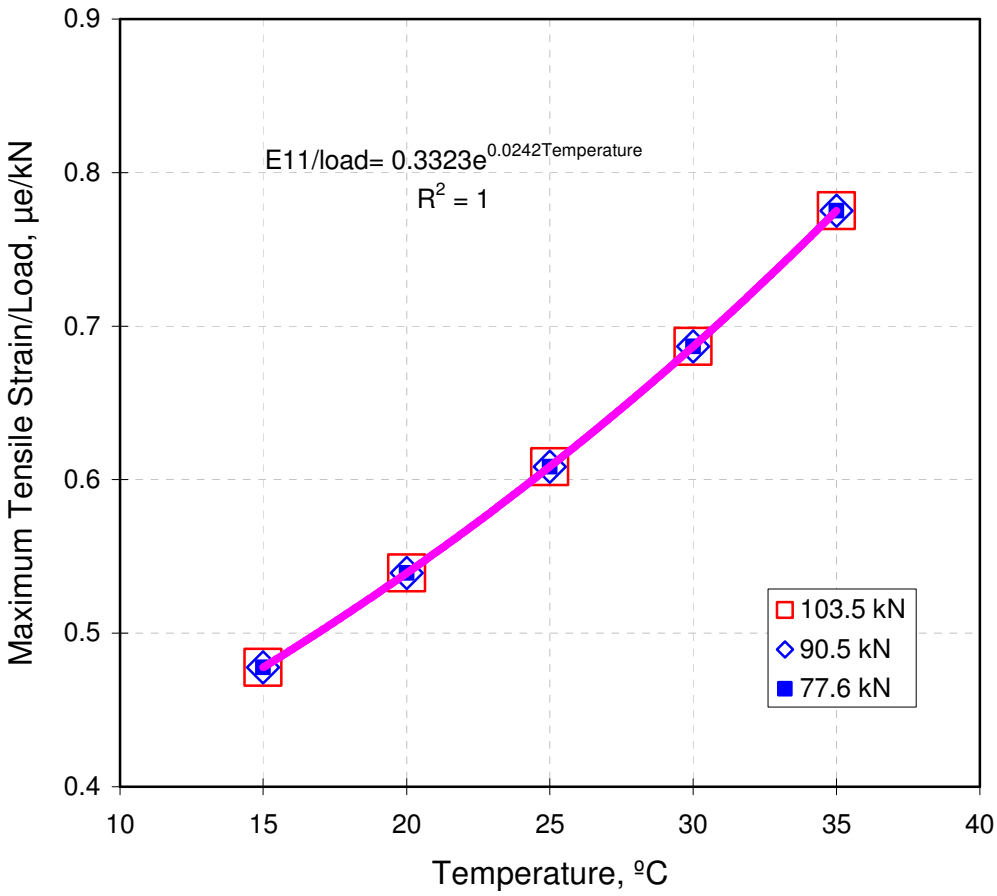

Figure 6.4 Effect of load level on maximum tensile strain

6.5 The Effect of Traffic Speed

Field-measured pavement response data revealed that the traffic speed had a significantly impact on pavement response. The effect of traffic speeds on the maximum tensile strain at the bottom of the FRL layer is researched with the developed viscoelastic FE model in this section, assuming that the traffic speed is 88.5 km/h (55 mph). Two

additional lower speeds were considered: 8 km/h (5 mph) and 40.2 km/h (25 mph). These speed levels were analyzed at three different pavement temperature profiles respectively, each of which was represented by the temperature at mid-depth of the ODOT302 layer including: 11.5$^{\circ}C$ (52.7$^{\circ}F$), 25.6$^{\circ}C$ (78.1$^{\circ}F$), and 34.2$^{\circ}C$ (93.6$^{\circ}F$). The tire pressure was again taken as 724 kPa (105 psi) for all speeds and a total of 9 runs were performed. The results of these analyses are shown in Figure 6.5.

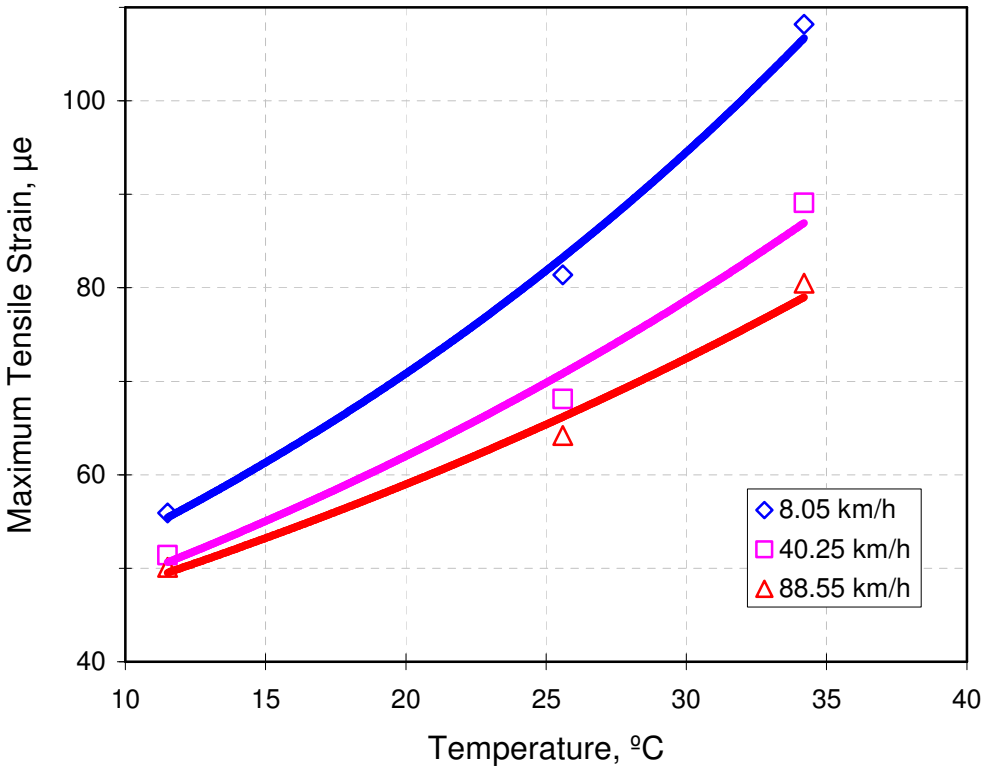

Figure 6.5 Effect of vehicle speed on maximum tensile strain

This figure indicates that the maximum tensile strain significantly increased as the traffic speed decreased from 88.5 km/h (55 mph) to 8 km/h (5 mph). The ratio of maximum-tensile-strain/speed greatly depends on the speed itself and it increased with a decrease in the traffic speed. Thus, the speed effect is not negligible and should be included in the mechanical analysis, since the time dependency of HMA materials is pronounced.

6.6 Summary

This chapter focused on parametric studies using the developed viscoelastic FE model after it was verified and calibrated to field-measured pavement responses obtained at the U.S. 30 perpetual pavement.

The sensitivity of the maximum tensile strain to thickness values of the ODOT302 and the aggregate base layers was investigated, indicating that the pavement would be prone to fatigue cracking damage in the summer. A new profile consisting of a 254 mm (10 in) thick ODOT302 layer and a 304.8 mm (12 $in.$) thick aggregate base layer was suggested. The comparative study of thickness design revealed that PerRoad would yield a pavement structure with less thickness compared with the developed viscoelastic FE mode, which would not be conservative for design purposes.

Small variations of layer modulus, in general, do not have significant impact on the fatigue resistance of the pavement. A design nomograph was developed for selecting the pavement temperature at which the maximum tensile strain will not exceed 70 microstrains. The ratio of maximum-tensile-strain/load was found to be independent of

the axle load magnitude, indicating that a good linear relationship exists. It was also found that the maximum tensile strain significantly increased as the traffic speed decreased from 88.5 km/h (55 mph) to 8 km/h (5 mph) and the ratio of maximum-tensile-strain/speed greatly depends on the traffic speed and it increased with a decrease in the traffic speed.

7 USING FWD TESTS TO PREDICT PAVEMENT RESPONSE

7.1 Overview

The Falling Weight Deflectometer (FWD) is a non-destructive testing device which applies dynamic loading to the pavement surface, constituting a good simulation in magnitude and duration to that of a single moving wheel load. The FWD has been extensively and successfully used to estimate the layer stiffness and to evaluate the pavement structural condition for pavement rehabilitation, overlay design, and quality control (Khosla and Ali, 1989; Roque et al., 1995; Zaghloul and Kerr, 1999; Sargand et al., 2002; Pologruto, 2006; Joh et al., 2006).

During the construction of the U.S. 30 perpetual pavement, FWD testing was performed by ODOT to detect any weak areas and to assess construction quality after the completion of each layer. Upon the completion each of the test sections and before they were opened to the traffic, FWD testing was also performed on top of the pavement surface.

This part of the study is dedicated to using FWD deflection data to predict pavement responses (the maximum tensile strain and the maximum vertical compressive strain) under vehicular loading after the completion of the perpetual pavement. If pavement responses estimated from the FWD are higher than the prescribed limits, necessary remediation measures may be undertaken to decrease these responses to fall below the prescribed limits. Thus, the primary objective of this chapter is to develop FWD deflection-based statistical models to facilitate the prediction of pavement response

of newly-constructed perpetual pavements and then the assessment of construction quality.

7.2 FWD FE Model

To distinguish from the developed viscoelastic FE model described in Chapter 5, the FE model developed in this chapter is referred to as the FWD FE model. The FWD FE model was built out of the developed viscoelastic FE model in Chapter 5 with only one FWD load applied at the center of the model. Except for the applied load, the pavement structure, material properties, and all boundary conditions remained same. One FWD haversine loading waveform was applied to the pavement surface as shown in Figure 7.1. The loading duration was verified with field-measured pavement responses and the loading pressure was assumed to be uniformly distributed considering the radius of the FWD loading plate of $150\,mm$ $(5.91\,in.)$.

During the field testing study, one FWD test was performed at the location of each sensor to make sure it worked well prior to the initiation of the CLV tests. Data collected from these FWD tests was employed to calibrate the FWD FE model. It is worth mentioning that all units adopted in this chapter are based on British system of measurement except for temperature (degree C), to closely represent current practice.

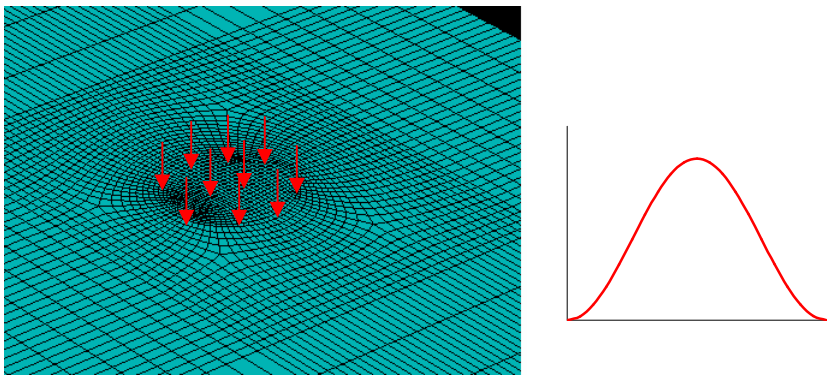

Figure 7.1 FWD loading and magnitude curve

7.3 Factors Considered

To make the FWD deflection based statistical models more practically applicable, the following factors were initially considered:

- *Pavement Temperature (T_{pav}).* The temperature factor was considered in the models to tailor them to the temperature conditions normally encountered in the field during FWD testing. Three temperature levels were used including: $11.5\,^{\circ}C$ ($52.7\,^{\circ}F$), $25.6\,^{\circ}C$ ($78.1\,^{\circ}F$), and $34.2\,^{\circ}C$ ($93.6\,^{\circ}F$), which represent the temperature at mid-depth of the ODOT302 layer. These temperature levels were selected based on the yearly in-situ monitoring record of pavement temperatures at the U.S. 30 test sections.

- *Resilient Modulus of the Subgrade (Mr_{sb}).* Although the resilient modulus of the subgrade is not affected by pavement temperature, it is dependent significantly on the moisture content of the subgrade and it has significant a significant impact on pavement deflection. The resilient modulus of the subgrade was taken into consideration at three levels including: 41.4 *kPa* (6 *ksi*), 69 *kPa* (10 *ksi* i), and 96.5 *kPa* (14 *ksi*).
- *Thickness of HMA layers (H_{ac}).* For a perpetual pavement to be constructed, it is assumed that typical configuration (material distribution) ODOT courses will be used. Thus the material modulus is not an important factor to be included into models. In contrast, the total HMA thickness is incorporated into models, emphasizing the design fundamentals of perpetual pavements. In accordance with its practice, this parameter is represented by the thickness of the ODOT302 layer, which is the most likely to be varied. Thus, three levels of ODOT302 layer thicknesses were used including: 228.6 *mm* (9 *in.*), 304.8 *mm* (12 *in.*), and 381 *mm* (15 *in.*).
- *Thickness of Aggregate Base (H_{base}).* From the results discussed in Chapter 6, it is known that the base modulus did not significantly affect pavement response. Also, an increase in base thickness leads to larger pavement deflections. Then only base layer thickness was considered, with values of: 152.4 *mm* (6 *in.*), 228.6 *mm* (9 *in.*), and 304.8 *mm* (12 *in.*).

A total of 81 ($3T_{pav} \times 3Mr_{sb} \times 3H_{ac} \times 3H_{base}$) cases were analyzed to establish the FWD deflection statistical models relating the FWD deflection to pavement responses. As can be been, the models to be developed more closely reflect the design methodology of perpetual pavements in which the approach is more a design for the maximum tensile strain than a design for the incremental damage, including that fact that the thickness factor is more accounted for in modelss to limit the maximum tensile strain less than 70 microstrains without any fatigue cracking generating.

7.4 Results

After all 81 analyses were completed, analysis of variance (ANOVA) was used to further evaluate the significance of the factor under consideration to the maximum tensile strain and the maximum vertical compressive strain. The results of ANOVA are listed in Table 7.1. An F value represents a measure of how different the mean is relative to the variability within each variable. To understand ANOVA results, the p-value is of most importance, which indicates how significant effect of the independent variable on the dependent variable.

As it can be seen in Table 7.1, if p is set to be less than 0.05, the resilient modulus of subgrade soils and the thickness of aggregate base should be excluded for building the E_{11} model and the resilient modulus of subgrade soils should be excluded for constructing the E_{33} model, meaning the resilient modulus of subgrade soils and the thickness of aggregate base are insignificant to the maximum tensile strain and the resilient modulus of subgrade soils is not significant to the maximum vertical compressive strain.

Table 7.1 ANOVA Results

Factor	E_{11}		E_{33}	
	F	p	F	p
Mr_{sb}	0.1192	0.73	0.2230	0.64
H_{ac}	150.41	0	151.6925	0
T_{pav}	39.8465	$1.49\text{x}10^{-8}$	31.2290	$3.1517\text{x}10^{-7}$
H_{base}	0.1638	0.68	4.0495	0.04759
D_1	357.9361	0	195.7335	0

Following this guidance, two FWD deflection-based statistical models were obtained by performing regression analyses on the computer results using the statistical software AXUM version 7.0 (2001). Two regression models were:

$$E_{11} = 38.5924 - 2.6625H_{ac} + 0.3925T_{pav} + 3.3406D_1$$

$$R^2 = 0.9671, \qquad (7-1)$$

$$E_{33} = 126.1282 - 6.0782H_{ac} + 0.9553T_{pav} - 1.8891H_{base} + 2.5097D_1$$

$$R^2 = 0.9481, \qquad (7-2)$$

Where, E_{11} = Maximum tensile strain at the bottom of the FRL layer, με,

E_{33} = Maximum vertical compressive strain on top of the subgrade, με,

H_{ac} = Thickness of the ODOT302 layer, $in.$,

H_{base} = Thickness of aggregate base, $in.$,

T_{pav} = Temperature at mid-depth of the ODOT302 layer, $^{\circ}C$,

D_1 = FWD deflection at the center of the loading plate, mil.

The coefficients of determination (R^2) of equations (7 – 1) and (7 – 2) revealed that both the maximum tensile strain and the maximum vertical compressive strain are significantly related to the independent variables included in the equation. Provided the values of those factors are known, the maximum tensile strain and the maximum vertical compressive strain can be predicted with confidence.

It is instructive to note that the load magnitude of FWD tests used in equations (7 – 1) and (7 – 2) was $40\,kN$ ($9\,kips$). If any other FWD load magnitude is used, it can be easily converted to $40\,kN$ ($9\,kips$) since the load-deflection relationship for the FWD is linearly proportional. Figure 7.2 presents the relationship between FWD deflection D_1 and applied load. From which, a load multiplier of $0.5993\,mil/kip$ ($0.00221\,mm/kN$) is determined.

If the field-measured asphalt concrete (AC) temperature is unavailable, the AC temperature can be predicted by the regression model developed by Figueroa (2004). The average AC temperature (approximately equal to the temperature at mid-depth of the ODOT302 layer considered in this study) is related to the air temperature by the equation:

$$P = C_1 + C_2 \cdot A + C_3 \cdot A^2 \qquad (7-4)$$

Where, C_1, C_2, C_3 = Regression constants,

P = Average pavement temperature, $^{\circ}C$,

A = Air temperature, $^{\circ}C$.

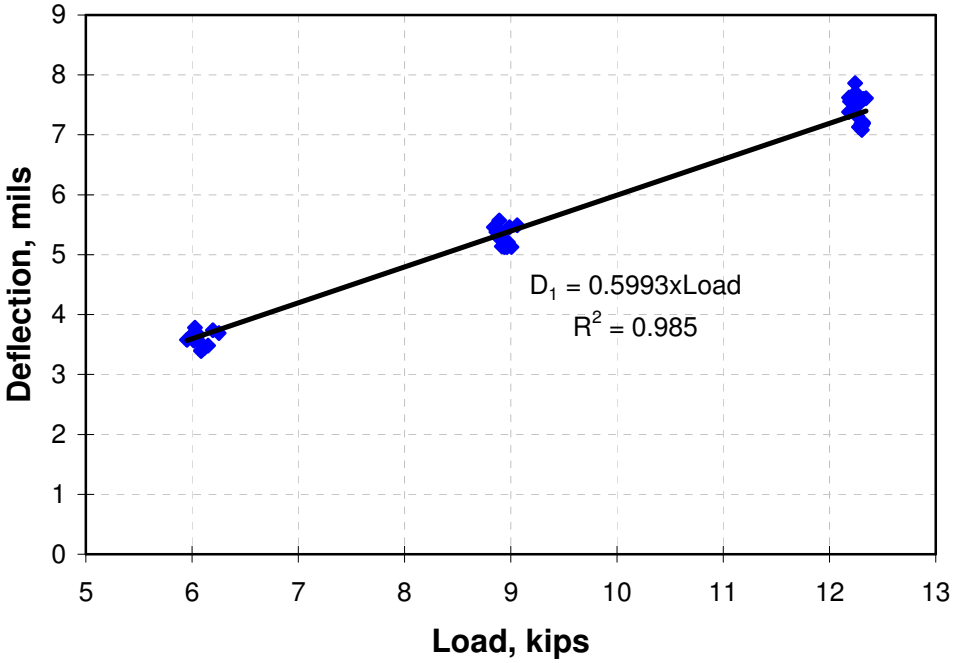

Figure 7.2 FWD deflection vs. load

In the same study, Figueroa (2004) developed regression constants for different climatic zones including eight counties throughout the state of Ohio and these are provided as shown in Table 7.2.

Table 7.2 Average AC Temperature vs. Air Temperature Coefficients (after Figueroa)

Location	No. Points	C_1	C_2	C_3	R^2
North[†]	75414	4.1409	0.9423	0.0027	0.8640
Central[*]	118290	4.8118	0.8860	0.0052	0.8418
South[+]	61152	5.2834	0.9113	0.0055	0.8431
All Sites[#]	254856	4.7055	0.9107	0.0045	0.8475
Ohio Test Road	24133	5.0952	0.8889	0.0114	0.9117

†: Lucas, Wood (2.85) and Wood (8.1).
*: Crawford, Knox, and Licking.
+: Adams and Athens.
#: Adams, Athens, Crawford, Knox, Licking, Lucas, Wood (2.85) and Wood (8.1).

7.5 Summary

An FWD FE model was developed in this chapter to construct two FWD statistical models that can be used to predict the maximum tensile strain and the maximum vertical compressive strain for a pavement structure similar to that built at the U.S. 30 perpetual pavement. A load multiplier was proposed to convert the FWD load to $9\,kips$ if the applied FWD load is not $9\,kips$. Based on the regression models developed by Figueroa (2004), the asphalt concrete temperature can be estimated from the air temperature if there are no field-measured pavement temperatures available. These models are important in practice to assess pavement construction quality using the FWD.

8 CONCLUSIONS AND RECOMMENDATIONS

A three dimensional FE model employing a linear viscoelastic constitutive relationship for HMA materials was developed in this research to predict the response of the pavement structure subjected to dynamic vehicular loading. The laboratory-determined viscoelastic material properties were successfully incorporated into this model. This model was first calibrated to field-measured pavement responses from CLV tests and then further evaluated at different vehicular speeds and pavement temperatures. Parametric studies were undertaken to examine the effects of layer thickness, layer modulus, pavement temperature, load level, and vehicular speed. Finally, FWD deflection-based statistical models were developed to predict pavement response for the purpose of construction quality assessment of perpetual pavements.

This research led to the following major findings:

- The good agreement between the calculated and the measured maximum tensile strain and maximum vertical stress suggested that the constitutive behavior of HMA materials under study may be adequately described by a 5-term Prony series. The developed FE model accurately predicted the strain and stress responses.
- The developed viscoelastic FE model predicted the pavement deflection less accurately mostly due to the non-linearity of unbound granular materials. The pavement deflection was generally overestimated by about 13 percent.

- The developed viscoelastic FE model was calibrated to field-measured pavement response (e.g. strain, stress, and deflection) simultaneously. It is believed that, in comparison with the calibration of strains and stresses, the calibration of deflections could be improved to achieve the same prediction accuracy as long as the effect of non-linearity of granular materials is included in the FE model.
- In comparison with the viscoelastic FE model, the elastic FE model without considering the effect of vehicular speeds significantly underestimated pavement response, which would not be conservative for design purposes.
- Thickness designs by PerRoad may not be conservative, which could lead to premature failure of the pavement. The thickness design by the PerRoad should be validated by other programs that include viscoelastic constitutive models, such as the one developed in this research.
- Layer modulus variation did not affect pavement response as significantly as layer thicknesses. The modulus of the FRL mix has the most marked impact on the maximum tensile strain.
- A nomograph relating the maximum tensile strain to pavement temperature was developed. It is a very practical tool to guide in new perpetual pavement design with the aim at limiting the maximum tensile strain to less than 70 microstrains.

- Results of the study on the effect of load level showed that the ratio of maximum-tensile-strain/load is independent of the axle load, meaning that the maximum tensile strain varied linearly with the axle load.
- The traffic speed played a significant role in the maximum tensile strain. The ratio of maximum-tensile-strain/speed increased with a decrease in the traffic speed.
- An FWD FE model was developed in this study to construct two FWD deflection-based statistical models that can be used to predict the maximum tensile strain and the maximum vertical compressive strain for a perpetual pavement structure similar to that built at the U.S. 30 perpetual pavement. These models can be used to evaluate the pavement structure condition to detect weak areas and to assess pavement construction quality.

Although the developed viscoelastic FE model excellently simulated pavement response, some improvements could be made to make this FE model more effective and accurate. At the same time, more factors could be incorporated into the FWD deflection model to make it more versatile. The recommendations for future research include:

- Inclusion of the non-linearity of unbound granular materials into the viscoelastic FE model to help improve the accuracy in predicting the pavement deflection. The universal model suggested by the AASHTO 2002 Design Guide could be a good choice.

- The utilization of infinite elements to idealize areas far away from the region of interest in the FE model. Infinite elements can provide “quiet” boundaries to the FE model in dynamic analyses, which may for the most part minimize edge effects.
- Up to three key factors including pavement temperature and the thicknesses of the HMA and base layers were considered in the developed FWD deflection-based statistical models in this research. In future studies, more factors such as the asphaltic mix modulus and the thickness of each AC layer could be added into these models such that they can be extended to apply to overlay design where FWD testing is preformed.

9 LIST OF REFERENCES

AASHTO. (1992). *Resilient modulus of unbound granular base/subbase materials and subgrade soils, SHRP Protocol P46: AASHTO Standard Test Designation T*–294–92, American Association of State Highway and Transportation Officials, Washington, D.C.

AASHTO. (2002). *AASHTO 2002 Pavement Design Guide*, American Association of State Highway and Transportation Officials, Washington, D. C.

ABAQUS, (2006). *User's Manual Version 6.6-3*, Hibbitt, Karlsson & Sorensen, Pawtucket, R. I.

ABAQUS, (2006). *Theory Manual Version 6.6-3*, Hibbitt, Karlsson & Sorensen, Pawtucket, R. I.

Abraham, H. (1929). *Asphalts and Allied Substances: Their Occurrence, Modes of Production, Uses in the Arts and Methods of Testing*, Third Edition. D. Van Nostrand Co., Inc. New York, NY.

Asphalt Pavement Alliance (APA), (2002). *Perpetual Pavements: A Synthesis*, Asphalt Pavement Alliance, Lanham, MD.

Asphalt Pavement Alliance (APA), (2004). *A Guide to PerRoad 2.4 Software*, Lanham, MD.

AXUM, (2001). *User's Guide 7.0*, Lucent Technologies, Inc.

Barber, E. S. (1946). "Application of Triaxial Compression Test Results to the Calculation of Flexible Pavement Thickness," *Proceedings, Highway Research Board*, pp 26-39.

Burmister, D. M. (1943). "The theory of Stresses and Displacements in Layered Systems and Application to the Design of Airport Runways," *Proceedings, Highway Research Board*, Vol. 23, pp 126-144.

Burmister, D. M. (1945). "The General Theory of Stresses and Displacements in Layered Soil Systems," *Journal of Applied Physics*, Vol. 16, pp 84-94, 126-127, 296-302.

Carpenter, S. H., Ghuzlan, K. A., SHEN, S. (2003). "Fatigue Endurance Limit for Highway and Airport Pavements," *Transportation Research Record No. 1832*, pp 131-138, Transportation Research Board, National Research Council, Washington, D. C.

Chehab, G. R. (2002). *Characterization of Asphalt Concrete in Tension Using a ViscoElastoPlastic Model*, Dissertation, Department of Civil and Environmental Engineering, North Carolina State University.

Christensen, R. M. (1982). *Theory of Viscoelasticity*. 2nd Ed., Academic Press, New York.

Daniel, S. J. (2001). *Development of a Simplified Fatigue Test and Analysis Procedure using a Viscoelastic Continuum Damage Model its Implication to WestTrack Mixtures*, Dissertation, Department of Civil and Environmental Engineering, North Carolina State University.

De Jong, D. L., Peatz, M. G. F., and Korswagen, A. R. (1973). *Computer Program BisarLayered Systems Under Normal and Tangential Loads*, External Report AMSR.0006.73, Konin Klijke Shell-Laboratorium, Amsterdam.

Duncan, J. M., Monismith, C. L., and Wilson, E. L. (1968). "Finite Element Analysis of Pavements," *Highway Research Record 228*, pp 18-33, Highway Research Board.

Elseifi, M. A., Al-Qadi, I. L., Yoo, P. J., and Janajreh, I. (2005). "Quatification of pavement Damage Caused by Dual and Wide-Base Tires," *Journal of the Transportation Research Board* No. 1940, pp 125-135, National Research Council, Washington, D. C.

Elseifi, M. A.; Al-Qadi, I. L.; Yoo, P. J. (2006 a). "Viscoelastic Modeling and Field Validation of Flexible Pavements," ASCE *Journal of Engineering Mechanics*, Vol. 132 No. 2, pp 172-178.

Elseifi, Mostafa A; Dessouky, Samer H; Al-Qadi, Imad L; Yang, Shih-Hsien, (2006 b). "Viscoelastic Model to Describe Mechanical Response of Bituminous Sealants at Low Temperature," Transportation Research Record: *Journal of the Transportation Research Board*, No. 1958, pp 82-89, Transportation Research Board, Washington D.C.

Ferry, J. D. (1980). *Viscoelastic Properties of Polymers*, 3rd Ed., Wiley, New York.

Figueroa, J. (2004). *Long Term Monitoring of Seasonal and Weather Stations and Analysis of Data from SHRP pavements*, Report FHWA/OH-2004/004, Department of Civil Engineering, Case Western Reserve University, Cleveland, Ohio

Flexible Pavements of Ohio (FPO). (2004). *Ohio Asphalt (spring)*, Columbus, Ohio.

Harichandran, R. S, Baladi, G. Y., and Yeh, M. (1989). *Development of a Computer Program for Design of Pavement Systems Consisting of Bound and Unbound Materials*, Department of Civil and Environmental Engineering, Michigan State University.

Huang, Y. H. (1969). "Finite Element Analysis of Nonlinear Soil Media," *Proceedings, Symposium on Application of Finite Element Methods in Civil Engineering*, pp 663-693, Vanderbilt University, Nashville, TN.

Huang, Y. H. (2004). *Pavement Analysis and Design*, 2nd Ed., Pearson Printice Hall, Upper Saddle River, NJ

Hwang, D., and Witczak, M. W. (1979). *Program DAMA (Chevron), User's Manual*, Department of Civil Engineering, University of Maryland.

Joh, S. H., Kang, T. H., Kwon, S. A., and Won, M. C. (2006). "Accelerated Stiffness Profiling of Aggregate Bases and Subgrades for Quality Assessment of Field Compaction," *Journal of the Transportation Research Board* No. 1975, pp 63-72, Transportation Research Board, National Research Council, Washington, D. C.

Kansas State Highway Commission, (1947). *Design of Flexible Pavements Using the Triaxial Compression Test*, Bulletin 8, Highway Research Board.

Khosla, N. P., and Ali, N. A. (1989). "A Mechanistic Method for Evaluation of Layer Moduli and Overlay Design," *First International Symposium on Nondestructive Testing of Pavements and Backcalculation of Moduli*, pp 355-367, American Society for Testing and Materials, West Conshohocken, PA.

Kopperman, S., Tiller, G., and Tseng, M. (1986). *ELSYM5, Interactive Microcomputer Version, User's Manual*, Report No. FHWA-TS-87-206, Federal Highway Administration.

Lee, S. (2003). *Long-Term Performance Assessment of Asphalt Concrete Pavements Using the Third Scale Model Mobile Loading Simulator and Fiber Reinforced Asphalt Concrete*, Dissertation, Department of Civil and Environmental Engineering, North Carolina State University.

Liao, Y., Kovach J., and Mann, B. (2005). *Asphalt Mix Design Report for the 9th Annual FPO Asphalt Mixture Performance Competition*, Department of Civil Engineering, Ohio University, Athens, Ohio.

Liao, Y., Sargand, S. M., Khoury, I. S., and Harrigal, A. (2007). "*In-Depth Investigation of Premature Distresses of Four Ohio SHRP Test Road Sections,"* 86th TRB Annual Meeting (CD-ROM), Jan. 21-25, 2007, Transportation Research Board, National Research Council, Washington, D. C.

LTPP Protocol P07, (2001). *Test Method for Determining the Creep Compliance, Resilient Modulus and Strength of Asphalt Materials Using the Indirect Tensile Test Device*, Long-Term Pavement Performance Team, Federal Highway Administration, McLean, Virginia

Masada, T. (2001). *Laboratory Characterization of Materials and Data Management for Ohio-SHRP Project (U.S. 23)*, Report No. FHWA/OH-2001/07, Department of Civil Engineering, Ohio University, Athens, Ohio.

Masada, T., Sargand, S. M., and Liao, Y. (2006). "Resilient Modulus Prediction Model for Fine-Grained Soils in Ohio: Preliminary Study," *International Conference on Perpetual Pavement (CDROM)*, Columbus, Ohio.

Mateos, A.; Snyder, M. B. (2002). "Validation of Flexible pavement Structural Response Models with data from the Minnesota Road Research Project," *Transportation Research Record,* No. 1806, pp 19-29, Transportation Research Board, Washington D.C.

Mikhail, M. Y.; Mamlouk, M. S. (1997). "Effect of Vehicle-Pavement Interaction on Pavement Response," *Transportation Research Record,* No. 1570, pp 78-88, Transportation Research Board, Washington D.C.

Mun, S. H. (2003). *Nonlinear Finite Element Analysis of Pavements and Its Application to Performance Evaluation*, Dissertation, Department of Civil and Environmental Engineering, North Carolina State University.

NCHRP, (1997). *Recommended Standard Test Method for Determining the Resilient Modulus of Bituminous Mixtures by Indirect Tension*, Transportation Research Board, National Research Council, Washington D.C.

NCHRP, (2002). *Simple Performance Test for Superpave Mix Design: Appendix A – Test Method for Dynamic Modulus of Asphalt Concrete Mixtures for Fatigue Cracking*, Transportation Research Board, National Research Council, Washington D.C.

Ohio Department of Transportation (ODOT). (2004). *http://www.flexiblepavements.org/documents/way30ppprojectarticle.pdf*.

Park, S. W., and Schapery, R. A. (1999). "Methods of Interconversion between Linear Viscoelastic Materials Functions. Part I – A Numerical Method Based on Prony Series," *Int. J. Solis Struc.*, Vol. 36, No. 11, 1653–1675.

Schapery, R. A. (1984). "Correspondence Principles and a Generalized J-Integral for Large Deformation and Fracture Analysis of Viscoelastic media, *Int. J. Fract.*, Vol. 25, pp. 195–223.

Schapery, R. A., and Park, S. W. (1999). "Methods of Interconversion between Linear Viscoelastic Materials Functions. Part II – An Approximate Analytical Method," *Int. J. Solis Struc.*, Vol. 36, No. 11, 1677–1699.

Pirabarooban, S., Zaman, M., Tarefder, R. A. (2003). "Evaluation of Rutting Potential in Asphalt Mixes Using Finite Element Modeling," The Transportation Factor 2003. *Annual Conference and Exhibition of the Transportation Association of Canada*. (Congres et Exposition Annuels de l'Association des transport du Canada), Transportation Association of Canada.

Pologruto, M. (2006). "Study of In Situ Pavement Material Properties Determined from FWD Testing," *Journal of Transportation Engineering*, Vol. 132 No. 9, pp 742-750, American Society of Civil Engineers, Reston, Virginia.

Raad, L., and Figueroa, J. L. (1980). "Load Response of Transportation Support Systems," *Transportation Engineering Journal*, ASCE, Vol. 106, No. TE1, pp 111-128.

Roque, R., Romero, P., Shen, X., and Ruth, B. E. (1995). "Prediction of Asphalt Pavement Structural Layer Moduli Using Optimized FWD Configuration (With Discussion)," *Journal of the Association of Asphalt Paving Technologists*, Vol. 64, pp 278-305, Association of Asphalt Paving Technologists, White Bear Lake, MN.

Sargand, S. M. (2002). *Determination of Pavement Layer Stiffness on the Ohio SHRP Test Road Using Non-Destructive Testing Techniques*, Report FHWA/OH-2002/035, Department of Civil Engineering, Ohio University, Athens, OH.

Sargand, S. M., Khoury, I. S., Romanello, M. T., and Figueroa, J. L. (2006). "Seasonal and Load Response Instrumentation of the Way-30 Perpetual Pavement," *International Conference on Perpetual Pavement (CDROM)*, Columbus, Ohio.

Sector, K. E.; and Monismith, C. L. (1961). "Analysis of Triaxial Test Data on Asphalt Concrete Using Viscoelastic Principles," *Highway Research Board Proceedings,* Vol. 40, pp 295-314, Highway Research Board, Washington, D. C.

Sousa, J. B., Craus, J., and Monismith, C. L. (1991). "*Summary Report on Permanent Deformation in Asphalt Concrete*," SHRP-A/IR-91-104, Transportation Research Board, National Research Council, Washington, D. C.

Terzaghi, K. (1943). *Theoretical Soil Mechanics*, Wiley, New York.

Warren, H., and Dieckmann, W. L. (1963). *Numerical Computation of Stresses and Strains in a Multiple-layer Asphalt Pavement System*, Internal Report, Chevron Research Corporation, Richmond, CA.

Weissman, S., Harvey, J., Long, F., and Monismith, C. L. (1998). "*Material Modeling for Asphalt Mix and Pavement Analysis/Design Rutting and Fatigue Considerations*," Proceedings of the First National Symposium on 3D Finite Element Modeling for Pavement Analysis & Design, pp 179-225, Charleston, West Virginia.

Wen, H. F. (2001). *Fatigue Performance Evaluation of WesTrack Asphalt Mixtures Based on Viscoelastic Analysis of Indirect Tensile Test*, Dissertation, Department of Civil and Environmental Engineering, North Carolina State University.

Williams, M. L., Landel, R. F., and Ferry, J. D. (1955). "The Temperature Dependency of Relaxation Mechanisms in Amorphous Polymers and Other Glass Forming Liquid," *The Journal of The American Chemical Society*, Vol. 77, No. 14, pp 3701-3707.

Zaghloul, S. M., and Kerr, J. B. (1999). "Reduced Rehabilitation Cost from Use of Falling Weight Deflectometer," *Transportation Research Record* No. 1655, pp 16-24, Transportation Research Board, National Research Council, Washington, D. C.

Zhao, Y. Q. (2002). *Permanent Deformation Characterization of Asphalt Concrete Using a Viscoelastoplastic Model*, Dissertation, Department of Civil and Environmental Engineering, North Carolina State University.